

Efficacy of climate forcings

J. Hansen,^{1,2} M. Sato,² R. Ruedy,³ L. Nazarenko,² A. Lacis,^{1,4} G. A. Schmidt,^{1,4} G. Russell,¹ I. Aleinov,² M. Bauer,² S. Bauer,² N. Bell,² B. Cairns,⁵ V. Canuto,¹ M. Chandler,² Y. Cheng,³ A. Del Genio,^{1,4} G. Faluvegi,² E. Fleming,⁶ A. Friend,⁷ T. Hall,^{1,5} C. Jackman,⁶ M. Kelley,⁷ N. Kiang,¹ D. Koch,^{2,8} J. Lean,⁹ J. Lerner,² K. Lo,³ S. Menon,¹⁰ R. Miller,^{1,5} P. Minnis,¹¹ T. Novakov,¹⁰ V. Oinas,³ Ja. Perlwitz,⁵ Ju. Perlwitz,² D. Rind,^{1,4} A. Romanou,^{1,4} D. Shindell,^{1,4} P. Stone,¹² S. Sun,^{1,12} N. Tausnev,³ D. Thresher,⁴ B. Wielicki,¹¹ T. Wong,¹¹ M. Yao,³ and S. Zhang²

Received 7 January 2005; revised 3 June 2005; accepted 27 June 2005; published 28 September 2005.

[1] We use a global climate model to compare the effectiveness of many climate forcing agents for producing climate change. We find a substantial range in the “efficacy” of different forcings, where the efficacy is the global temperature response per unit forcing relative to the response to CO₂ forcing. Anthropogenic CH₄ has efficacy ~110%, which increases to ~145% when its indirect effects on stratospheric H₂O and tropospheric O₃ are included, yielding an effective climate forcing of ~0.8 W/m² for the period 1750–2000 and making CH₄ the largest anthropogenic climate forcing other than CO₂. Black carbon (BC) aerosols from biomass burning have a calculated efficacy ~58%, while fossil fuel BC has an efficacy ~78%. Accounting for forcing efficacies and for indirect effects via snow albedo and cloud changes, we find that fossil fuel soot, defined as BC + OC (organic carbon), has a net positive forcing while biomass burning BC + OC has a negative forcing. We show that replacement of the traditional instantaneous and adjusted forcings, Fi and Fa, with an easily computed alternative, Fs, yields a better predictor of climate change, i.e., its efficacies are closer to unity. Fs is inferred from flux and temperature changes in a fixed-ocean model run. There is remarkable congruence in the spatial distribution of climate change, normalized to the same forcing Fs, for most climate forcing agents, suggesting that the global forcing has more relevance to regional climate change than may have been anticipated. Increasing greenhouse gases intensify the Hadley circulation in our model, increasing rainfall in the Intertropical Convergence Zone (ITCZ), Eastern United States, and East Asia, while intensifying dry conditions in the subtropics including the Southwest United States, the Mediterranean region, the Middle East, and an expanding Sahel. These features survive in model simulations that use all estimated forcings for the period 1880–2000. Responses to localized forcings, such as land use change and heavy regional concentrations of BC aerosols, include more specific regional characteristics. We suggest that anthropogenic tropospheric O₃ and the BC snow albedo effect contribute substantially to rapid warming and sea ice loss in the Arctic. As a complement to a priori forcings, such as Fi, Fa, and Fs, we tabulate the a posteriori effective forcing, Fe, which is the product of the forcing and its efficacy. Fe requires calculation of the climate response and introduces greater model dependence, but once it is calculated for a given amount of a forcing agent it provides a good prediction of the response to other forcing amounts.

Citation: Hansen, J., et al. (2005), Efficacy of climate forcings, *J. Geophys. Res.*, 110, D18104, doi:10.1029/2005JD005776.

¹NASA Goddard Institute for Space Studies, New York, New York, USA.

²Columbia University Earth Institute, New York, New York, USA.

³SGT Incorporated, New York, New York, USA.

⁴Department of Earth and Environmental Sciences, Columbia University, New York, New York, USA.

⁵Department of Applied Physics and Applied Mathematics, Columbia University, New York, New York, USA.

⁶NASA Goddard Space Flight Center, Greenbelt, Maryland, USA.

⁷Laboratoire des Sciences du Climat et de l'Environnement, Orme des Merisiers, Gif-sur-Yvette, France.

⁸Department of Geology, Yale University, New Haven, Connecticut, USA.

⁹Naval Research Laboratory, Washington, D. C., USA.

¹⁰Lawrence Berkeley National Laboratory, Berkeley, California, USA.

¹¹NASA Langley Research Center, Hampton, Virginia, USA.

¹²Center for Meteorology, Massachusetts Institute of Technology, Cambridge, Massachusetts, USA.

1. Introduction

[2] A climate forcing, measured in W/m^2 , is an imposed change of the planetary energy balance. Common examples of forcing agents are an increase of atmospheric CO_2 or a change of solar irradiance. It is implicitly assumed in most discussions of global climate change that global forcings of the same magnitude will yield similar changes of global mean temperature. Hansen et al. [1997a], hereinafter referred to as RFCR (Radiative Forcing and Climate Response), examined this assumption for a wide range of forcing agents, showing that, although it is a good approximation in many cases, there are a number of forcing agents, such as changes of ozone and absorbing aerosols, for which the climate response is atypical, unique to the forcing agent, and a function of its spatial distribution.

[3] The effectiveness of climate forcings has practical relevance because of the need to assess and compare the climate impact of different changing atmospheric constituents [IPCC, 2001]. Strategies to slow global warming will be most beneficial if they are well informed about the effectiveness of all significant forcings in altering global temperature.

[4] The global mean response to a forcing is a convenient metric, and it has been argued that global mean warming provides one useful criterion to help evaluate the degree of imposed climate change that would constitute dangerous anthropogenic interference [Hansen, 2004]. However, evaluation of the impacts of climate change, including detection and attribution of the causes of climate change, also requires knowledge of the spatial distribution of climate effects and an understanding of how this spatial distribution depends upon specific forcing mechanisms.

[5] In this paper we make numerical climate simulations to investigate the efficacy of many climate forcings that are believed to affect global climate, essentially the forcings considered by IPCC [2001]. For the sake of a compact overview, we emphasize investigation of the global efficacy of the forcings. However, the climate simulations yield information with spatial detail for many climate variables. We provide examples of the climate response here and make our climate model diagnostics available for investigation by others.

[6] Section 2 outlines our approach and the rationale for it. Section 3 defines the climate forcings that we use and includes examples of simulated climate responses. We note the efficacies of the forcings in section 3, but do not attempt detailed explanations. Section 4 compares side-by-side the spatial distribution of climate responses to many climate forcings. Section 5 summarizes and compares the global efficacies, which determine the effective climate forcings as discussed in section 6. In section 7 we examine in detail the efficacies of two important anthropogenic climate forcings: methane and soot. In section 8 we summarize implications of the prior calculations and estimate the net effective climate forcing during the industrial era.

2. Approach

2.1. Definition of Efficacy

[7] We define the efficacy of a climate forcing as the global mean temperature change per unit forcing produced

by the forcing agent relative to the response produced by a standard CO_2 forcing from the same initial climate state. We introduced the efficacy concept and terminology at a workshop on air pollution as a climate forcing [Hansen, 2002] because it was realized that the climate effect of pollutants such as soot and ozone was complex, depending especially on their spatial distribution [RFCR; Forster et al., 1997, 2000; Shine and Forster, 1999; Ramaswamy et al., 2001; Joshi et al., 2003]. CO_2 provides an apt basis for comparison, because the anthropogenic increase of atmospheric CO_2 is the largest anthropogenic climate forcing [IPCC, 2001]. Attempts to slow global warming must focus primarily on restricting CO_2 emissions. Therefore, in considering the merits of reducing other forcings, it is helpful to know their contributions to global warming relative to that of CO_2 .

[8] Use of CO_2 as the standard differs from the approach in RFCR, which compared the global temperature response to given forcing with the response to a spectrally uniform solar irradiance forcing. A CO_2 standard seems better not only for the practical reason given above, but because actual solar forcing is complex and the climate response to it is not well known. Solar irradiance change has a strong spectral dependence [Lean, 2000], and resulting climate changes may include indirect effects of induced ozone change [RFCR; Haigh, 1999; Shindell et al., 1999a] and conceivably even cosmic ray effects on clouds [Dickinson, 1975]. Furthermore, it has been suggested that an important mechanism for solar influence on climate is via dynamical effects on the Arctic Oscillation [Shindell et al., 2001, 2003b]. Our understanding of these phenomena and our ability to model them are primitive, which argues against using solar forcing as a standard for comparing simulated climate effects.

[9] We calculate climate change and efficacy using measured or estimated changes of forcing agents between 1880 and 2000, or, in some cases, the estimated changes between 1850 and 2000. In cases where there is a reasonably well-understood causal relationship between one forcing agent and another, e.g., increasing methane causes increased tropospheric ozone and increased stratospheric water vapor, we also estimate the full efficacy of the primary forcing agent including these indirect effects.

2.2. Atmospheric Model

[10] The global climate model that we employ is the GISS model E [Schmidt et al., 2005], which has been adopted as the new standard GISS model with the present version designated as model III. Model E is a reprogrammed, modularized and documented version of prior GISS climate models including improved representations of several physical processes. Schmidt et al. [2005] provide extensive comparisons of the atmospheric model climatology with observations. Principal model shortcomings include $\sim 25\%$ regional deficiency of summer stratus cloud cover off the west coast of the continents with resulting excessive absorption of solar radiation by as much as 50 W/m^2 , deficiency in absorbed solar radiation and net radiation over other tropical regions by typically 20 W/m^2 , sea level pressure too high by 4–8 hPa in the winter in the Arctic and 2–4 hPa too low in all seasons in the tropics, deficiency of rainfall over the Amazon basin by about 20%, deficiency in summer cloud cover in the western United States and

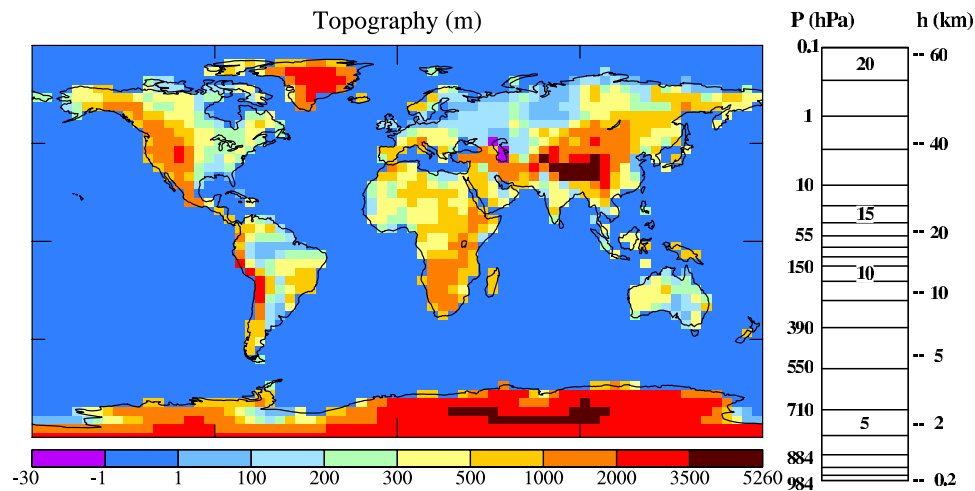


Figure 1. (a) Topography in the $4^\circ \times 5^\circ$ climate model, and (b) vertical layering in 20-layer model.

central Asia by $\sim 25\%$ with a corresponding $\sim 5^\circ\text{C}$ excessive summer warmth in these regions.

[11] *Schmidt et al.* [2005] compare simulations with $2^\circ \times 2.5^\circ$ and $4^\circ \times 5^\circ$ horizontal resolutions, finding that the climatology of the $4^\circ \times 5^\circ$ version is almost as realistic as the finer resolution in most respects. We employ the $4^\circ \times 5^\circ$ resolution here, for which the topography is shown in Figure 1a. Thus the model used here differs from that in RFCR in horizontal resolution ($4^\circ \times 5^\circ$ instead of $8^\circ \times 10^\circ$) and geography (realistic global continents instead of “Wonderland” geography with repeating 120° sectors).

[12] Model physical representations are also improved over those in RFCR, which employed model physics from GISS model II [*Hansen et al.*, 1983]. The most important improvements (Figure 1b) are in the vertical resolution (20 layers instead of 9; designated M20 in *Schmidt et al.* [2005]), the higher model top (at 0.1 hPa instead of 10 hPa), and reduced stratospheric drag. Drag in the top model layer is the minimum required for numerical stability. A much weaker constant drag coefficient is applied throughout the stratosphere to slow the mean zonal stratospheric wind slightly for better accord with observations. Stratospheric zonal structure, its interannual variability, and the zonal temperature structure are generally realistic, although the polar lower stratosphere is as much as $5\text{--}10^\circ\text{C}$ too cold in the winter. This simple stratosphere is a stepping stone toward the implementation of a physically-based representation of gravity-wave drag. The present documentation of the 20-layer model’s behavior is intended to set the stage for comparison of model versions with successively more detailed stratospheric treatments, with the aim of determining the level of stratospheric detail required for climate studies.

2.3. Ocean Models

[13] Our philosophy is that it is instructive to attach the identical atmospheric model to alternative ocean representations [*Hansen et al.*, 1997b]. We include calculations here for ocean A (observed sea surface temperature [SST] and sea ice [SI]), ocean B (Q-flux ocean, with ocean heat transports specified from the implied ocean heat transports in ocean A simulations), and ocean C (Russell dynamic

ocean model [*Russell et al.*, 1995]), with emphasis on ocean C. One merit of ocean C, compared to other dynamical oceans that we employ, is its efficiency. It adds negligible computation time to that for the atmosphere, when the ocean resolution is the same as that for the atmosphere, as is the case here. Ocean C has 13 layers of geometrically increasing thickness, four of these in the top 100 m, and employs the KPP [*Large et al.*, 1994] parameterization for vertical mixing, and the Gent-McWilliams parameterization [*Gent et al.*, 1995; *Griffies*, 1998] for eddy-induced tracer transports. Ocean C at this coarse resolution has realistic overturning rates and inter-ocean transports, but it does not yield El Niño-like variability. Thus, to the extent that the El Niño dynamics play a role in the climate response to radiative forcings [*Mann et al.*, 2005], we would not expect the version of ocean C employed here to capture that effect. Also the deep-water production in the North Atlantic Ocean does not go deep enough in ocean C and the Southern Ocean is too well-mixed near Antarctica [*Liu et al.*, 2003]. Global sea ice cover is realistic, but this is achieved with too much sea ice in the Northern Hemisphere and too little in the Southern Hemisphere. Simulations with ocean E, which has hybrid coordinates with constant- z layers near the surface, isopycnic layers in the bulk of the ocean [*Bleck*, 2002], and a higher horizontal resolution that yields El Niño-like variability, will be presented elsewhere.

2.4. Timescales

[14] The climate simulations in RFCR focused on the equilibrium response with a mixed layer Q-flux ocean. For practical applications, however, it is better to model the full ocean and examine the temporal response. We illustrate mainly the 100-year response (mean for years 81–120), which is the timescale emphasized by *IPCC* [2001] in its definition of global warming potentials.

2.5. Nature and Definition of Forcings

[15] RFCR, as an early investigation of how climate response depends on climate forcings, emphasized idealized geographical distributions, e.g., most forcings were globally or zonally uniform. Here we use more realistic distributions of the spatially variable forcings such as ozone, aerosol and

vegetation changes. We employ several alternative definitions of radiative forcing, for the sake of characterizing the forcing agents better and aiding interpretation of the climate responses that they evoke.

[16] The simplest forcing, and the only pure forcing, is the instantaneous forcing, F_i . F_i is the radiative flux change at the tropopause after the forcing agent is introduced with the climate held fixed. The reason to use the instantaneous flux at the tropopause, rather than the flux at the top of the atmosphere, is that, as shown by *Hansen et al.* [1981], it provides a good approximation to F_a , the flux change at the top of the atmosphere (and throughout the stratosphere) after the stratosphere is allowed to adjust radiatively to the presence of the forcing agent.

[17] The adjusted radiative forcing, F_a , might be expected to be a good measure of the radiative forcing acting on the climate system and relevant to long-term climate change. The reason to anticipate this is that the stratospheric temperature adjusts rapidly, in comparison with the response time of the troposphere, which is tightly coupled to the ocean, and most forcing agents are present longer than the stratospheric radiative relaxation time. Thus F_a , the flux at the top of the atmosphere and throughout the stratosphere after the stratospheric temperature has come to radiative equilibrium, is the principal measure of climate forcing employed in RFCR and by *IPCC* [2001].

[18] Ultrapurists may object to calling F_a a forcing, and object even more to forcings defined below, because they include feedbacks. F_a allows only one climate feedback, the stratospheric thermal response to the forcing agent, to operate before the flux is computed. The rationale for considering additional forcing definitions, which allow more feedbacks to come into play, is the desire to find a forcing definition that provides a better measure of the long-term climate response to the presence of the forcing agent. Specifically, we seek a forcing that is proportional to the equilibrium global temperature response, with the same proportionality constant for all forcing agents. For the reason mentioned above and illustrated in RFCR, F_a tends to provide a better indication of the global climate response than F_i . Because our interest is in the long-term climate response, which is delayed decades to centuries by the ocean's thermal inertia, it is reasonable to allow additional fast feedback processes to operate, as these feedbacks are felt as forcings by the ocean and thus affect the long-term climate response. Of course such mechanisms (fast feedbacks) may have differing degrees of realism from one model to another, so a forcing that includes fast feedbacks may have greater model dependence, but, partly for this reason, quantification of multiple forcing definitions is a useful analysis tool.

[19] *Shine et al.* [2003] suggest a forcing definition, F_g , computed by fixing both SST and T_g , the ground temperature of non-ocean areas. They find that F_g provides a better measure of the equilibrium climate response than F_i or F_a in their intermediate-complexity model. Calculation of F_g in a GCM that includes physical and biological processes at the land surface requires prescription among alternative programming choices that hold T_g fixed, and thus F_g may not have a unique value. We tried several alternatives (e.g., fixing only T_g , fixing T_g and T_s , also fixing surface fluxes), but were unable to find a prescription yielding F_g values

that were a good predictor of the climate response. This difficulty may be a consequence of unique characteristics of the GISS model [*Hansen et al.*, 1983; *Schmidt et al.*, 2005] such as parameterization of surface fluxes in terms of T_g and T_s , and the planetary boundary layer treatment, which internally has subgrid scale vertical resolution. *Shine et al.* [2003] find that F_g provides a good prediction of temperature change in their model.

[20] We define another measure of the climate forcing, a fixed SST forcing,

$$F_s = F_o + \delta T_o / \lambda, \quad (1)$$

by running the climate model with SST and SI fixed. F_o and δT_o are, respectively, the flux change at the top of (and throughout) the atmosphere and the global surface air temperature change after the forcing is introduced with SST and SI fixed. F_o is the "quasi forcing" of *Rotstayn and Penner* [2001]. λ is the model's equilibrium climate sensitivity ($^{\circ}\text{C}$ per W/m^2 , evaluated from doubled CO_2). Thus the fixed sea surface forcing, F_s , allows the tropospheric temperature and land surface, as well as the stratospheric temperature, to adjust to the presence of the forcing agent. The rationale is that F_o is the relevant forcing for predicting that portion of the equilibrium temperature change that occurs after the SST has adjusted. However, we must also include the temperature change, δT_o , that occurs with the forcing present but before the SST is allowed to change. The predicted equilibrium global temperature change is $\Delta T_s (t \rightarrow \infty) = \lambda F_s = \delta T_o + \lambda F_o$. *Hansen et al.* [2002] discussed F_s but did not note the desirability of including the second term ($\delta T_o / \lambda$) to obtain a better estimate of F_s . The reason to include this term is apparent, because it accounts for the fact that the global surface temperature has already partially adjusted to the forcing when the flux is calculated.

[21] One merit of both F_g and F_s is that they avoid the task of defining the tropopause level. F_i and F_a are sensitive to the choice of tropopause level [*Forster et al.*, 1997; RFCR], and the definition of the tropopause level differs from one climate model to another. A disadvantage of F_g and F_s is that they require running the global climate model for at least several years to minimize the noise due to chaotic weather in the model. As both F_g and F_s allow the troposphere to adjust, thus including such feedbacks as the aerosol semi-direct effect on cloud cover, we would anticipate comparable performance from these two definitions of climate forcing.

[22] *Gregory et al.* [2004] suggest that calculations of the forcing can be obviated in cases for which a climate model run exists in which the forcing was added suddenly to a model control run and then held constant for a long simulation. An estimate of the forcing is obtained by regressing the flux at the top of the atmosphere against the change in surface air temperature, with the flux at zero temperature change being the estimated forcing. This approach allows both stratospheric, tropospheric, and land surface feedback mechanisms to operate. Thus the forcing so obtained, which we designate F_s^* , is an approximation of F_s . Our climate model runs allow ready computation of F_s^* as well as F_s , so our tabulated forcing comparisons below include F_s^* . The regression to $t = 0$ depends upon the

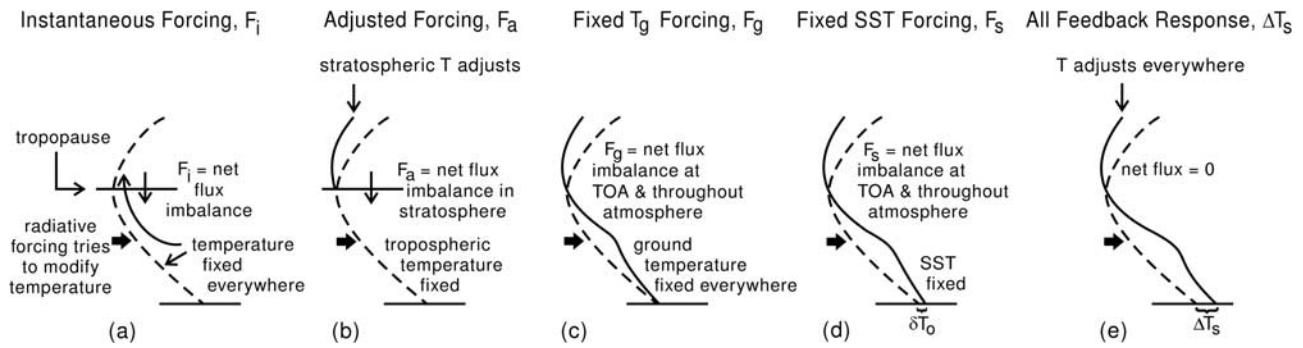


Figure 2. Cartoon comparing (a) F_i , instantaneous forcing, (b) F_a , adjusted forcing, which allows stratospheric temperature to adjust, (c) F_g , fixed T_g forcing, which allows atmospheric temperature to adjust, (d) F_s , fixed SST forcing, which allows atmospheric temperature and land temperature to adjust, and (e) ΔT_s , global surface air temperature calculated by the climate model in response to the climate forcing agent.

number of years in the simulation. We tried several alternatives to find the run length that gives the “best” result in the sense of “predicting” most accurately the global temperature response to the forcing. Use of only several years near $t = 0$ yields an inaccurate result because of the noise in a short response, while use of 100 years gives too much weight to results far from $t = 0$. Usually 10-year to 30-year run lengths give the best results, i.e., they yield a value for E_s^* closest to unity. We include results for 10-year runs in our tabulated comparisons below. Our several tables show that F_s^* usually provides a good measure of the forcing for forcings that are not too small.

[23] The cartoons in Figure 2 compare alternative forcing definitions. We calculate F_s for all forcings and F_i and F_a for cases in which they are readily computed. We suggest that F_s has a good physical basis, because the time constant for the surface soil temperature to adjust usually is short, more like the time constant for the troposphere than the time constant for the ocean. Nevertheless, each of the forcing definitions needs to be judged on its practical utility for climate change analyses, and computation of several of them may aid understanding of climate forcing mechanisms.

[24] Corresponding to F_i , F_a , F_g and F_s are the efficacies E_i , E_a , E_g and E_s . We normally refer to E_a as the efficacy, because F_a is the standard forcing employed by *IPCC* [2001]. However, as we shall see, E_s often provides a better prediction of the climate response and in some cases it is difficult to compute or uniquely define F_a and thus E_a .

3. Climate Forcings

[25] We define here climate forcing agents used in our climate simulations and include examples of the surface air temperature response to the forcings. We note the resulting efficacies, but do not discuss them in detail. A more comprehensive comparison of the climate responses to these forcings is provided in section 4. This aids discussion of efficacies in section 5 and effective climate forcings in section 6.

[26] We compute F_i , F_a , F_s and F_s^* for most forcing mechanisms to aid understanding and to allow other researchers easy comparison with our results. We use the World Meteorological Organization [*WMO*, 1957; *Reichler et al.*, 1996] tropopause definition in computing F_i and F_a .

Nominally the WMO tropopause is set at the lowest level at which the lapse rate ($-dT/dz$) decreases to 2K/km or less and if the average lapse rate from this level to any level within the next higher 2 km does not exceed 2K/km. Figure 3 compares the fixed tropopause level that we used in prior papers [e.g., *Hansen et al.*, 2002] with the WMO

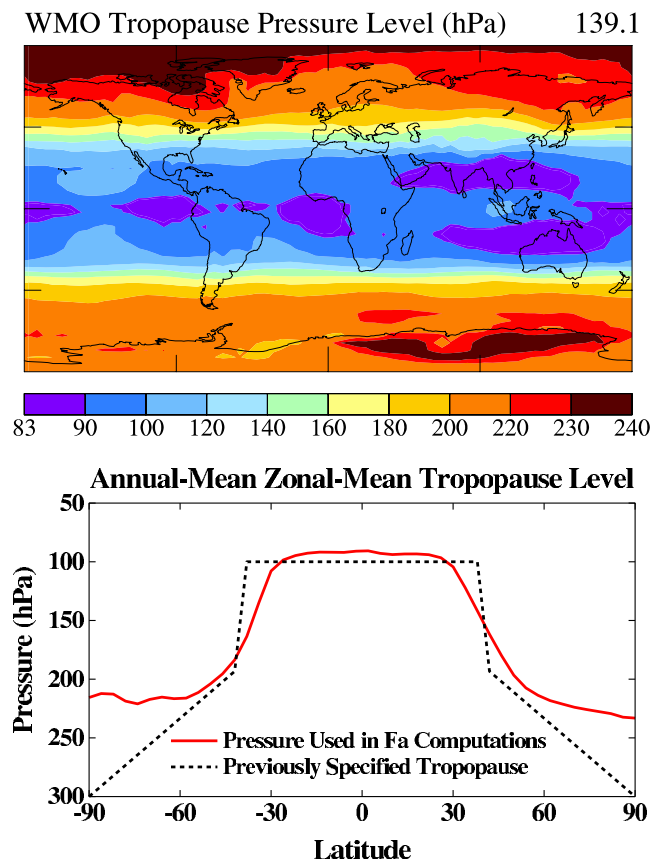


Figure 3. Tropopause pressure level in GISS model III with 1880 atmospheric and surface conditions as computed with the *WMO* [1957] tropopause definition. The “previously specified tropopause” was employed by *Hansen et al.* [2002] and is used in our present paper for calculations of F_a .

tropopause level in the control run of model III with 1880 atmospheric composition and ocean surface conditions. We include in Table 1 and later tables Fa' , the adjusted forcing based on the tropopause level used by Hansen *et al.* [2002]. A principal merit of the WMO tropopause definition is that it allows the specified tropopause level to change as the climate changes.

[27] We note here that most simulations in this paper were made with the identical computer program for modelE, identified by the prefix E2 in the run name. However, the E2 code did not include programming for the aerosol indirect effects, AIE_{CldAlb} and AIE_{CldCvr} , or snow albedo increments proportional to BC deposition. The modelE program including code for these effects is identified by the prefix E3. A separate control run was made for E3 and several of the simulations made with E2 were repeated with E3 in order to verify that the model sensitivity was not modified to a detectable amount by these changes.

3.1. Greenhouse Gases

3.1.1. Carbon Dioxide

[28] The climate forcing by CO_2 in the present GISS model III is at the high end of the range estimated by IPCC [Ramaswamy *et al.*, 2001]. Specifically, doubled CO_2 in our current model, from the 1880 value of 291 ppm to 582 ppm, yields $F_i = 4.52 \text{ W/m}^2$, $F_a = 4.12 \text{ W/m}^2$ and $F_s = 4.11 \text{ W/m}^2$ ($F_o = 3.78 \text{ W/m}^2$, $\delta T_o = 0.22^\circ\text{C}$, $\lambda = 2/3^\circ\text{C per W/m}^2$). IPCC [Ramaswamy *et al.*, 2001] estimates F_a for doubled CO_2 to be in the range 3.5–4.1 W/m^2 . If the actual CO_2 forcing is at the low end of this range, our CO_2 forcing and simulated climate response will be reduced as much as 15%. However, the climate forcing efficacy is a relative measure that is independent of uncertainty in the CO_2 forcing.

[29] Figure 4 shows the heat flux into the planetary (ocean) surface (Figure 4a), surface air temperature (Figure 4b), and ocean ice cover (Figure 4c) for the first 300 years of the coupled model (ocean C) control run (no forcing) and doubled CO_2 experiment. We employ no flux corrections. The control run has a drift of 0.06°C per century during the 300 years based on the linear trend and still has a flux into the ocean of about 0.2 W/m^2 at year 300. We make five $2 \times CO_2$ runs initiated at successive 30-year intervals of the control run, in order to define precisely the model's sensitivity. At the same points we initiate additional control runs (not included in Figure 4), to allow subtraction of an accurate mean control run. Most of our subsequent figures are the difference between experiment runs and control run means.

[30] Figure 4 shows the temporal response of global surface air temperature to doubled CO_2 for the coupled model, relative to the control run, and for the mixed layer and full-ocean Q-flux models. After 100 years, specifically the 81–120 year mean, the coupled model has achieved about 70% of its estimated equilibrium response. The Q-flux mixed layer model has an equilibrium sensitivity of 2.7°C for doubled CO_2 (Figure 4), i.e., $\sim 2/3^\circ\text{C per W/m}^2$. The (ocean C) coupled model's equilibrium climate sensitivity for doubled CO_2 is also $\sim 2.7^\circ\text{C}$, based on the remaining energy imbalance at 200 years ($2.2^\circ\text{C} + 0.75 \text{ W/m}^2 \times 2/3^\circ\text{C per W/m}^2$). The climate sensitivity of model III is thus well within the range $3 \pm 1^\circ\text{C}$ for

doubled CO_2 that has been inferred from paleoclimate evidence [Hansen *et al.*, 1984, 1993].

[31] Figure 5 shows the geographical distributions of F_i , F_a and F_o for doubled CO_2 obtained as a mean for years 11–100 of a 100-year model run with fixed observed SSTs and sea ice, with F_o shown at both the planetary surface and the top of the atmosphere. The fixed SST forcing, F_s , is the sum of $\delta T_o/\lambda$ and global integral of F_o , which is independent of altitude in the atmosphere. The maps of F_i and F_a are similar, as expected. F_o at the surface shows that the energy associated with the energy imbalance is deposited especially in the Indian, Western Pacific, and Tropical Atlantic oceans.

[32] We calculate the climate forcings and simulate the climate response for a wide range of CO_2 amounts (0.125, 0.25, 0.5, 1, 1.25, 1.5, 2, 4, 8 times the 1880 amount) in order to characterize the nonlinearity of the modeled response. We refer not to the nonlinearity of the forcing as a function of CO_2 amount, which is well known, but rather to the nonlinearity of the global mean response as a function of the magnitude of the forcing. This latter nonlinearity is a fundamental characteristic of the climate system, which we discuss in section 5.

[33] Figure 6a shows the adjusted forcing as a function of CO_2 amount. Figure 6b is the simulated surface air temperature change as a function of CO_2 amount. There is increased curvature in the line formed by the points in Figure 6b, compared with the line in Figure 6a. This increased curvature is the climate system nonlinearity discussed in section 5.

[34] The efficacy E_a is the global temperature response per unit forcing for a given forcing agent relative to the response to a standard CO_2 forcing from the same initial climate state. Specifically, we use 100-year (mean for years 81–120) responses of the GISS coupled climate model. For the standard forcing we use $1.5 \times CO_2$ (relative to 1880), as discussed in section 5.

[35] Figure 6c shows the ratio of the simulated global mean temperature change to the adjusted forcing, $\Delta T_s/F_a$, and its normalized value, which is the efficacy E_a . The efficacy of CO_2 increases as the CO_2 amount increases. This is a result of climate feedback processes as discussed in section 5.

[36] We note that the large standard deviation for the five $1/2 CO_2$ runs (0.055°C) arises from a single run that yielded a global cooling of only 1.68°C . The five members of the ensemble were obtained from ocean-atmosphere initial conditions spaced at 30-year intervals of the control run. It would be informative to have a far larger ensemble, with 100 or more members, allowing a statistical study of responses to a forcing. The climate model is highly efficient if run on a single processor and many computers now have 1000 or more processors, so the resource requirements are feasible.

[37] The spatial distribution of F_s for a sequence of CO_2 amounts is shown in Figure 7, which also includes each of the forcings used in simulations with the GISS model for the 2007 IPCC report. These forcings are all collected in Figure 7 for ease of intercomparison of forcings and response. The coupled model 81–120 year response to each of these forcings is illustrated in section 4. The transient response to transient forcings, submitted to

Table 1. Forcings and Efficacies for Greenhouse Gases

GHG Changes	Run Names	Fi	Fa ^a	Fa ^a	Fs	Fs ^{a,b}	δTo	ΔTs	Ei	Ea	Es	Es [*]	Fe ^c
1 × CO ₂ = 291 ppm													
0.125 × CO ₂	E2CO2E	-12.68	-10.94	-	-10.30	-10.10	-0.61	-4.56	0.78	0.90	0.95	0.98	-9.84
0.25 × CO ₂	E2CO2Q	-8.88	-7.74	-7.56	-7.44	-7.21	-0.43	-3.32	0.81	0.92	0.96	0.99	-7.16
0.5 × CO ₂	E2CO2H	-4.61	-4.07	-3.99	-3.91	-3.84 ± 0.27	-0.22	-1.78 ± 0.05	0.83	0.94	0.98 ± 0.03	1.00	-3.84
1.25 × CO ₂	E2e1Q	1.44	1.30	1.29	1.32	1.23 ± 0.14	0.07	0.58 ± 0.03	0.88	0.97	0.95 ± 0.05	1.03	1.26
1.5 × CO ₂	E2e1H	2.64	2.39	2.37	2.38	2.11	0.12	1.10	0.90	1.00	1.00	1.13	2.38
2 × CO ₂	E2e2	4.52	4.12	4.08	4.11	3.95 ± 0.11	0.22	1.96 ± 0.02	0.93	1.02	1.03 ± 0.01	1.07	4.22
4 × CO ₂	E2e4	9.27	8.53	8.41	8.58	8.14	0.45	4.06	0.95	1.03	1.02	1.08	8.77
8 × CO ₂	E2e8	14.65	13.53	13.29	13.97	13.37	0.73	7.02	1.04	1.12	1.09	1.13	15.16
Specified Changes													
W-MT GHGs(1880→2000) ^d	E2GHG	2.52	2.40	2.31	2.55	2.54 ± 0.10	0.14	1.21 ± 0.02	1.04	1.09	1.02 ± 0.02	1.03	2.61
CO ₂ (291→370 ppm) ^d	No Runs	1.55	1.40	-	-	-	-	-	-	-	-	-	-
CH ₄ (837→1752 ppb) ^d	No Runs	0.51	0.53	-	-	-	-	-	-	-	-	-	-
CH ₄ (837→3504 ppb)	E2CH4x2	1.10	1.15	1.05	1.20	1.18 ± 0.12	0.07	0.59 ± 0.01	1.15	1.10	1.05 ± 0.02	1.07	1.27
CH ₄ (837→9000 ppb)	E2CH4x5	2.11	2.17	2.00	2.28	2.29	0.13	1.14	1.16	1.13	1.08	1.07	2.46
N ₂ O (278→316 ppb) ^d	No Runs	0.15	0.15	-	-	-	-	-	-	-	-	-	-
N ₂ O (278→1898 ppb)	E2N2Ox6	3.55	3.47	3.28	3.62	3.49	0.21	1.67	1.02	1.04	1.00	1.04	3.62
MPTGs + OTGs (2000) ^d	No Runs	0.30	0.30	-	-	-	-	-	-	-	-	-	-
CFC11 + CFC12 (4 × 2000)	E2CFCx4	1.02	1.04	1.01	1.41	1.38	0.08	0.64	1.34	1.32	0.97	0.99	1.37
Stratospheric H₂O by CH₄ Oxidation													
1880 to 2000 CH ₄	E2eh4-E2o	-	-	-	0.061	0.036 ± 0.01	0.000	0.027 ± 0.01	-	-	0.96 ± 0.31	1.49	0.058
none to 2000 CH ₄	E2eh4-noch4	-	-	-	0.105	0.108 ± 0.06	0.002	0.042 ± 0.02	-	-	0.87 ± 0.34	0.85	0.091
O₃ (1880→2000)													
Whole Atmosphere	E2oz	0.438	0.281	-	0.256	0.203 ± 0.12	0.019	0.107 ± 0.02	0.53	0.82	0.90 ± 0.13	1.14	0.231
Troposphere	E2ozT	0.408	0.337	0.300	0.335	0.276 ± 0.09	0.015	0.128 ± 0.03	0.68	0.82	0.83 ± 0.16	1.00	0.276

^aFa uses tropopause defined by WMO [1957], while Fa' uses the Hansen *et al.* [2002] tropopause.

^bFs* is asymptotic (ΔTs→0) planetary flux imbalance based on first 10 years of simulation with the specified agent.

^cFe = EaFa = EsFs = ΔTs/(ΔTs/Fa)_{1.5×CO₂} = ΔTs/0.463.

^dGreenhouse gas amounts are 1880–2000 changes from Hansen and Sato [2004]. MPTGs are Montreal Protocol trace gases, and OTGs are other trace gases tabulated by Hansen and Sato [2004].

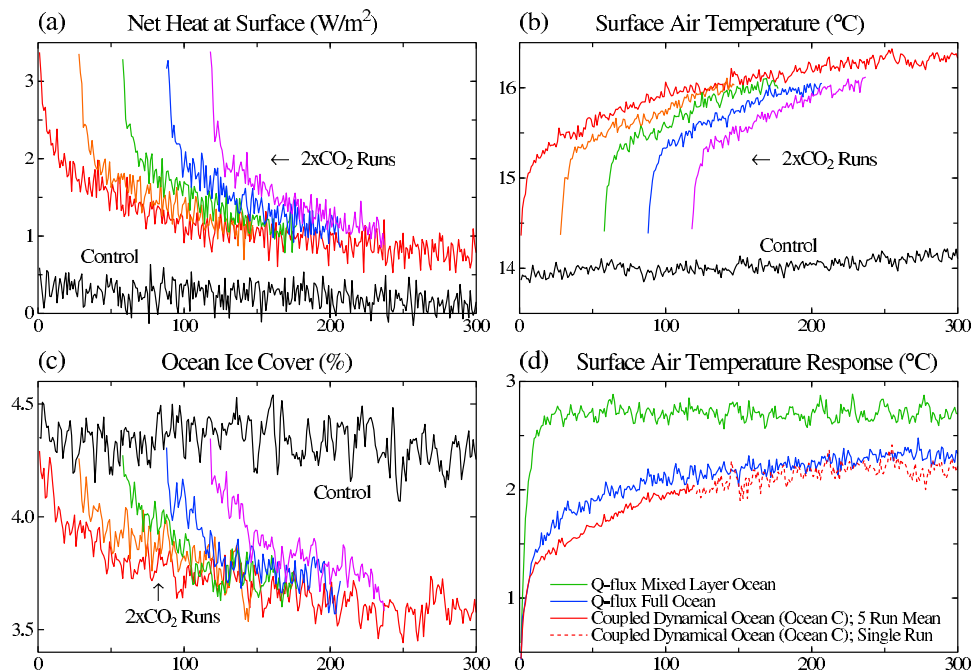


Figure 4. (a) Heat flux into the planetary surface, (b) surface air temperature, and (c) ocean ice cover in doubled CO₂ experiments and control run of the coupled atmosphere–ocean model III. (d) Global surface air temperature responses to doubled atmospheric CO₂ (291 → 582 ppm) after subtraction of appropriate control runs, for several ocean representations, all with atmosphere model III.

IPCC, is described by Hansen *et al.* [2005, also manuscript in preparation, 2005].

3.1.2. Other Well-Mixed Greenhouse Gases

[38] In addition to CO₂, methane (CH₄), nitrous oxide (N₂O) and the chlorofluorocarbons (CFCs) are significant anthropogenic greenhouse gases whose long-term perturbations are reasonably well-mixed in the troposphere. The climate response to changes of these gases is not necessarily similar to the climate response to a CO₂ forcing of the same magnitude, although that assumption is often implicit in climate change studies. CO₂ changes in our model are approximated as spatially uniform in the troposphere and stratosphere, which, except for a small effect due to a lag in CO₂ perturbations being mixed upward, should be a good approximation, as CO₂ is not dissociated in the stratosphere. CH₄, N₂O and CFC perturbations, on the other hand, have spatial distributions that are fit to observed abundances as reported by Minschwaner *et al.* [1998]. These gases thus are uniformly mixed in the troposphere and fall off exponentially in the stratosphere with scale heights 50, 30 and 30 km for CH₄, N₂O, and CFCs, respectively. There is also a latitudinal gradient in amount, ranging from 1% for N₂O to 9% for methane, based on data of Minschwaner *et al.* [1998].

[39] Our 120-year coupled model simulation with all well-mixed GHGs (CO₂, CH₄, N₂O and CFCs) increased from 1880 to 2000 values yields $\Delta T_S = 1.21 \pm 0.02^\circ\text{C}$ for years 81–120, where the indicated uncertainty is the standard deviation of the five ensemble members. $\Delta T_S = 1.21^\circ\text{C}$ corresponds to an efficacy $E_a \sim 109\%$. This result implies, because more than half of the GHG forcing for that period is from CO₂, that the efficacy of the non-CO₂ gases is substantially higher than 100%. To verify this, we carried

out simulations individually for CH₄, N₂O and CFC forcings. Simulations with individual gases used changes larger than those observed for the sake of assuring a substantial response relative to unforced model variability. Runs were made for CH₄ changes 2 and 5 times the 2000 atmospheric amount and for an N₂O change 6 times the atmospheric amount.

[40] GHG forcings and responses are listed in Table 1. The forcings and efficacies in Table 1 include only direct effects; indirect effects of CH₄ on O₃ and H₂O and indirect effects of CFCs on O₃ are discussed in later

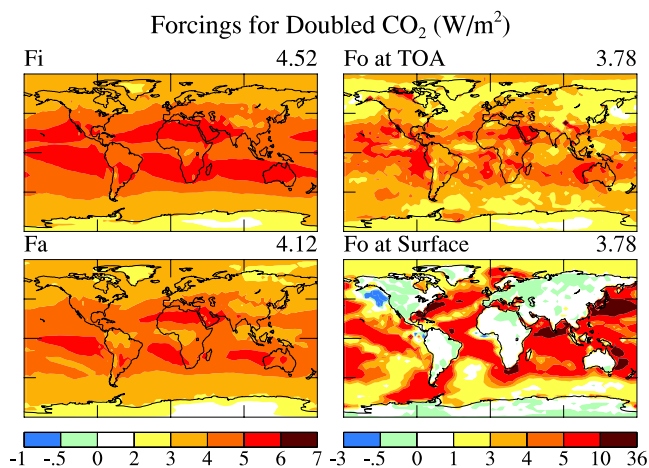


Figure 5. Alternative climate forcing definitions for doubled CO₂. Fi is evaluated at the tropopause and Fa at the top of the atmosphere. Fo is shown at both the top of the atmosphere and the planetary surface.

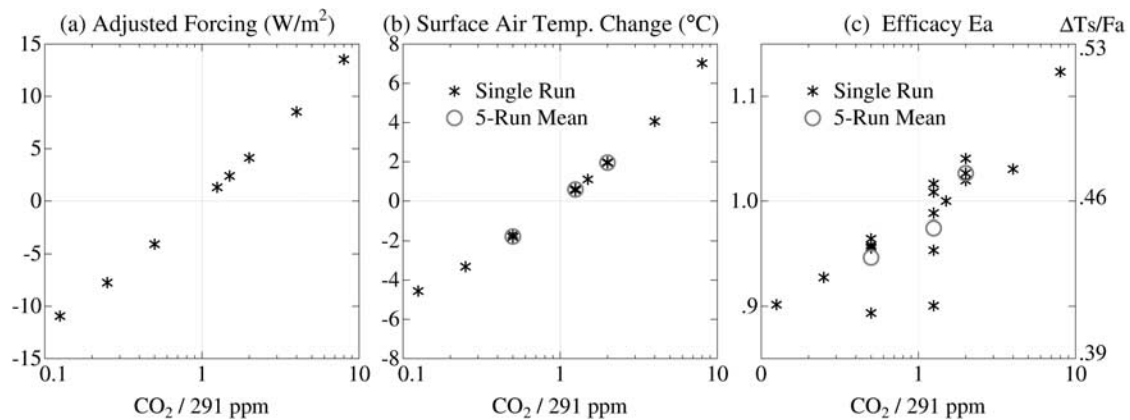


Figure 6. (a) Adjusted forcing, F_a , as a function of CO_2 amount relative to the control run with $\text{CO}_2 = 291$ ppm. (b) Mean 81–120 year global temperature change (ΔT_s) as a function of CO_2 amount. Asterisks are results for single runs and open circles are 5-run ensemble means. (c) Ratio of 81–120 year temperature change to F_a . Scale on the left is the efficacy E_a , obtained by dividing $\Delta T_s/F_a$ by the value of $\Delta T_s/F_a$ for $1.5 \times \text{CO}_2$.

sections. The global mean surface air temperature response, ΔT_s , is the mean for years 81–120 for either a single run or a 5-member ensemble, with the latter identified by the presence of the standard deviation in the ΔT_s column. The CH_4 , N_2O and CFC forcings yield efficacies $E_a \sim 110\%$, 104% and 132% relative to the standard CO_2 forcing, respectively. In interpreting the results the nonlinearity of the response should be borne in mind. For example, a CH_4 increase to 9000 ppb yields $E_a \sim 113\%$, while an increase to 3504 ppb yields $E_a \sim 110\%$. Judging from the ensemble runs the typical one standard deviation uncertainty in the forcings is $\sim 2\%$. Causes of higher efficacies for non- CO_2 gases are discussed in section 5.

[41] Geographical distributions of the greenhouse gas forcings are shown in Figure 8, along with the surface air temperature response to the forcings. The spatial patterns of the responses to the well-mixed GHGs are remarkably similar when normalized by F_s , the global mean fixed sea surface forcing. The spatial responses are discussed in section 4 and the global mean efficacies in section 5.

3.1.3. Stratospheric Water Vapor

[42] The direct climate forcing by CH_4 is second only to CO_2 among the well-mixed anthropogenic greenhouse gases. In addition, if CH_4 increases, so too does stratospheric H_2O and tropospheric O_3 . These well-established indirect effects contribute to the total efficacy of CH_4 as a climate forcing.

[43] Figure 9a shows the production rate of H_2O from CH_4 oxidation in our climate model for tropospheric CH_4 abundance 1740 ppbv, based on the two-dimensional model of Fleming *et al.* [1999]. The H_2O production rate is scaled linearly with atmospheric CH_4 abundance. We assume a two-year lag between surface CH_4 change and the CH_4 perturbation that affects stratospheric H_2O production. We use the surface CH_4 chronology in Table 1 of Hansen and Sato [2004].

[44] Figure 9b shows observed stratospheric H_2O based on satellite observations [Randel *et al.*, 2001]. The simulated stratospheric H_2O in the 1880 control runs is shown in

Figures 9c and 9d, for the fixed sea surface model and the coupled atmosphere-ocean model, respectively.

[45] We carry out a series of simulations with the ocean A (fixed SST) and ocean C (coupled atmosphere-ocean) models to examine individually the effects on stratospheric H_2O of CH_4 oxidation, other climate forcings with SST fixed, and tropospheric climate change. Climate forcings such as CO_2 and O_3 alter the temperature profile in the stratosphere in addition to changing tropospheric climate. By means of the fixed SST runs we can separate the effect of these forcings on H_2O via stratospheric temperature change from the effect via tropospheric warming.

[46] Conclusions about stratospheric H_2O based on the present model are limited, because of the model's crude vertical resolution (Figure 1) in the region of the tropical tropopause, i.e., the “cold-trap” that is believed to limit transport of water into the stratosphere. Although, as a result, the changes in water vapor transport into the stratosphere as a function of climate forcings may not be accurate, it is useful to record our present results for comparison with later higher resolution studies.

[47] The second row in Figure 9 shows the atmospheric H_2O in years 11–100 of fixed SST runs with no CH_4 oxidation, with CH_4 oxidation of 2000, with “all forcings” of 2000 including CH_4 oxidation, and with “all forcings” plus 1990s SST. The third row in Figure 9 shows the impact on atmospheric H_2O of each of these changes. The fourth row in Figure 9 shows atmospheric H_2O in two experiments with the coupled model and resulting changes of H_2O relative to appropriate controls. The first experiment has only the forcing of the 1880–2000 CH_4 -derived H_2O and the second experiment has “all forcings” for 2000. “All forcings” refers to the year 2000 forcings defined specifically in section 4.2, with the predominant forcings being greenhouse gases and aerosols.

[48] Several conclusions can be gleaned from comparisons of these runs with each other and with observations. The H_2O abundance in the cold-trap region, i.e., at low latitudes just above the tropopause, is similar to the abundance that would exist throughout the stratosphere if there

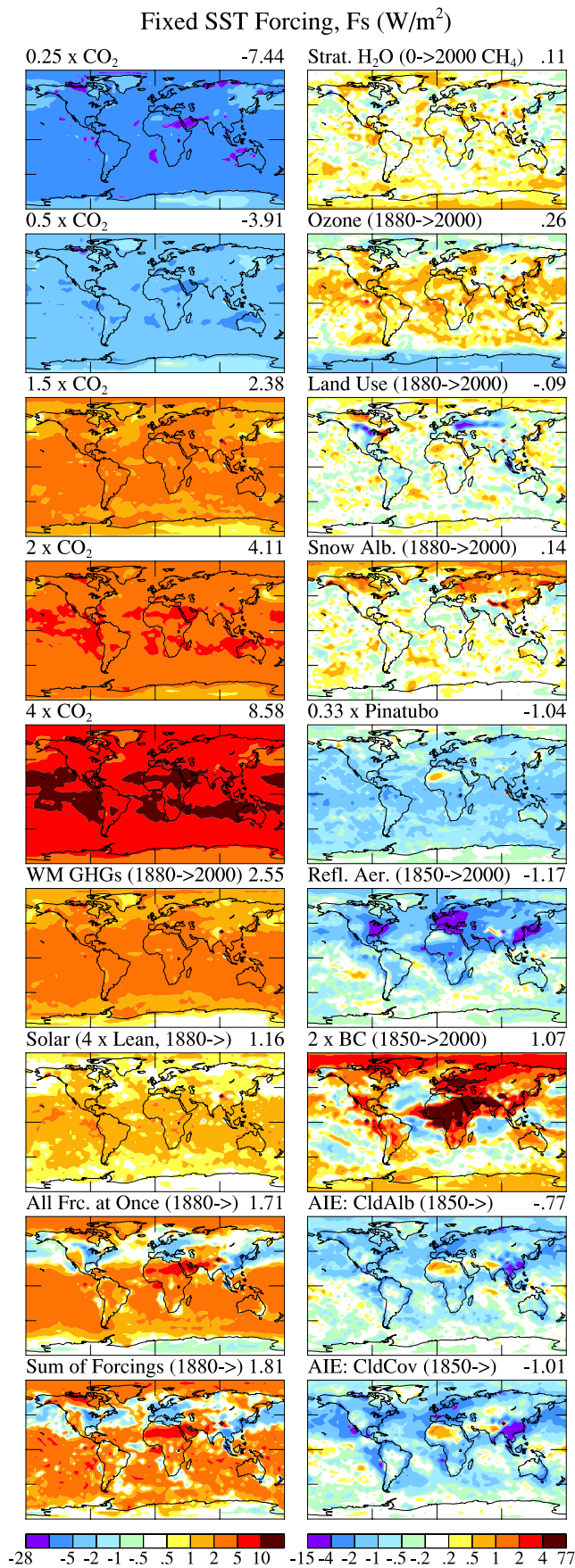


Figure 7. Fixed SST forcings, F_s , for specified CO₂ changes and other forcing mechanisms (section 3).

were no CH₄ oxidation (Figure 9e). This is consistent with the simple Brewer-Dobson picture of the mean circulation in the stratosphere, with rising air at low latitudes and sinking at the poles, as shown by the model's stream function in section 4. H₂O produced in the tropical middle stratosphere (Figure 9a) is carried upward and poleward by the Brewer-Dobson circulation. Descending motion at the poles carries H₂O-richer air downward, but the equilibrium distribution of H₂O at high latitudes in the lower stratosphere is less than that in the air descending from the middle stratosphere, probably because of horizontal mixing of air in the lower stratosphere. There is also vapor condensation during winter cooling, but this is a small term in the water budget and the condensate usually evaporates rather quickly. The formation and sedimentation of polar stratospheric cloud particles, which act as a sink of water vapor in the winter stratosphere, is not included in the model.

[49] One implication of these simulations is that the CH₄ indirect climate forcing via oxidation to stratospheric H₂O is small. It is difficult to compute F_i or F_a due to CH₄-derived H₂O, because we do not have an easy way to compute the H₂O change without including some feedback effects. We obtain the H₂O distribution by inserting the CH₄ source function into the climate model, allowing the model to determine a new H₂O distribution including the CH₄ source function. This is done with fixed SST and SI, so the resulting radiative flux change is F_s . The resulting F_s is small, 0.11 and 0.06 W/m^2 , for the CH₄ changes to 2000 CH₄ from zero CH₄ and from 1880 CH₄, respectively. The forcing is small because the H₂O increase near the tropopause is small (Figures 9i and 9j).

[50] The small CH₄-derived forcing contrasts with much larger estimates of the empirical H₂O “forcing” that would be obtained based on observed H₂O changes [Forster and Shine, 1999; Oinas et al., 2001; Smith et al., 2001], which are as large as 0.12–0.20 W/m^2 per decade. However, as those authors note, the observed H₂O change includes feedback effects as well as CH₄-derived H₂O change. Our simulations show that CH₄ oxidation contributes little to increase of H₂O near the tropopause, where H₂O is a very effective climate forcing [Lacis et al., 1990; RFCR; Forster and Shine, 2002]. CH₄ oxidation causes a large increase in upper stratospheric H₂O, but H₂O increase there does not yield much forcing because that region, which is convectively stable and optically thin, is not tightly coupled with the troposphere.

[51] Another implication of the simulations summarized in Figure 9 is that there is no apparent need for a source of stratospheric H₂O other than CH₄ oxidation and tropospheric warming. Stratospheric H₂O observations have been interpreted as increasing at a rate twice that expected from CH₄ oxidation alone [Rosenlof et al., 2001], but our simulations suggest that CH₄-derived H₂O plus tropospheric warming can account for observed levels of stratospheric H₂O (Figure 9b). These two sources yield stratospheric H₂O much larger than the uniform ~ 3 ppmv that would exist in the absence of either source (Figure 9e). Indeed, the simulated H₂O for the 1990s (Figures 9h and 9o) is somewhat larger than observed. This excess may not be significant; it could arise from (1) the fact that we include no photo-destruction of H₂O in the upper atmosphere, which is a small sink, (2) a too slow removal of strato-

Greenhouse Gas Forcings and Surface Temperature Response

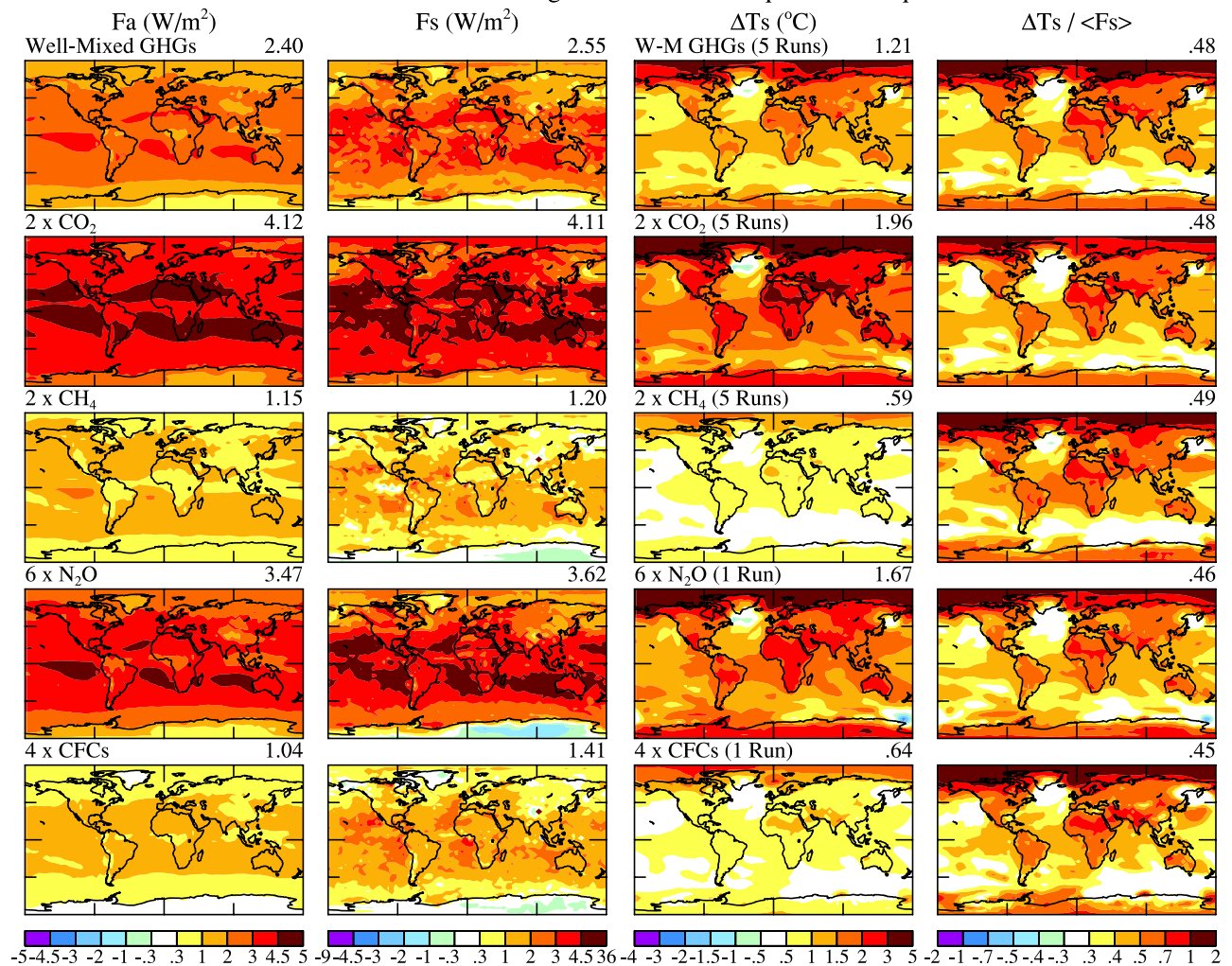


Figure 8. Climate forcings F_a and F_s for various changes of greenhouse gases, 81–120 year surface air temperature response (ΔT_s), and the normalized response ($\Delta T_s / \langle F_s \rangle$), where $\langle F_s \rangle$ is the global mean. $2 \times \text{CO}_2$ is doubling of the 1880 amount (291 ppm). $2 \times \text{CH}_4$ refers to a doubling of the 2000 CH_4 amount, as specified in Table 1, and the N_2O and CFC changes have analogous meanings (see Table 1). Well-mixed GHGs are the 1880–2000 change including trace gases [Hansen and Sato, 2004].

spheric H_2O via the model's Brewer-Dobson circulation at the polar winter sinks, (3) a too large source specification (Figure 9a), or (4) excessive input of tropospheric H_2O through the cold-trap.

[52] Figure 9p shows explicitly that the contribution of tropospheric climate change to the H_2O amount in the middle and upper stratosphere is small, less than 0.2 ppm. On the other hand, tropospheric climate change contributes substantially to the H_2O increase in the lower stratosphere (Figure 9p) near the tropopause, much more than the CH_4 -derived H_2O , the latter being shown in Figures 9i, 9j, 9k, and 9n.

[53] The efficacy of CH_4 -derived stratospheric H_2O is difficult to evaluate accurately, because the forcing is so small. However, because it is small, its precise value is not very important. From a 5-run ensemble of simulations we find that E_s does not differ significantly from unity, $E_s = 0.96 \pm 0.31$ for the 1880–2000 CH_4 change (Table 1).

3.1.4. Ozone

[54] O_3 change of the past century includes both a long-term tropospheric O_3 increase due mainly to human-made increases of CH_4 , NO_x (nitrogen oxides), CO (carbon monoxide), and VOCs (volatile organic compounds), and stratospheric O_3 depletion during the past few decades due to human-made Cl and Br compounds (halogens). However, the effects of tropospheric air pollution and ozone depleting halogens are not isolated, respectively, to the troposphere and stratosphere. For example, it is apparent that O_3 depletion at the South Pole extends all the way to the surface. O_3 depletion due to halogens must extend more generally into the troposphere, because a significant fraction of tropospheric O_3 originates in the stratosphere. However, this effect may be small because the photochemical adjustment time for tropospheric ozone is short in regions with substantial sunlight, so changes of input from the stratosphere may have little impact (the system is highly buffered).

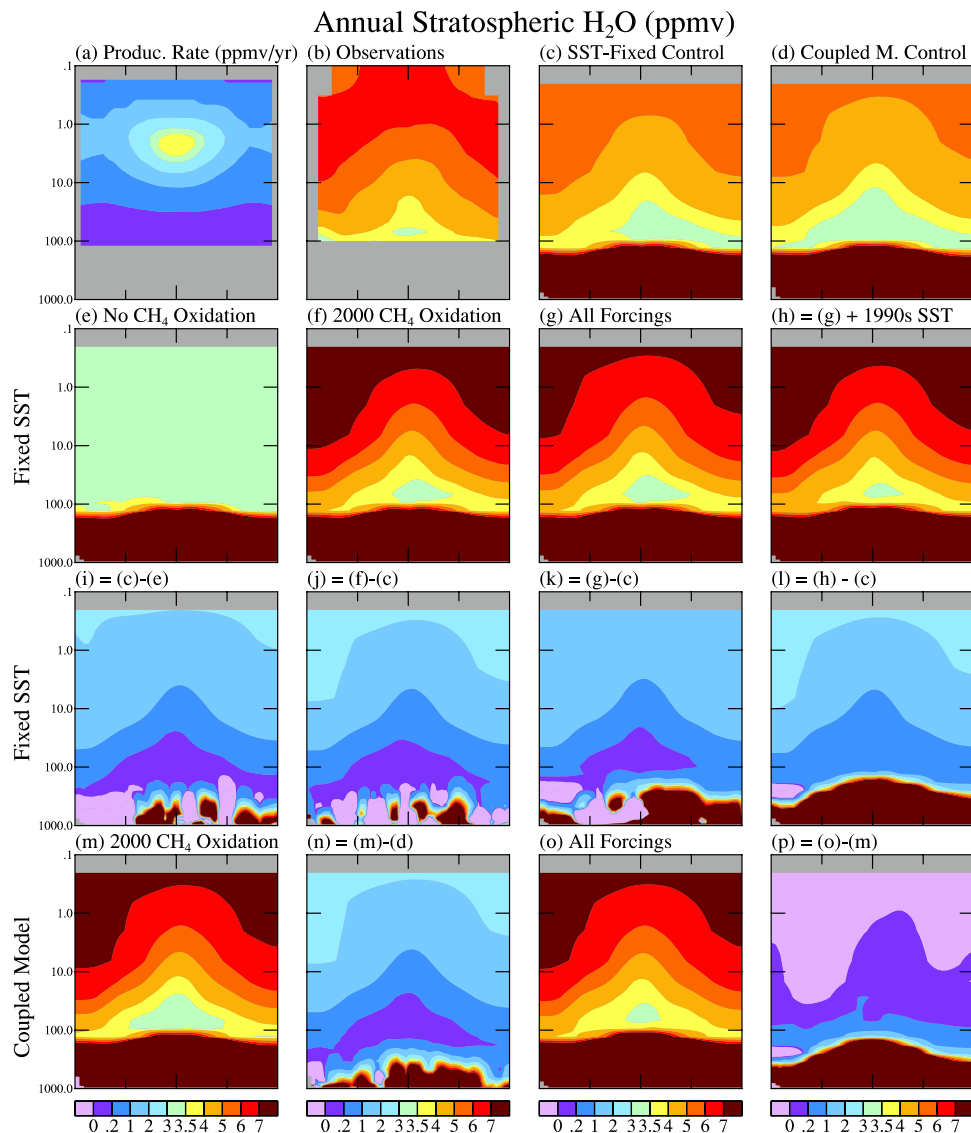


Figure 9. (a) Annual stratospheric H₂O production rate for tropospheric CH₄ abundance of 1740 ppbv based on two-dimensional model of *Fleming et al.* [1999], (b) observed H₂O [*Randel et al.*, 2001], (c) Fs control run with 1880 atmosphere and fixed sea surface, (d) coupled model control run with 1880 atmosphere, (e, f, g, h) Fs runs with no CH₄-derived H₂O, 2000 CH₄-derived H₂O, “all forcings” (see text), and all forcings plus 1990s SSTs, (i, j, k, l), differences showing the effect on H₂O of the four Fs simulations, (m) H₂O in years 81–120 of the coupled model driven by the single forcing due to CH₄-derived H₂O of 2000, (n) Δ H₂O in (m) relative to 1880 control run, (o) H₂O in the coupled model driven by all 1880–2000 forcings, and (p) Δ H₂O in Figure 9o relative to Figure 9m. Fs runs are years 11–100 mean and 120-year coupled model runs are years 81–120 mean.

[55] Preferably, for the sake of isolating the effects of different mechanisms of change, we would specify the O₃ change throughout the atmosphere due to tropospheric air pollution and separately specify the O₃ depletion throughout the atmosphere due to halogens. Such O₃ change fields were not readily available at the time of our simulations, so our experiment set-up is somewhat different than that.

[56] Our first O₃ simulation uses tropospheric O₃ change (the troposphere for this purpose is taken as extending to 150 hPa in the tropics, lowering from 150 to 200 hPa between 45 and 60° latitude, and to 290 hPa poleward of 60°) for 1880–2000 (Figure 10a) from a chemical transport

model [*Shindell et al.*, 2003a]. The chemical transport model was run for the period 1850–2000 driven by prescribed changes in ozone precursor emissions and climate conditions. This provides an estimate for the effect of tropospheric air pollution on tropospheric O₃.

[57] Our second O₃ simulation adds to this tropospheric O₃ change the stratospheric O₃ change from the observational analysis of *Randel and Wu* [1999]. Some impact of stratospheric O₃ depletion on tropospheric O₃ change is included by extrapolating O₃ trends in the Antarctic all the way to the surface and by reducing the O₃ growth rates in the Arctic troposphere region (Figure 10b).

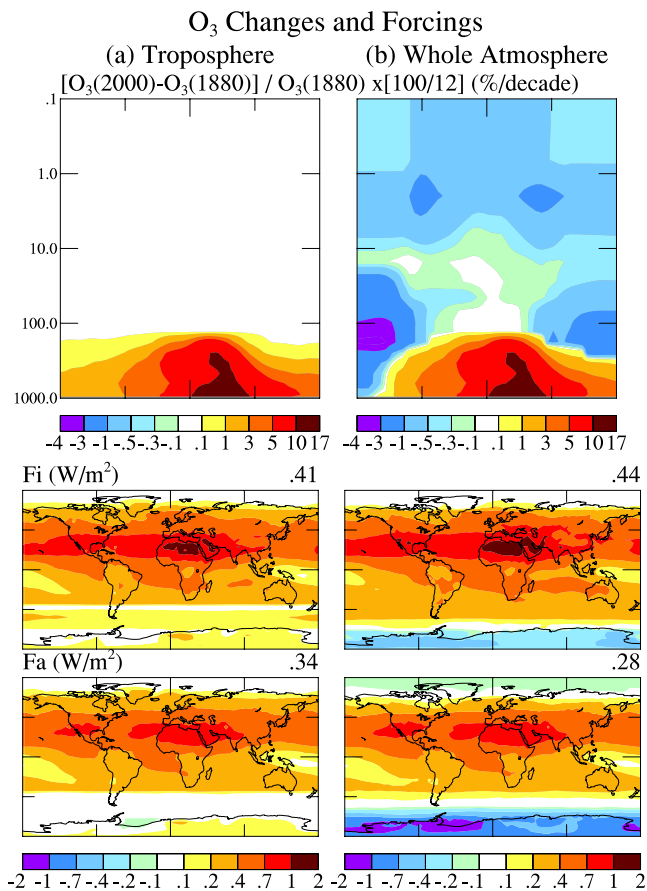


Figure 10. (a) Tropospheric O₃ and (b) whole atmospheric O₃ changes employed in 120-year climate simulations, and the instantaneous and adjusted forcings.

[58] This combined O₃ change may not fully account for the effects of halogen-induced stratospheric ozone depletion on the troposphere, as no changes are made to tropospheric O₃ trends outside of the polar regions. However, since the downward flux of ozone into the troposphere is largest at high latitudes during the colder half of the year, when polar ozone depletion also maximizes, we have likely captured the bulk of the stratospheric influence on tropospheric O₃ via transport. Halogen depletion of stratospheric O₃ probably reduces tropospheric O₃ to some degree at all latitudes via transport, but it may allow greater in situ production by permitting more UV flux to reach the troposphere. Hence the climate forcing and response that we obtain by subtracting cases 1 and 2 can be viewed as reasonable estimate of the actual halogen effect, though subject to these additional non-negligible uncertainties.

[59] Fi is a poor indicator of expected climate response for O₃ changes, as shown in detail in Table 3 of RFCR. Fa usually provides a better measure of the expected climate response to O₃ change, and in most cases Fa is smaller than Fi. This is the case for our tropospheric O₃ and total O₃ changes, as shown in Figure 10.

[60] The adjusted climate forcing is $F_a = 0.34 \text{ W/m}^2$ for the simulated 1880–2000 tropospheric O₃ change. This compares to a range from 0.28 to 0.43 W/m^2 and a mean 0.34 W/m^2 for 11 model studies reviewed by *Ramaswamy*

et al. [2001]. Thus our tropospheric O₃ forcing is in the middle of the range for these other models. However, our calculation is for the period 1880–2000 rather than the entire period of anthropogenic influence. If pre-1880 O₃ change were included, our forcing presumably would increase modestly.

[61] The adjusted climate forcing for the combined stratospheric and tropospheric O₃ change is $F_a = 0.28 \text{ W/m}^2$. The difference between this and the tropospheric O₃ forcing, -0.06 W/m^2 , is perhaps a lower limit on the magnitude of the O₃ forcing due to Cl/Br, for the reason given above. However, this small negative forcing due to Cl/Br should be more realistic than large negative forcings estimated several years ago [RFCR; *Forster and Shine*, 1997]. As discussed by *Forster* [1999], the earlier results were influenced by spurious satellite analyses of large O₃ depletion near the tropical tropopause. Note that the negative stratospheric O₃ forcing has much smaller numerical value than the positive CFC forcing, so the net direct plus indirect CFC forcing has substantial positive value.

[62] We find an efficacy for the standard adjusted forcing $E_a \sim 0.82 \pm 0.16$ for the tropospheric O₃ change and $E_a = 0.82 \pm 0.13$ for the total atmosphere O₃ change (Table 1). $E_a < 1$ for tropospheric O₃ agrees with results from an earlier GISS model [*Hansen*, 2002]. *Mickley et al.* [2004] obtain 30% greater increase of global surface air temperature for CO₂ than tropospheric O₃, corresponding to an efficacy of 77%. The fact that the efficacy is not too far from unity for either of our atmospheric O₃ changes is in part an accidental averaging effect, as there can be large variations of the efficacy depending on the location of the O₃ change [RFCR; *Christiansen*, 1999; *Stuber et al.*, 2005]. O₃ efficacies are discussed further in section 5.

3.2. Aerosols

3.2.1. Volcanic Aerosols

[63] Volcanic aerosols cause a large, albeit transitory, climate forcing that provides a useful test for climate models [*Hansen et al.*, 1978; *Robock*, 2000; *Soden et al.*, 2002; *Shindell et al.*, 2004; *Stenchikov et al.*, 2004] that has not yet been fully exploited. We consider here a specific volcanic eruption, that of Mt. Pinatubo in 1991, for the sake of testing the accuracy of our calculated volcanic aerosol forcing. Pinatubo aerosol properties are the most accurately measured of all volcanoes [*McCormick et al.*, 1995; *Russell et al.*, 1996].

[64] Stratospheric aerosol properties that we employ are reported in an update of the data set of *Sato et al.* [1993], which is available at <http://www.giss.nasa.gov/data/strataer> and is illustrated in Figure 3 of *Hansen et al.* [2002]. During the period of Pinatubo, the aerosol properties in the updated *Sato et al.* [1993] data set are based primarily on SAGE (Stratospheric Aerosol and Gas Experiment) satellite data [*McCormick et al.*, 1995] via the retrieval algorithm of *Lacis et al.* [2000]. Here we look at the forcing by the Pinatubo aerosols, because recent reanalysis of Earth Radiation Budget Experiment (ERBE) wide-field-of-view satellite observations [*T. Wong et al.*, 2004] provides a useful comparison.

[65] The radiation scheme in the current GISS model yields a mean forcing $F_a = -2.90 \text{ W/m}^2$ for the 12-months following Pinatubo (July 1991 to June 1992). The forcing is

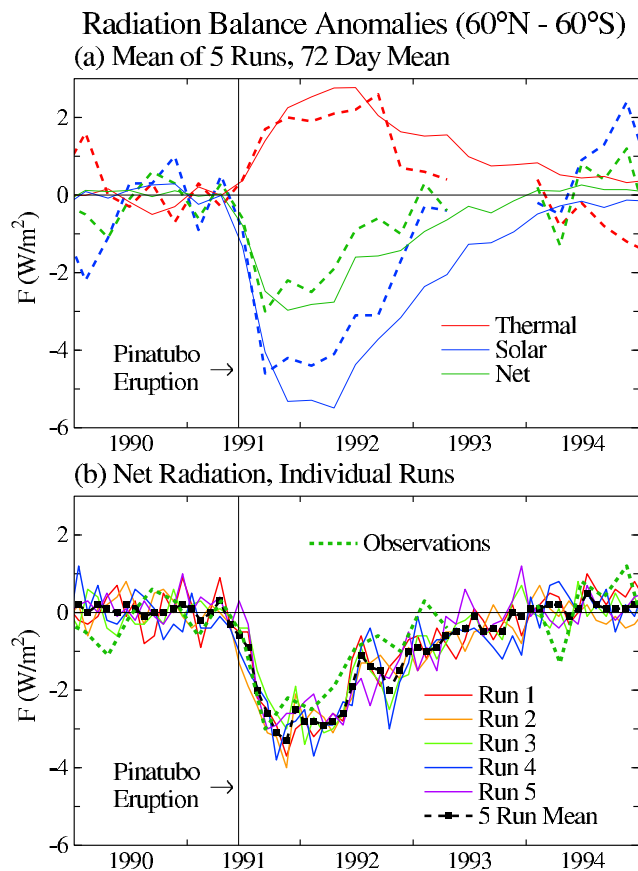


Figure 11. Comparison of top-of-the-atmosphere fluxes as simulated by the present model using the Pinatubo optical properties of Figure 3 of Hansen *et al.* [2002] and as observed by ERBE [T. Wong *et al.*, 2004]. Model (solid lines) and observations (dashed lines) refer to the latitude region 60N–60S. As in Hansen *et al.* [1996], the means for the period 1985–1989 were used to remove the seasonal cycle and anomalies are relative to the 12 months preceding the Pinatubo eruption. (a) Compares the ensemble mean simulations to observations of reflected solar radiation, emitted thermal radiation, and net radiation at the top of the atmosphere, with both observations and model at 72-day resolution. (b) Shows the variability of net radiation at monthly resolution among the five model runs.

not quite linear for optical depths as large as that of Pinatubo (0.12 at $\lambda = 0.55 \mu\text{m}$ for the 12 months following the eruption), as we find $F_a = -1.01 \text{ W/m}^2$ for optical depth one-third that of Pinatubo. The one-third Pinatubo case, for which we carry out an ensemble of 120-year climate simulations, implies an F - τ (forcing, optical depth) relation

$$F_a(\text{W/m}^2) \sim -25 \tau, \quad (2a)$$

while the full Pinatubo case yields

$$F_a(\text{W/m}^2) \sim -24 \tau. \quad (2b)$$

When we use a globally uniform distribution of aerosols with $\tau = 0.1$ and constant size distribution of effective

radius $0.51 \mu\text{m}$ and effective variance 0.35, rather than the specific geographically and temporally varying Pinatubo distributions, we obtain $F_a = -2.38 \text{ W/m}^2$, thus the same relation as above. Past versions of the GISS model have yielded values ranging from -30τ [Lacis *et al.*, 1992] to -21τ [Hansen *et al.*, 2002]. Changes in the calculated sensitivity occur because of changes in the model vertical resolution, number of spectral bands and k -distributions in the solar and thermal radiation calculations [Lacis and Oinas, 1991], method of parameterizing the integration over angles, and other factors. The present model has higher vertical and spectral resolutions than those in our prior Pinatubo calculations. We subjectively estimate the uncertainty in our current value as $\sim 15\%$.

[66] For comparison with Pinatubo observations we use the coupled model (with the Russell ocean C) driven by “all” forcings, which are summarized and tabulated in section 4 below. For the brief period around the Pinatubo eruption, the changing stratospheric aerosol forcing overwhelms changes of other forcings such as slowly increasing greenhouse gases. We include the Pinatubo comparison in this paper on forcings, because it provides the best measure of the model response to an isolated forcing. Model results for the full period 1880–2003 are included in our transient simulations carried out for IPCC [Hansen *et al.*, 2005, also manuscript in preparation, 2005].

[67] Figure 11 compares ERBE top-of-the-atmosphere radiative flux anomalies [T. Wong *et al.*, 2004] with results of the current model. The modeled solar flux anomaly peaks at about 6 W/m^2 , about 1 W/m^2 larger than observed. The modeled reduction of thermal radiation to space peaks about $1/2 \text{ W/m}^2$ larger than reported for ERBE. The net radiation anomaly, which is the forcing, peaks at about 3 W/m^2 in both the model and observations, although it averages about $1/2 \text{ W/m}^2$ larger in the model than in the observations for the calendar year 1992. ERBE measurement uncertainty is estimated at $\sim 0.4 \text{ W/m}^2$ (B. Wielicki, private communication, 2004). Figure 11b shows the variability of the calculated forcing among the five ensemble members. The real-world El Niño of 1992, not included in the climate model, may have affected the planetary radiation balance. We conclude that the modeled and observed radiation imbalance are in good agreement.

[68] Our maximum forcing of $\sim 3 \text{ W/m}^2$ for Pinatubo is smaller than the $\sim 5 \text{ W/m}^2$ obtained by Andronova *et al.* [1999]. As discussed by Hansen *et al.* [2002], we believe that SAGE data [McCormick *et al.*, 1995], retrieval analysis [Lacis *et al.*, 2000], and supporting aerosol microphysical data [Russell *et al.*, 1996] are more accurate than the data employed by Andronova *et al.* [1999].

[69] We obtain an efficacy $E_a \sim 91\%$ for Pinatubo aerosols (Table 2). Thus the F - τ relation for the effective forcing, $F_e = E_a F_a$, is

$$F_e(\text{W/m}^2) \sim -23 \tau, \quad (2c)$$

for the one-third Pinatubo optical depth, and

$$F_e(\text{W/m}^2) \sim -22 \tau, \quad (2d)$$

for the full Pinatubo optical depth.

Table 2. Clear-Sky Aerosol Optical Depths ($\lambda = 0.55 \mu\text{m}$), Global Forcings, and Efficacies for 1850–2000 Changes in GISS Model III^{ab}

Aerosols	Name	T_{control}^a	T_{exper}^a	Fi	Fa	Fa ^b	Fs	Fs ^{ab}	δT_o	ΔT_s	Ei	Ea	Es	Es*	Fe ^b
Direct Effects															
$0.33 \times \text{Pinatubo}$	E2PIN	0.000	0.040	-1.09	-1.01	-0.98	-1.04	-0.94 ± 0.23	-0.02	-0.43 ± 0.01	0.84	0.91	0.88	1.00	-0.92
Pinatubo	No Runs	0.000	0.120	-3.17	-2.90	-	-	-	-	-	-	-	-	-	-
All Trop. Aerosols	E2TRA	0.089	0.141	-0.44	-0.40	-0.36	-0.572	-0.83 ± 0.21	-0.04	-0.292 ± 0.01	1.44	1.56	1.10 ± 0.03	0.76	-0.63
	E3TRA	0.089	0.141	-0.44	-0.40	-0.36	-0.637	-0.74	-0.04	-0.318	1.57	1.70	1.08	0.92	-0.69
Reflective Aerosols	E2noBC	0.017	0.063	-1.11	-1.10	-1.09	-1.17	-0.97	-0.06	-0.55	1.06	1.08	1.01	1.22	-1.18
2($\Delta\text{BCI} + \Delta\text{BCB}$)	E2BC × 2	0.002	0.017	1.28	1.32	1.40	1.07	0.76	0.07	0.42	0.70	0.68	0.84	1.18	0.90
	E2SU × 2	0.007	0.053	-1.27	-1.26	-1.26	-1.31	-1.19	-0.08	-0.63	1.08	1.09	1.04	1.12	-1.37
	E2NO3 × 5	0.002	0.036	-1.01	-1.00	-1.00	-1.06	-0.95	-0.05	-0.48	1.03	1.04	0.98	1.06	1.04
	No Runs	0.000	0.008	-0.171	-0.134	-	-	-	-	-	-	-	-	-	-
	1 × ΔOCI	0.000	0.046	-0.171	-0.134	-	-	-	-	-	-	-	-	-	-
	6 × ΔOCI	0.000	0.046	-0.171	-0.134	-	-	-	-	-	-	-	-	-	-
	1 × ΔOCB	0.009	0.009	-0.164	-0.129	-	-	-	-	-	-	-	-	-	-
	6 × ΔOCB	0.009	0.054	-0.164	-0.129	-	-	-	-	-	-	-	-	-	-
	1 × ΔBCI	0.000	0.005	0.446	0.492	-	-	-	-	-	-	-	-	-	-
	2 × ΔBCI	0.000	0.010	0.935	0.964	1.02	0.81	0.71 ± 0.17	0.06	0.35 ± 0.03	0.81	0.78	0.93 ± 0.07	1.07	0.76
	1 × ΔBCB	0.002	0.003	0.188	0.194	-	-	-	-	-	-	-	-	-	-
	6 × ΔBCB	0.002	0.017	0.986	1.028	1.09	0.73	0.50 ± 0.10	0.00	0.27 ± 0.03	0.60	0.58	0.81 ± 0.08	1.19	0.59
	Unif. BC in layer 1	0.000	0.0125	0.45	0.44	0.45	2.01	1.96	0.22	0.97	4.72	4.74	1.05	1.07	2.10
	Unif. BC in layer 2	0.000	0.0125	0.59	0.59	0.59	1.69	1.59	0.17	0.74	2.70	2.72	0.95	1.01	1.60
	Unif. BC in layer 3	0.000	0.0125	0.93	0.93	0.93	2.02	1.87	0.14	0.92	2.12	2.14	0.98	1.06	1.98
	Unif. BC in layer 4	0.000	0.0125	1.31	1.30	1.31	0.97	0.96	0.12	0.46	0.76	0.77	1.04	1.04	1.00
	Unif. BC in layer 5	0.000	0.0125	1.53	1.51	1.52	0.64	0.74	0.08	0.30	0.42	0.43	1.02	0.87	0.65
	Unif. BC in layer 6	0.000	0.0125	1.72	1.71	1.72	0.85	0.82	0.06	0.39	0.49	0.50	1.00	1.04	0.85
	Unif. BC in layer 7	0.000	0.0125	2.00	1.98	1.99	0.81	0.41	0.03	0.35	0.37	0.38	0.92	1.83	0.75
	Unif. BC in layer 8	0.000	0.0125	2.36	2.25	2.26	0.94	0.55	0.02	0.32	0.30	0.31	0.74	1.27	0.70
	2 × ΔBCI in layer 2	0.000	0.010	0.54	0.54	0.54	-	-	-	0.54	2.18	2.19	-	1.30	1.14
	2 × ΔBCI in layer 5	0.000	0.010	1.05	1.05	1.05	-	-	-	0.30	0.61	0.62	-	1.82	0.61
	6 × ΔBCB in layer 2	0.002	0.017	0.48	0.47	0.48	-	-	-	0.48	2.17	2.18	-	1.38	1.00
	6 × ΔBCB in layer 5	0.002	0.017	1.16	1.15	1.16	-	-	-	0.21	0.40	0.40	-	3.15	0.42
Sea Salt	E2noSLT	0.038	0.000	-1.16	-1.15	-1.15	-1.12	-1.19	-0.01	-0.53	0.99	1.00	1.03	0.97	-1.15
Soil Dust	E2noDST	0.030	0.000	-0.75	-0.74	-0.73	-0.71	-0.68	-0.04	-0.30	0.87	0.88	0.91	0.96	-0.65
Indirect Effects															
Direct + AIE _{CldAlb}	E3IE1	-	-	-	-	-	-1.40	-1.21	-0.08	-0.70	-	-	1.07	1.23	-1.52
AIE _{CldAlb} only	E3IE1-E3TRA	-	-	-	-	-	-0.77	-0.79	-0.04	-0.38	-	-	1.07	1.03	-0.82
Direct + AIE _{CldCov}	E3IE2	-	-	-	-	-	-1.64	-1.40	-0.08	-0.77 ± 0.03	-	-	1.01 ± 0.04	1.18	-1.65
AIE _{CldCov} only	E3IE2-E3TRA	-	-	-	-	-	-1.01	-0.87 ± 0.05	-0.05	-0.45 ± 0.04	-	-	0.97 ± 0.08	1.13	-0.98

^aAerosol optical depths are for the 1850 amount and the experiment [1850 amount + factor × (2000–1850) amount].^bFor Fa', Fs*, and Fe definitions, see footnotes a, b, and c of Table 1.

[70] The efficacy of aerosol forcings is discussed in section 5. The simulated climate response to volcanic aerosols is compared with the response to other forcings in section 4. Regarding the realism of this volcanic aerosol forcing and our climate model's ability to simulate resulting climate effects, *Shindell et al.* [2004] show that this aerosol forcing yields stratospheric warming, regional surface "winter warming," and summer continental cooling following Pinatubo consistent with observations (as obtained in other studies [*Robock*, 2000]), and in our transient simulations carried out for IPCC we show that the model response after the notorious Krakatau volcano is reasonably consistent with observations. However, with the ocean resolution in our current simulations the model would not be capable of capturing an effect of volcanic aerosols occurring via modification of El Niño dynamics such as suggested by *Mann et al.* [2005].

3.2.2. Tropospheric Aerosols

[71] Present day tropospheric aerosols in the GISS model III are described by *Schmidt et al.* [2005]. The time-variable aerosols that yield climate forcings are: sulfate, nitrate, black carbon (BC) and organic carbon (OC), with the distributions and histories of these based on simulations of *Koch et al.* [1999] and *Koch* [2001], except nitrate. "Natural" sulfate aerosols are time-independent, i.e., there is no attempt to simulate possible feedbacks of climate change on the sulfur cycle [*Lovelock et al.*, 1972; *Shaw*, 1983, 1987]. Present-day nitrate is from *Liao et al.* [2004], with nitrate at earlier times reduced in proportion to global population. BC and OC are subdivided into two source distributions: fossil fuels and biomass burning, the latter including agricultural fires, primarily in the tropics, and forest fires that are more widely distributed especially in Asia and North America. Aerosols from biofuels are not included. OC emissions are taken as proportional to BC emissions, with the OM/BC mass ratio being 4 for fossil fuels and 7.9 for biomass burning, where OM is organic matter and it is assumed that $OM = 1.3 \times OC$ [*Koch*, 2001].

[72] The aerosols are approximated as externally mixed for radiative calculations. Absorption by BC was increased a factor of two over that calculated for external mixing to approximate enhancement of absorption that accompanies realistic internal mixing of BC with other aerosol compositions [*Chylek et al.*, 1995; *Schnaiter et al.*, 2005]. The BC and OC masses from the *Koch* [2001] simulations were multiplied by factors 1.9 and 1.6, respectively, to obtain best correspondence with multispectral AERONET observations [*Sato et al.*, 2003]. The GISS model includes the effect of humidity on sulfate, nitrate and OC aerosol sizes [*Schmidt et al.*, 2005; A. A. Lacis, http://gacp.giss.nasa.gov/data_sets/lacis/database.html], which substantially increases the aerosol optical depths and radiative forcings. Resulting aerosol optical depths and forcings are listed in Table 2. Forcings by individual aerosol compositions are small, so it would require a large number of climate simulations to obtain a good signal/noise ratio in the climate response. Thus we increased the 1880–2000 change of individual aerosols by a factor such that the resulting forcing is of the order of 1 W/m^2 . A forcing of 1 W/m^2 is small enough that the climate response should be close to linear with aerosol amount, as we verified empirically. Figure 12 and Table 2

give individual aerosol forcings and simulated 100-year surface temperature responses.

[73] The efficacies for the direct aerosol forcings range from $E_a = 58\%$ for BC from biomass burning to $E_a = 109\%$ for sulfate (Table 2), as discussed in section 5. These efficacies refer to spatial distributions of aerosols obtained from the GISS tracer transport model. Biomass burning causes local cooling in the tropical Africa region of burning, and even E_s , the global efficacy relative to F_s , is significantly less than unity (0.81 ± 0.08) for BC aerosols from biomass burning.

[74] When all tropospheric aerosols, BC plus the several reflective aerosols, are included in the same run, the climate response corresponds to an efficacy $E_a \sim 160\%$. This is an expected result, reflecting the fact that the BC efficacy is significantly less than unity. If positive and negative aerosol forcings are combined, the net forcing can be small and the resulting efficacy of the net forcing can take on almost any value, as found in RFCR.

[75] The efficacy of BC aerosols is very sensitive to their vertical distribution, varying from more than 100% for BC in the planetary boundary layer to 30–50% for BC in the upper troposphere. Experiments in which the BC aerosols are placed at different heights in the atmosphere, included in Table 2, are discussed in section 6. The quantitative results depend upon the realism of the cloud modeling.

[76] The spatial pattern of the global thermal response to aerosol forcings has a high degree of similarity among different aerosols, when the response is normalized by the global mean forcing (fourth column of Figure 12). Of course there is some local response to regional aerosol concentrations, such as cooling under the biomass aerosols in central Africa, yet there is substantial global coherence in the response to various forcings.

3.3. Clouds

[77] Clouds affect the amount of sunlight absorbed by the Earth and terrestrial radiation to space. Even small imposed cloud changes can be a large climate forcing. Cloud changes due to human aerosol and gaseous emissions or natural forcings such as volcanic emissions and incoming cosmic rays are difficult to quantify because of the large natural variability of clouds, cloud feedbacks on climate that occur simultaneously with imposed cloud changes, and imprecise knowledge of the driving human and natural climate forcing agents.

[78] Knowledge of imposed cloud changes could be advanced via precise composition-specific global monitoring of aerosols and cloud microphysical properties [*Mishchenko et al.*, 2004] supplemented by appropriate field campaigns, cloud modeling, and laboratory studies [*Lohmann and Feichter*, 2005]. In the meantime, cloud forcings in climate models are probably best viewed as sensitivity studies. Various observational constraints allow rationalization of the overall magnitude of assumed cloud forcings, but these constraints are imprecise and their interpretations are debatable. Nevertheless, if the relationships employed for the spatial and temporal distribution of the cloud forcing have justification, it may be possible to draw meaningful conclusions. Furthermore, there is one cloud forcing, the production of contrails by aircraft, with useful cloud change observations.

Tropospheric Aerosol Forcings and Surface Temperature Response

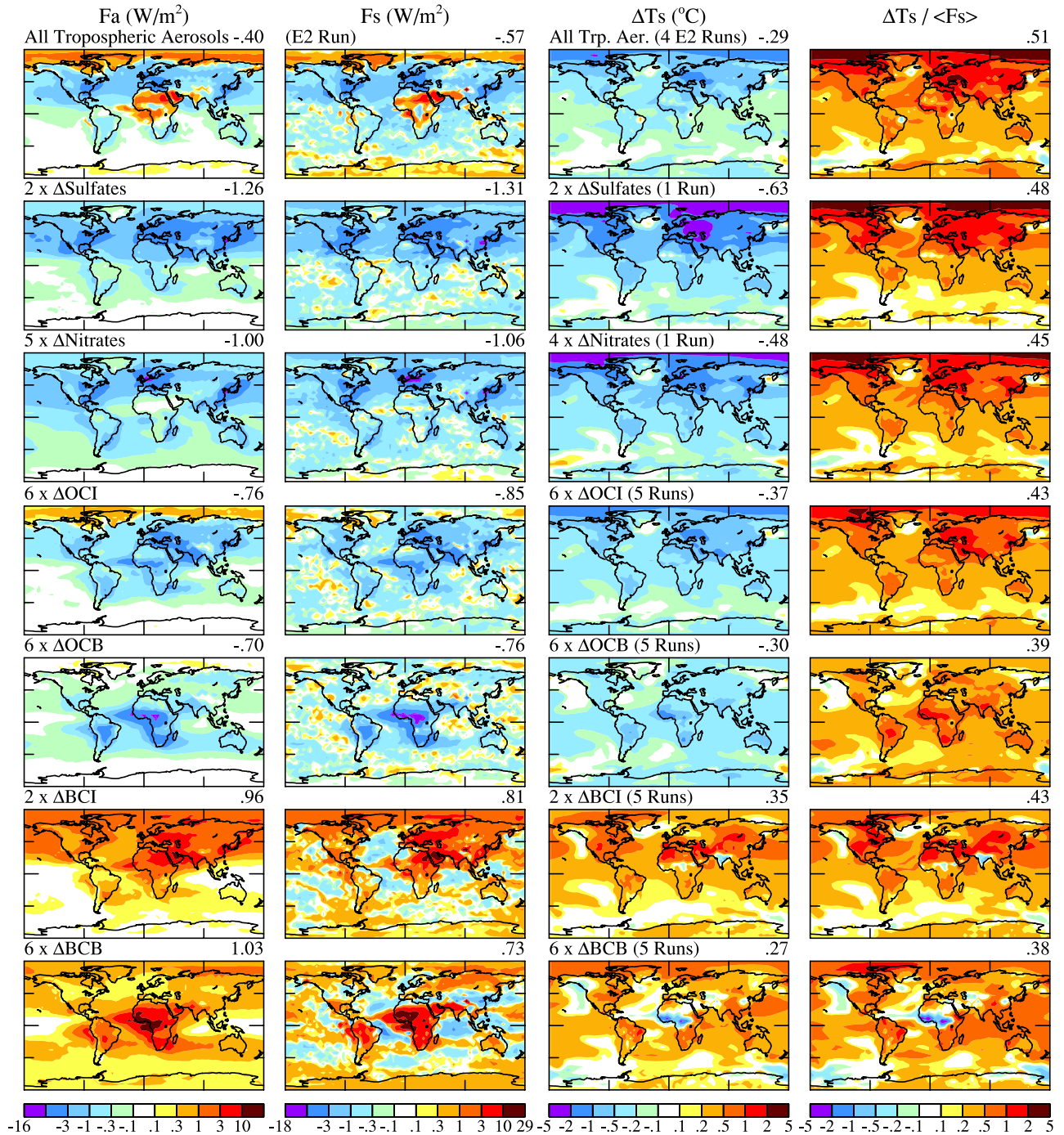


Figure 12. Tropospheric aerosol forcings for 1850–2000, 100-year surface air temperature response (mean for years 81–120), and this response normalized by the global mean $\langle Fs \rangle$, in the GISS coupled climate model (ocean C). Changes of individual tropospheric aerosol amounts are multiplied by the indicated factors.

3.3.1. Aerosol Indirect Effects

[79] We investigate the efficacies of the aerosol indirect effects, AIE_{CldAlb} and AIE_{CldCvr} , via parameterizations that are included as options in model III. We define AIE_{CldAlb} and AIE_{CldCvr} as the change in cloud albedo and the change in cloud area, respectively, due to an imposed change of aerosol amount. The effect of a change in aerosol absorption

is book-kept separately as the semi-direct effect (RFCR). Thus AIE_{CldAlb} includes the *Twomey* [1977] effect of increased cloud albedo due to an imposed increase of cloud condensation nuclei with resulting smaller cloud droplets and larger cloud optical depth, and AIE_{CldCvr} includes the *Albrecht* [1989] effect of increased cloud cover due to an imposed increase of cloud condensation nuclei with result-

ing smaller cloud drops, reduced precipitation, and increased cloud lifetime. Our AIE_{CldAlb} and AIE_{CldCvr} , however, do not refer to specific mechanisms, but rather to the net effect of added aerosols. AIE_{CldAlb} and AIE_{CldCvr} so defined are observable as changes of cloud albedo per unit cloud area and changes of cloud cover, respectively. We argue below that empirical data suggest AIE_{CldCvr} to be the dominant aerosol indirect effect.

[80] We assume that the climatically most important aerosol indirect effects are those that alter low clouds, because changes of low clouds cause the largest forcing and because anthropogenic aerosols are abundant in the lower atmosphere. Thus our parameterization is developed for clouds beneath the 720 hPa level. However, there may be other significant aerosol indirect effects; for example, *Lohmann* [2002] suggests that soot particles act as ice nuclei posing a “glaciation indirect effect” that increases precipitation from midlevel clouds and tends to reduce the magnitude of AIE_{CldCvr} at those levels.

[81] Empirical data support the reality of aerosol indirect effects, but *IPCC* [2001] could conclude only that the indirect effect was potentially larger than anthropogenic CO_2 forcing, but opposite in sign and too poorly understood to assign a quantitative value. Cloud-resolving models [*Ackerman et al.*, 2004] suggest that the increase of cloud water content due to aerosols may be less than portrayed in global models that yield large aerosol indirect effects, which would reduce AIE_{CldAlb} but not necessarily AIE_{CldCvr} . Part of the difficulty in modeling AIE_{CldAlb} and AIE_{CldCvr} from first principles is the fact that modeling of clouds themselves, and the climate producing them, is still crude. Also, aerosols, rather than being neat externally mixed compositions, include messy composites that are difficult to simulate.

[82] Understanding of aerosol indirect effects will require more realistic modeling and high precision global observations. Aerosol-cloud modeling needs to be interactive with the simulated climate. Such modeling is being pursued at GISS [*Menon et al.*, 2002a; *Menon and Del Genio*, 2005] and other laboratories. Here we use a parameterization of aerosol indirect effects for low-level warm stratiform clouds, based in part on more complete aerosol-cloud modeling, with the hope of learning something from numerical experimentation.

[83] The parameterization is via empirical effects of aerosols on cloud droplet number concentration (CDNC) [*Menon and Del Genio*, 2005]. We include four time-variable aerosols: sulfate (S), nitrate (N), black carbon (BC), and organic carbon (OC), with the distributions and histories of each of these based on simulations of *Koch et al.* [1999] and *Koch* [2001]. We multiply cloud cover (C_c) and optical depth (C_d), computed by the climate model without aerosol indirect effects, by the factors

$$C_c : 1 + C_2 \times \Delta CDNC \times V_f$$

$$C_d : 1 + C_1 \times \Delta CDNC \times V_f$$

C_1 and C_2 are constants, $\Delta CDNC$ is the change of cloud droplet number concentration due to added aerosols (relative to the control run for 1850), and V_f specifies the apportionment of CDNC (and thus cloud cover change) among model layers.

[84] Thus C_1 and C_2 determine the magnitude of the two aerosol indirect effects, $\Delta CDNC$ determines the geographical distribution and temporal variations, and V_f determines the vertical distribution. V_f was obtained from interactive aerosol-cloud simulations of *Menon and Del Genio* [2005]. Specifically, we distribute the cloud cover and optical depth changes vertically among the lowest six model layers in proportions, starting from the lowest layer, 0.35, 0.20, 0.10, 0.17, 0.10, and 0.08.

[85] $\Delta CDNC$ is computed from the number of added aerosols in the region of low clouds in the GISS model, i.e., at altitudes below the 720 hPa level, which comprises the lowest six layers in the GISS 20-layer model. $\Delta CDNC$ is obtained by computing CDNC for the control run and experiment aerosol distributions, using in both cases the empirical result from *Gultepe and Isaac* [1999]

$$CDNC = \begin{matrix} 162 \times \log_{10}(N_a) - 273 & \text{ocean} \\ 298 \times \log_{10}(N_a) - 595 & \text{land} \end{matrix} \quad (3)$$

N_a is the number concentration of soluble aerosols (cm^{-3}),

$$N_a = \sum_i S_i N_i \quad (4)$$

for $N_i = N_{BlackCarbon}, N_{OrganicCarbon}, N_{Sulfates}, N_{SeaSalt}, N_{Nitrates}$. S_i is the soluble fraction of aerosol N_i .

[86] Soil dust was not included because its solubility is uncertain and with the dust size distribution in our present model its contribution would be small. Active (soluble) aerosol numbers were obtained from aerosol masses with the assumption that the soluble fractions were 0.6/0.8, 0.8, 1, 1, 1, and densities were 1, 1, 1.77, 2, and 1.7 g/cm^3 for BC, OC, sulfate, sea salt, and nitrate, respectively. The BC soluble fraction was 0.6 for industrial (fossil fuel) BC and 0.8 for outdoor biomass burning BC. Mean particle sizes were radius 0.052 μm over land and 0.085 μm over ocean for all particles except sea salt, whose mean radius was taken as 0.44 μm .

[87] C_1 and C_2 should be chosen to give the correct global magnitudes for the indirect effects of aerosols on cloud albedo and cloud cover. Detailed aerosol-cloud-climate models yield a wide range for the indirect effects, from very small values to several W/m^2 for aerosol changes from the preindustrial era to the present [*IPCC*, 2001]. Thus these models, by themselves, do not concur on a well-defined value for AIE. However, we can use semi-empirical constraints on the AIE, i.e., constraints deduced from observations with the aid of models, to complete candidate parameterizations of the AIE.

[88] *Hansen et al.* [1995, 1997c] use observations of changes in the amplitude of the diurnal surface air temperature cycle, in combination with global climate model simulations, to infer a non-climatic increase of low cloud cover occurring predominately over land areas. They infer $AIE \sim -1 W/m^2$ for the industrial era with most of this forcing due to an increase of low cloud cover. Satellite measurements of the polarization of sunlight reflected by clouds are used by *Lohmann and Lesins* [2002] and *Quass et al.* [2004] to constrain aerosol-cloud models. Their analyses suggest that $AIE \sim -0.85 W/m^2$, with no numerical breakdown but with AIE_{CldCvr} providing a substantial

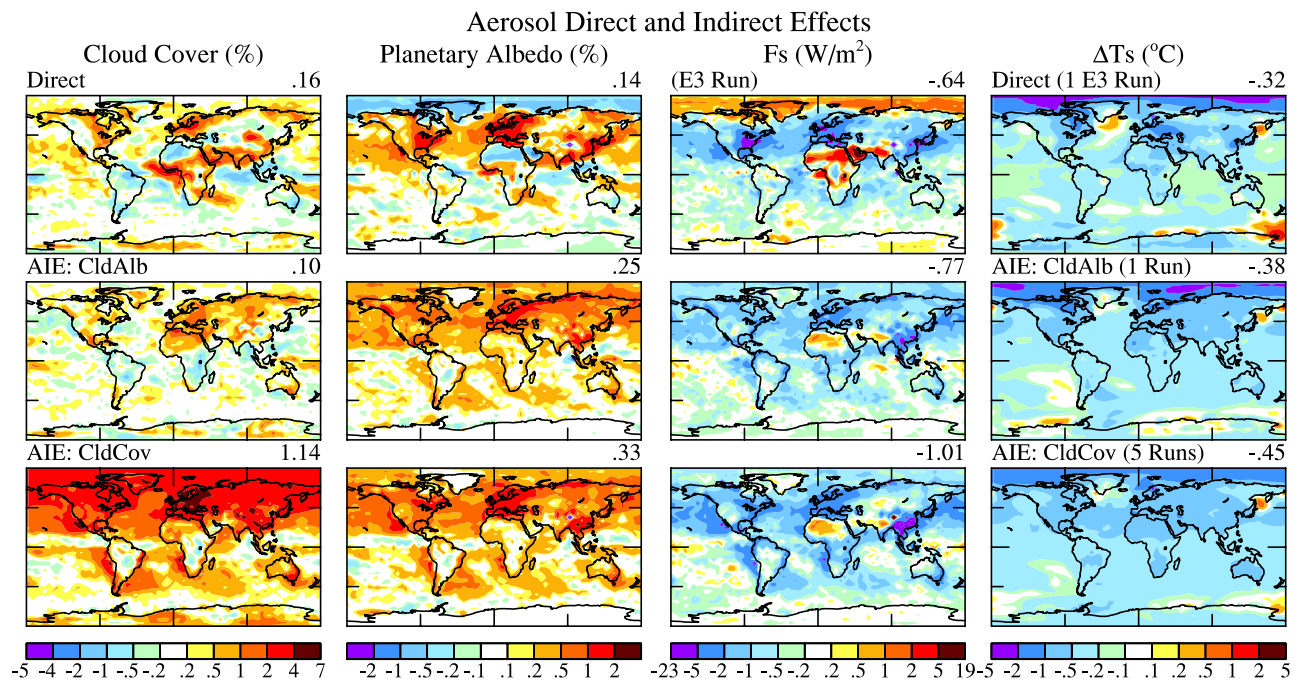


Figure 13. Changes of cloud cover, planetary albedo, and Fs in 100-year simulations with fixed SST for 1850–2000 changes of tropospheric aerosols in the GISS model (see Table 2). Changing aerosols are sulfates, nitrates, organic carbon, and black carbon. The final column is the change of surface air temperature at years 81–120 in the coupled climate model.

part of that forcing. *Kaufman et al.* [2005] use recent observations of the satellite instruments MODIS and MISR to infer that AIE probably is primarily due to AIE_{CldCvT} . Thus our first transient simulation for 1880–2003 employs $AIE_{CldCvT} \sim -1 W/m^2$ and $AIE_{CldAlb} = 0$ and in subsequent simulations we can test the impact of AIE_{CldAlb} . Our aim is to infer information in this way about both indirect effects.

[89] Based on these empirical analyses we chose values of C_1 and C_2 that would yield forcings of the order of $-1 W/m^2$. We found that $C_1 = 0.007$, $C_2 = 0$ yields a forcing $AIE_{CldAlb} \sim -0.77 W/m^2$ and $C_1 = 0$, $C_2 = 0.0036$ yields $AIE_{CldCvT} \sim -1.01 W/m^2$ for the assumed 1850–2000 aerosol changes in the GISS model (Table 2). We carried out 100-year Fs runs and 120-year coupled model runs for both of these forcings, as well as for the aerosols without either indirect effect. Figure 13 shows the resulting changes in cloud cover, planetary albedo, and net flux at the top of the atmosphere in the Fs runs, as well as the 81–120 year surface air temperature change in the coupled model runs. Cloud cover increase is caused mainly by AIE_{CldCvT} , although the other aerosol forcings tend to cool the atmosphere and increase cloud cover slightly. Although the forcings are more concentrated in regions of aerosol sources, the response of the coupled model is spread over a wider area.

[90] It would be valuable to know the portions of the indirect aerosol effect associated with each aerosol type. Many potential actions could be taken to alter aerosol emissions, and it would be useful to know beforehand which actions are most beneficial in a broad sense, including the climate effects. However, because of the complexity of aerosols, with internal and external mixtures of various compositions, our poor knowledge of aerosol source dis-

tributions, and the crude representations of aerosols in climate models, it is not possible today to do a good job of such an apportionment of the indirect effect.

[91] Nevertheless, we make an idealized apportionment here of the indirect effect among aerosol types. The main purpose is to provide a basis for discussion in section 6 about what would be needed for a more reliable evaluation. Here we treat soil dust, as well as sea salt, as a natural background aerosol, so it does not contribute to climate forcing. Although the fraction of soil dust that is of anthropogenic origin has been estimated to be as much as 20% [*Sokolik and Toon*, 1996] or even 30–50% [*Tegen and Fung*, 1995], recent studies [*Tegen et al.*, 2004] suggest that it is less than 10%. Humans also suppress soil dust emissions via irrigation and other practices, and human-induced climate change can alter soil dust emissions and atmospheric lifetime, but we have not tried to quantify any time variations of human effects on soil dust. Thus our present computation includes only sulfates, nitrates, black carbon and organic carbon as changing aerosols.

[92] We carried out climate simulations, both 120-year coupled model runs and 100-year Fs runs, in which we removed individually the indirect effect of each of the four time-variable aerosols. This was done by retaining the direct effect of all aerosols, but excluding a specific aerosol from calculation of the aerosol indirect effect on clouds. The results of such a run were then subtracted from the results of the run that included the full direct and indirect effects of all aerosols. Only the effect of aerosols on cloud cover, i.e., only AIE_{CldCvT} was included, but its forcing ($-1.01 W/m^2$) was such as to approximate our estimate for the total AIE. Our interest here is in the apportionment and spatial distribution of the indirect

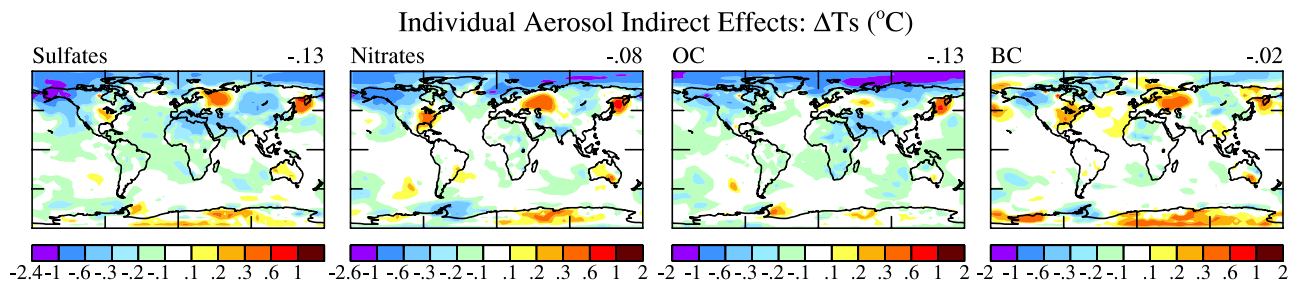


Figure 14. Effect of individual aerosol types on surface air temperature change in years 81–120 of the GISS coupled climate model III, as inferred from simulations in which the indirect effect on cloud cover of the single indicated aerosol type was removed.

effect, rather than its absolute value and division between AIE_{CldAlb} and AIE_{CldCvr} .

[93] Figure 14 shows the resulting indirect effects on surface air temperature for sulfates, nitrates, organic carbon and black carbon aerosols. Note that the sum for the four aerosol types is a cooling -0.35°C . This compares with -0.45°C global cooling due to the indirect effect of all four aerosol types included at the same time. The reason that the sum of the individual effects is smaller is saturation of the indirect effect. *Boucher and Pham* [2002] have noted that the indirect forcing saturates, i.e., it increases more slowly than linearly with increasing aerosol number. By removing the aerosol effects individually, we are treating each of the aerosols as if it were the fourth aerosol, i.e., the indirect effect of the other three aerosols is always there. This $+0.10^{\circ}\text{C}$ caused by saturation is the reason for regions of apparent warming in the United States and Europe in Figure 14.

[94] We conclude that with our external mixing approximation the aerosol indirect effect is apportioned as sulfates (36%), organic carbon (36%), nitrates (23%), black carbon (5%). There are many reasons why this apportionment

based on external mixing should be treated with caution, as discussed in section 6.

[95] We note that the tendency of the indirect aerosol effect to saturate, i.e., to be less effective as more aerosols are added, may have practical relevance. If policymakers were to hesitate in reducing aerosol pollution for the sake of retaining its cooling effect (to counter greenhouse warming), it should be pointed out that a much reduced aerosol load spread over a wide area would still produce a significant aerosol indirect effect. However, knowledge of aerosol climate effects is too crude for such recommendations, so efforts to reduce global warming now need to emphasize reduced greenhouse gas emissions.

3.3.2. Contrails

[96] Contrails produced by air traffic have become almost ubiquitous in the Northern Hemisphere, so it is natural to ask what effect they have on climate, especially since air traffic is projected to continue to increase through at least the first half of this century [*Penner et al.*, 1999]. *Minnis et al.* [2004] have compiled a comprehensive data set for observed contrail coverage in 1992 (Figure 15, upper left). This observed contrail coverage is increased by a spreading

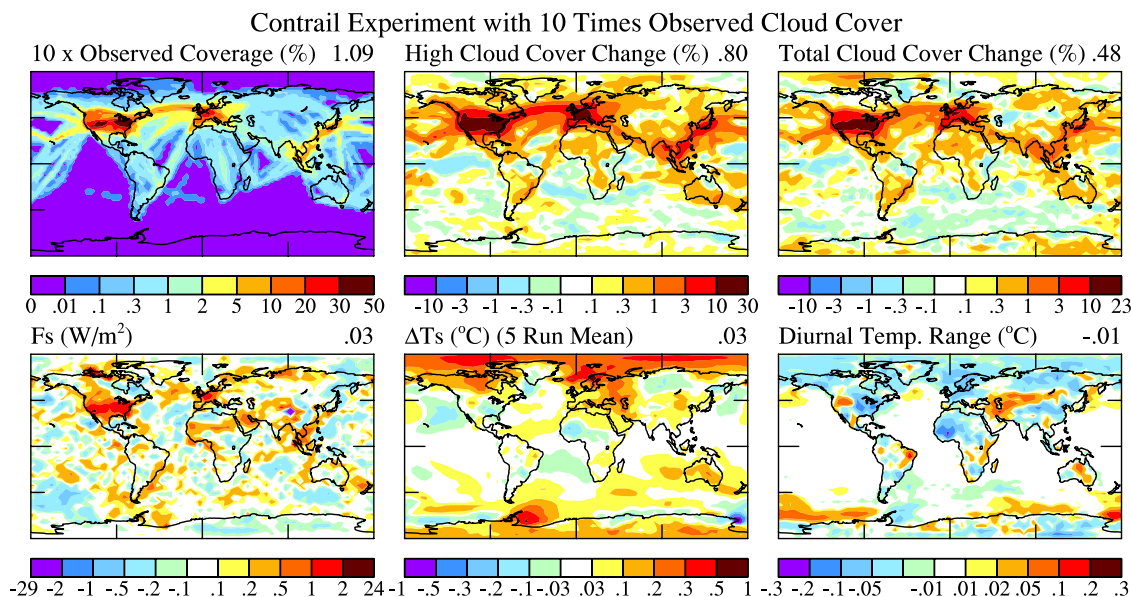


Figure 15. Observed contrail coverage in 1992 from *Minnis et al.* [2004] and simulated impact of the contrails, increased by a factor of 10, on high cloud cover, total cloud cover, F_s , surface air temperature, and the diurnal range of surface air temperature in years 81–120 of the coupled climate model.

factor to account for aging of linear contrails into natural-looking cirrus clouds and other cirrus clouds initiated by aerosols generated from aircraft exhaust [Jensen and Toon, 1994]. Minnis *et al.* [2004] estimate a spreading factor of two and use results of an equilibrium GCM simulation [Rind *et al.*, 2000], together with an assumption that the regional climate response is a function of the regional forcing, to estimate that cirrus trends over the United States caused a warming trend of 0.2–0.3°C per decade between 1975 and 1994, comparable to observed temperature change.

[97] We made climate simulations using the observed contrail coverage (Figure 15) multiplied by a factor of 10 to increase the signal/noise of the climate response. We assumed an optical depth of 0.25 and added the contrail-cirrus clouds in model layer 9 (210–285 hPa), essentially the values suggested by Minnis *et al.* [2004]. Our climate simulations included a 100-year Fs run (fixed SST) to define the climate forcing and a 5-member ensemble of 120-year coupled model runs. The cloud cover changes in the model, as seen by a ground observer or by a satellite, are reduced by overlap with clouds in other model layers. Resulting cloud cover changes are very similar in the 100-year Fs run and the 120-year coupled model run. Global high clouds increase 0.8% with maximum increase ~25% over the United States. Global total cloud cover increases about 0.5% with maximum increase ~20% over the United States. The high cloud and total cloud cover changes in the Fs run are shown in Figure 15.

[98] The resulting change in radiative flux at the top of the atmosphere in the Fs run (Figure 15) has a global mean 0.03 W/m² with a maximum of about 2 W/m² over the United States. The average global mean temperature change in years 81–120 of the ensemble of coupled model runs was 0.03°C. The global forcing is so small that we cannot define the global temperature response accurately with only five runs. The global mean temperature changes in years 81–120 were 0.011, 0.017, 0.019, 0.029, and 0.079°C in the five runs, so the standard deviation, 0.03°C, was as large as the mean temperature change. The simulated temperature change over the United States (Figure 15) is a few tenths of 1°C, which is only comparable to the standard deviation of the regional temperature change in the five control runs (section 5). Given that we used 10 times the observed contrail coverage, corresponding to an exaggeration by a factor of five if the spreading factor is two, it is clear that the effect of contrails on global and United States temperatures is very small.

[99] Our simulated climate response over the United States in 81–120 years is much smaller than even the decadal response of Minnis *et al.* [2004], even though our exaggerated contrail coverage is a factor of five larger than their assumed amount. Our calculated global radiative forcing, if reduced by a factor five, is 0.006 W/m², at the low end of the range 0.006–0.025 W/m² that they estimated. A factor of 2.5 in the estimated responses can be accounted for by the fact that they employed the equilibrium response of a climate model with high climate sensitivity, 5°C for doubled CO₂, while we use the 100-year response (1.96°C for doubled CO₂, Table 1) of a model with 2.7°C equilibrium sensitivity to doubled CO₂. Perhaps the primary reason for the difference is their assumption that the

regional climate forcing can be used to infer the regional climate response. Shine [2005] also concludes that Minnis *et al.* [2004] overestimate the effect of contrails for this reason. We do find a reduction of the amplitude of the diurnal temperature cycle in the United States (Figure 15), but, after reduction by a factor five, it is small because high clouds are relatively ineffective at influencing the diurnal cycle of Ts [Hansen *et al.*, 1995].

[100] The contrail forcing and the climate response are too small for reliable computation of the efficacy of the contrail forcing. However, in RFCR we showed, via equilibrium simulations with the Q-flux model, that high clouds have an efficacy substantially less than 100%. Ponater *et al.* [2005] examine the response of a global climate model to contrails, concluding that the effects of realistic contrail amounts on surface temperature are small with a response relative to an equal CO₂ forcing of 0.43/0.73, i.e., an efficacy ~59%.

3.4. Surface Properties

3.4.1. Land Use

[101] Changes of land-use have long been suspected of being a cause of regional and even global climate change [Sagan *et al.*, 1979; Henderson-Sellers and Gornitz, 1984], especially deforestation, which has occurred at both middle-high latitudes and in the tropics, often with forest replaced by cropland. Deforestation at high latitudes is an effective forcing, because forests with snow are darker than fields covered by snow. Hansen *et al.* [1998] calculated a global forcing of –0.21 W/m² for replacement of today’s land use pattern with natural vegetation, essentially the same as the –0.20 W/m² found by Betts [2001]. However, much of this land use change occurred prior to 1880. To examine the land use climate forcing of the past century, we have employed the time-dependent land-use data sets of Ramankutty and Foley [1999] and Klein Goldewijk [2001], finding similar climate forcings from these two data sets.

[102] Figure 7 shows the climate forcing that we obtain for the land use change between 1880 and 1990 for the land use data set of Ramankutty and Foley [1999]. The global mean forcing Fs = –0.09 W/m² includes the effects of albedo change, but also the effects on evapotranspiration of changed vegetation types. This result is consistent with the shortwave radiative forcing of –0.15 W/m² found by Matthews *et al.* [2003] for the period 1700–1992 using the same Ramankutty and Foley [1999] data set. The small land use global climate forcing that we find may not fully represent land use effects, as there are other land use activities, such as irrigation, that we have not included. Myhre and Myhre [2003] estimate a large range of uncertainty, from –0.6 to +0.5 W/m², for the land use climate forcing, with positive forcings from irrigation and human plantings. However, they conclude that the net land use forcing is probably negative. Brovkin *et al.* [2004], using a simplified climate model of unspecified sensitivity, obtain a global cooling of –0.12°C in the period 1880–2000 for the Ramankutty and Foley [1999] data set.

[103] We made an ensemble of five runs with the 1880–1990 land use change, because, unlike greenhouse gas or aerosol forcings, it is not easy to magnify the land use forcing. The ensemble-mean global-mean temperature change we find is –0.04 ± 0.02°C for years 81–120. The corresponding global efficacy is 1.02 ± 0.60. Although the

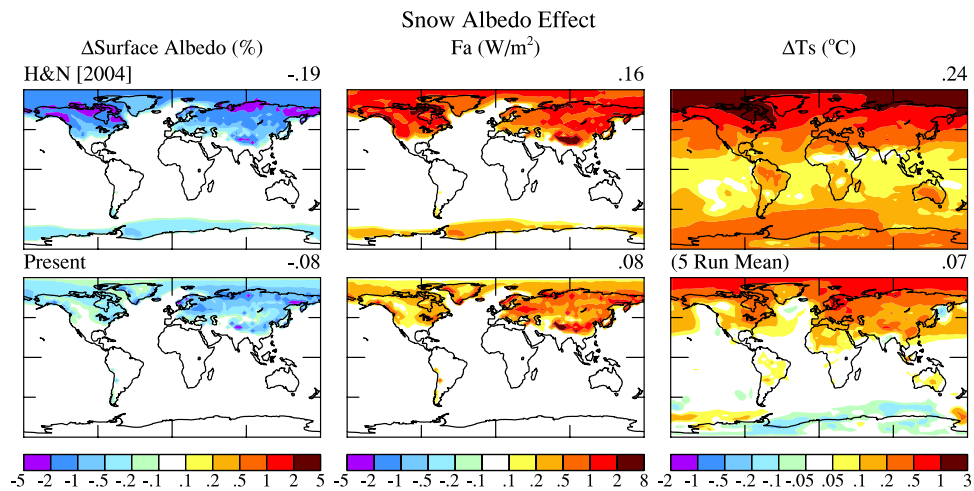


Figure 16. Geographical distributions of surface albedo changes, climate forcing F_s , and surface air temperature response in the (Q-flux model, equilibrium response) simulations of *Hansen and Nazarenko* [2004] and in our present (coupled model, 81–120 year response) simulations.

global mean climate response is small, because the global forcing is small, the regional response is readily apparent in the global map of the climate response, which is presented in section 4.

3.4.2. Snow Albedo

[104] *Clarke and Noone* [1985] measured soot in snow and ice at many locations around the Arctic in the early 1980s, finding an amount sufficient to have a significant effect on the albedo for solar radiation. *Hansen and Nazarenko* [2004] (hereinafter referred to as HN) made calculations of the climate effects assuming representative spectrally-integrated albedo changes of 1.5% in the Arctic and 3% in snow-covered Northern Hemisphere land regions, obtaining a global climate forcing of $\sim 0.16 \text{ W/m}^2$, which yielded equilibrium global warming of 0.24°C in a Q-flux model. The climate model was E037, the GISS model E as it existed in the summer of 2003, which had a sensitivity of 2.6°C for doubled CO_2 ($F_a \sim 4.1 \text{ W/m}^2$), implying a soot snow albedo efficacy $E_a \sim 236\%$.

[105] Soot effects on snow and ice albedos today are uncertain, in part because of the sparseness of measurements. There is evidence that Arctic BC pollution may have decreased in recent decades, [*Grenfell et al.*, 2002; *Sharma et al.*, 2004], probably because of decreased emissions from North America, Europe and Russia, despite an increase of emissions from the Far East. Even when the BC amount in snow is known, there is uncertainty about its effect on snow albedo, because the albedo change depends sensitively on the nature of the soot particles and how they are mixed with the snow and ice particles [*Warren and Wiscombe*, 1985; *Bohren*, 1986].

[106] Our present snow albedo specification differs from that of HN, as here we let the albedo change be proportional to the local BC deposition in the aerosol transport calculations of *Koch* [2001]. We still use a simple prescription, rather than detailed radiation calculations of soot and snow mixtures, because the latter require several arbitrary assumptions including a specification of how much soot is carried away in meltwater and how much is retained near the surface in the critical

times during and after surface melting. Application of an empirical scale factor in modeling the soot albedo effect may be justified by such considerations, but it is desirable to determine that scale factor from observations of the soot effect on snow albedo at several locations. In reality there is very little data available for soot amounts in snow and for their albedo effect.

[107] For the present calculation we chose a scale factor yielding a conservative estimate of the soot effect, with a global forcing of 0.08 W/m^2 , which is only about half as large as estimated by HN. The reason for use of a smaller scale factor is the suggestion in meager available observations that the BC in snow amounts measured by *Clarke and Noone* [1985], employed by HN, may be significantly larger than current BC amounts in the Arctic. The resulting BC albedo effect in the region of Arctic sea ice in our present model is only several tenths of 1% (Figure 16), as opposed to the 1.5% spectrally integrated (2.5% visible wavelengths) albedo change assumed by HN. The present snow albedo prescription yields an 81–120 year ensemble-mean global warming of 0.065°C and thus an efficacy of 171%.

[108] We made additional simulations to investigate the different responses of the prior model E037 and the current model III to snow albedo changes. The primary reason for the larger response in model E037 is the larger forcing assumed by HN. In addition, for the same forcing, model III yields a smaller response than model E037. Sea ice is more stable in model III than in E037, a change that is not necessarily more realistic, as simulated sea ice trends are smaller in model III and less than observed (*J. Hansen et al.*, manuscript in preparation, 2005). However, we have not studied the impact on model sensitivity of each change in model physics between E037 and model III. The larger response found by HN must be due largely to their assumed 1.5% sea ice albedo change, which contrasts with $\sim 0.4\%$ in our current snow albedo specification (Figure 16). The effectiveness of a forcing depends on its geographical distribution, and surface air temperature is especially sensitive

to sea ice cover. Thus it is important to obtain accurate measurements of the BC effect on sea ice albedo.

3.5. Solar Irradiance

[109] We carry out solar irradiance experiments of the classical sort [*Manabe and Wetherald, 1975; Wetherald and Manabe, 1975*], by altering the solar constant, as well as simulations in which the solar changes are largest at ultraviolet wavelengths in accord with observed solar variability. The latter simulations use the solar spectral changes of *Lean* [2000]. For both cases we find, in agreement with RFCR, that the direct solar forcing is less effective than an equivalent CO₂ forcing. We find $E_a \sim 92\%$ for the realistic spectral variations, as discussed in sections 4 and 5. However, we do not attempt to evaluate possible indirect effects of solar variability, such as on ozone amount, which have been suggested [*Haigh, 1994, 1999; RFCR; Shindell et al., 1999a*] to provide an enhancement of the direct solar forcing. *Shindell et al.* [2001] conclude that the ozone indirect forcing is small and its effect is primarily dynamic, not radiative.

4. Climate Model Responses

[110] The set of climate simulations carried out to investigate the efficacies of different climate forcing mechanisms provides fodder for other investigations. We compare several quantities here for the various forcings. More extensive diagnostics from these runs are available on the GISS web site.

[111] We emphasize the 100-year response (mean for years 81–120) of the coupled model runs. At that point the global mean temperature change is 0.78°C for the combination of nine forcings that we focus on. This warming is comparable to the observed global temperature increase of 0.6–0.7°C since 1880–1900, so comparisons with the real world are relevant. Bear in mind that the 100-year response to a fixed forcing can differ from the response to a gradually changing forcing. However, we would expect the transient 100-year response to fixed forcing to be much more relevant for comparison to the real world than the common equilibrium simulations with mixed layer ocean.

[112] One hundred-year Fs simulations, i.e., fixed SST runs, were made for the same forcing mechanisms as used for 120-year coupled model runs. Additional inferences can be drawn by comparing Fs and coupled model runs. It is not practical to illustrate most Fs runs here, but the diagnostics of all runs are available on the GISS web site.

4.1. Control Runs

[113] We illustrate here quantities whose sensitivities to forcings will be examined. Figures 17a and 17b show these quantities for years 11–100 of the 100-year Fs control run and for years 201–500 of the coupled model control run, respectively. Zonal mean quantities are shown only for the coupled model (Figure 17b), because the results for the Fs run appear identical.

[114] *Schmidt et al.* [2005] examine the degree of realism of the specified-SST model III in detail. Some prime deficiencies of the fixed SST version are mentioned in section 2.2 above. Comparison of Figures 17a and 17b shows that the coupled model retains about the same degree

of realism, except the ITCZ is less realistic, as shown by the precipitation patterns.

[115] Figure 17c shows the standard deviation of the quantities in Figure 17b, based on years 201–500 of the control run. The standard deviation provides a measure that helps evaluate the significance of the model response to forcings. The number on the upper right of each map is the global mean of the local standard deviation. The standard deviation of the global mean is much smaller, being 0.057°C and 0.007 mm/day, e.g., for temperature and precipitation.

[116] In interpreting the model response to forcings it is worth bearing in mind two major deficiencies of the present GISS model. One problem is the crude $4^\circ \times 5^\circ$ dynamical ocean, whose shortcomings include the absence of El Niño variability, too shallow overturning in the North Atlantic Ocean, excessive vertical mixing around Antarctica [*Liu et al., 2003*], and deepwater formation in the North West Pacific Ocean. A second deficiency is the simple representation of gravity wave effects in the stratosphere via a small constant drag coefficient. Although the stratospheric climatology is reasonably good, we cannot expect this model to yield realistic dynamical interactions between the troposphere and stratosphere. These two deficiencies are the focus of current GISS model development. We intend to repeat a subset of the present simulations with a model that has alleviated these problems.

4.2. Temperature and Precipitation Maps

[117] Figures 18 and 19 show the 100-year annual mean temperature and precipitation responses to a series of CO₂ forcings and each of the forcings used in our transient climate simulations for the 2007 IPCC report. The two panels in the lower left are the climate responses when “all forcings” are applied in the same run and the sum of the responses to the individual forcings. In Figures 18 and 19, forcings are from the year in parentheses to 2000, unless the forcing is specified explicitly. Results are 5-run ensemble means, unless specified as “1 run.” Tables 1–4 summarize the forcings, global temperature responses, and efficacies of the illustrated climate forcing mechanisms.

[118] The “all forcings” case includes the estimated forcings for the period 1880–2000. Specifically, it includes the well-mixed greenhouse gases (CO₂, CH₄, N₂O, and CFCs), CH₄-derived H₂O, O₃, land use changes, BC effects on snow albedo, direct effects of sulfate, nitrate, OC, and BC aerosols, and indirect effects of all these aerosols on clouds. The indirect aerosol effect is parameterized entirely as the cloud cover indirect effect with a forcing $F_s = -1.01 \text{ W/m}^2$ for 1850–2000 and $\sim -0.8 \text{ W/m}^2$ for 1880–2000. Volcanic aerosols are included in “all forcings” for our simulations with transient forcings, but their optical depth is zero in both 1880 and 2000 so they do not contribute to 120-year runs for fixed 1880 and 2000 forcings.

[119] The responses to CO₂ changes form a continuous sequence. The responses to negative and positive forcings are similar, but opposite in sign. Close examination reveals that there is a small asymmetry in the temperature response to positive and negative forcings, which is discussed below.

[120] Note in Figure 18 the nearly identical temperature response patterns for the $1.5 \times \text{CO}_2$ increase and the 1880–2000 increase of well-mixed greenhouse gases (GHGs). The fact that the global warming is $\sim 10\%$ larger for the GHGs

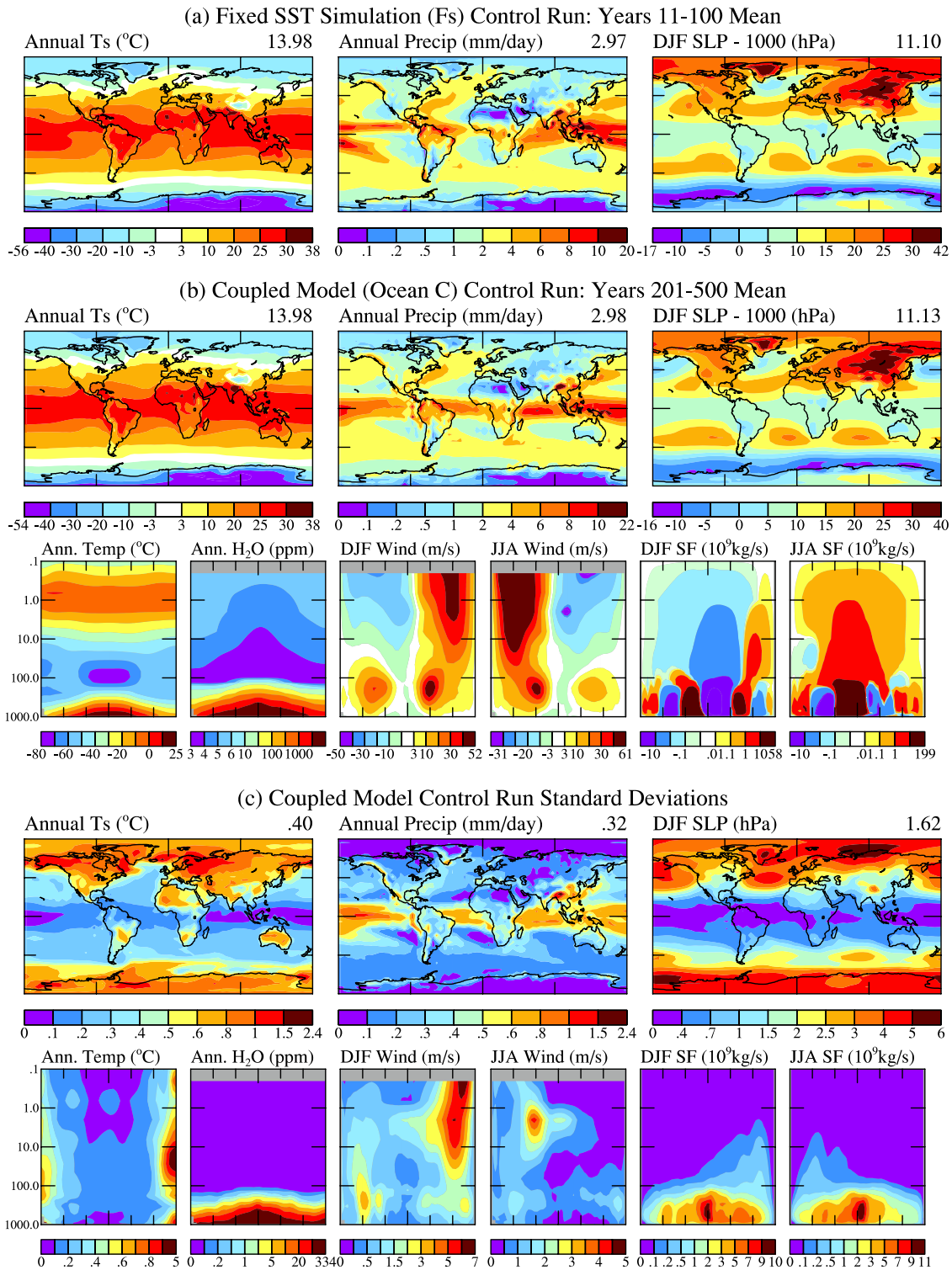


Figure 17. (a) Maps of annual surface air temperature, annual precipitation, and DJF sea level pressure for years 11–100 of fixed SST (Fs) control run, (b) the same maps plus zonal mean DJF and JJA latitude-height plots of temperature, water vapor, and stream function for years 201–500 of the coupled model III control run, and (c) standard deviations for years 201–500 of the coupled model III control run.

than for $1.5 \times \text{CO}_2$, despite their similar forcings (Fa), is a reflection of the higher efficacy of the non- CO_2 GHGs. [121] Regional climate changes simulated by the present model are not expected to be realistic, given the coarse model resolution and the inability of the coupled model to

accurately represent the ITCZ and other regional climate features. Nevertheless, meaningful statements about regional climate may be possible. As CO_2 increases, there is a robust intensification of the Hadley circulation (section 4.3), increase of rainfall in the Intertropical Convergence Zone

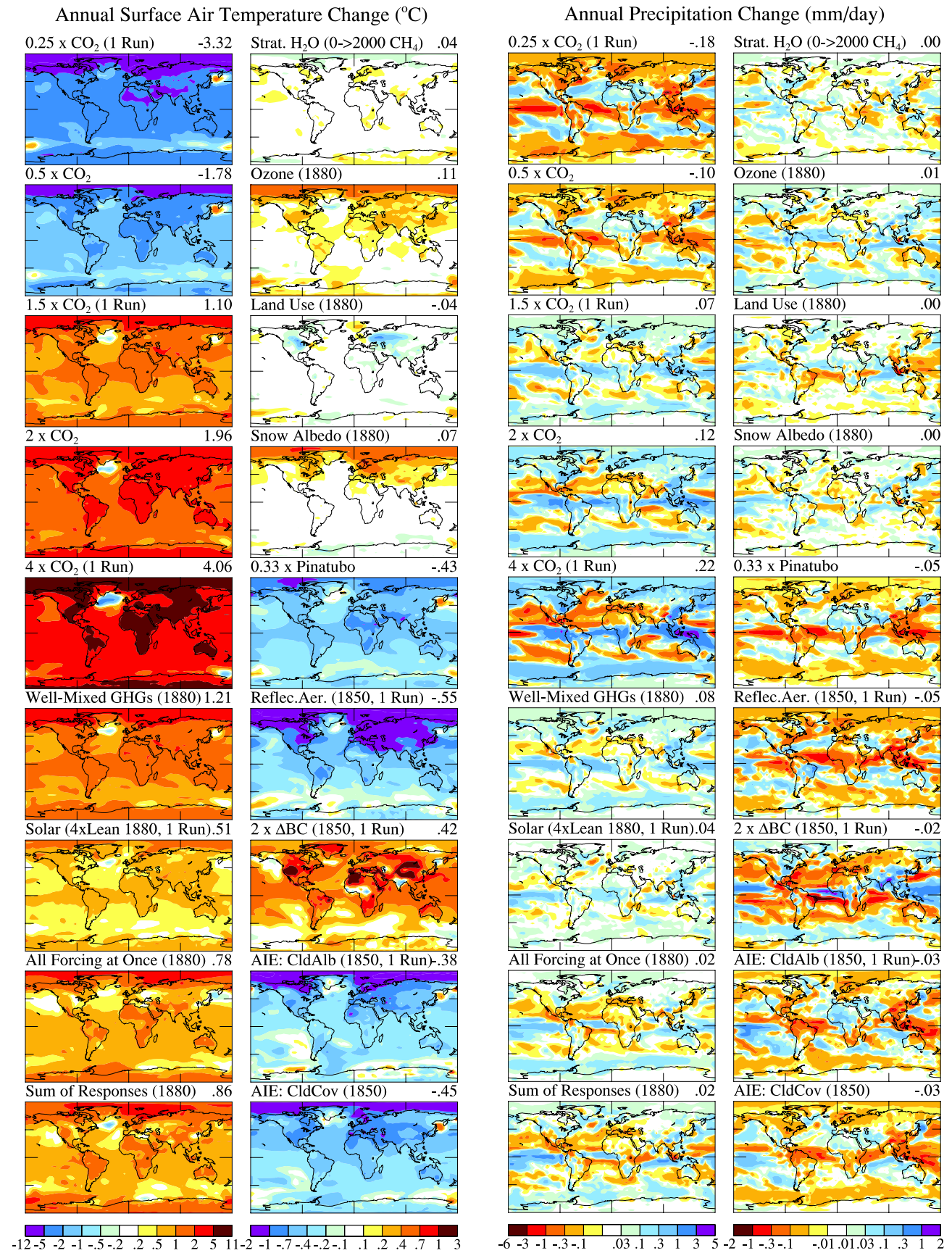


Figure 18. Temperature change in years 81–120 of coupled model simulations driven by the forcings of Figure 7.

Figure 19. Precipitation change in years 81–120 of coupled model simulations driven by the forcings of Figure 7.

(ITCZ), and intensification of dry conditions in subtropical regions including the Southwest United States, the Mediterranean region, and an expanding Sahelian region in Africa. Precipitation increases in the Eastern United States and at high latitudes in both hemispheres. These features survive in the model simulations that use all forcings of the past century. There is a suggestion of such precipitation tendencies in observations during recent decades of rapid global warming [Mitchell *et al.*, 2004].

[122] Substantial Arctic warming occurs in response to both anthropogenic ozone change and soot's snow albedo effect (Figure 18). Arctic warming occurs despite indications that sea ice cover, and thus Arctic surface air temperature, are less sensitive to forcings in the GISS model than in the real world (J. Hansen *et al.*, manuscript in preparation, 2005). Moreover, these warming contributions occur despite conservative estimates for both forcings: (1) Mickley *et al.* [2001], Shindell and Fulavegi [2002], and S. Wong *et al.* [2004], based on simulations and limited 19th century O₃ measurements, suggest that the anthropogenic tropospheric O₃ forcing might be larger than the 0.34 W/m² in our present simulations, and (2) we employ a soot albedo effect of only ~0.3–0.4 percent over Arctic sea ice (Figure 16), which compares with 1.5 percent of Hansen and Nazarenko [2004].

[123] The small soot albedo forcing (~0.25 W/m² over the Arctic Ocean) is effective because of positive feedbacks [Hansen and Nazarenko, 2004; Clarke and Noone, 1985]. Absorbed sunlight speeds snow “aging,” *i.e.*, growth of grain size, decreasing the snow albedo and hastening the first snow-melt, which darkens the albedo by tens of percent. The result is a longer snow-melt season and a greater area of open water, thus increased absorption of solar radiation by the ocean. When the Arctic Ocean refreezes in the winter, the thin single-year ice helps retain the ocean's heat while being more susceptible than multi-year ice to melting during the following summer. Thus soot may be a partial cause of reduced area and thickness of Arctic sea ice in the past half century [Rothrock *et al.*, 1999].

[124] These results imply that a strategy to reduce anthropogenic CH₄, O₃ and soot pollution could help slow Arctic climate change and minimize loss of summer sea ice as now inevitable additional global warming occurs in the 21st century [IPCC, 2001; Hansen *et al.*, 2005]. The magnitude of the soot contribution to ice loss needs to be assessed via measurements of soot content and its effect on snow albedo during spring just before the advent of the melt season.

[125] The response to “all forcings” in Figure 18 differs little from the sum of the responses to the individual forcings, the global warming being slightly larger for the sum of responses. This small non-linearity is reasonably consistent with results of Gillett *et al.* [2004] and Matthews *et al.* [2004], who found no non-linearity when combining multiple forcings, but it differs from the model of Feichter *et al.* [2004], which yielded significantly less warming for combined GHG plus aerosol forcing than for the sum of the individual responses.

[126] Some non-linearity is expected, as the efficacy of a forcing depends upon the magnitude of the forcing, and thus equal and opposite positive and negative forcings will not yield equal and opposite responses. Non-linearities arise

because the strength of climate feedbacks such as water vapor and sea ice depends upon the mean climate. In our model, *e.g.*, the efficacy increases as the mean climate warms, and thus the sum of the responses to equal positive and negative forcings is a warming. The opposite sign of the non-linearity in the model of Feichter *et al.* [2004] suggests that the efficacy of forcings in their model decreases as the magnitude of the forcing increases. This might occur, *e.g.*, if their model has a stronger sea ice feedback. These non-linearities are discussed further in section 5.1 via experiments with +2% So and –2% So forcings.

4.3. Zonal Mean Temperature and Water Vapor

[127] Figure 20 shows annual zonal mean changes of temperature and water vapor. Increasing CO₂ cools the stratosphere while warming the troposphere. Despite stratospheric cooling, H₂O increases there as CO₂ increases. The increased intensity of the Brewer-Dobson circulation (see below) increases the flux of moisture from the troposphere into the stratosphere in the tropics. Although the stratospheric climatology is realistic (Figure 17), the water vapor changes in the present model may not be accurate, because the vertical resolution near the tropopause (Figure 1) is inadequate to resolve small changes in the “cold-trap,” the minimum tropical temperature, which occurs in layer 12 at ~95 hPa in the 20-layer model. Nevertheless we record our present results for comparison with later higher resolution studies.

[128] The well-mixed GHGs increase middle stratospheric H₂O by several tenths of a ppm, which can account for a significant part of the observed stratospheric H₂O increase [Rosenlof *et al.*, 2001] despite slight cooling at the tropopause [Zhou *et al.*, 2001]. More important, from the standpoint of climate forcings, is the larger increase of H₂O near the tropopause. Substantial water vapor increase occurs well into regions of reduced temperature as can be seen from the side-by-side comparisons of ΔT and ΔQ.

[129] The case illustrated for increase of H₂O in the stratosphere due to CH₄ oxidation is for the change from no CH₄ to the CH₄ amount of 2000. The H₂O increase in this case is more than 3 ppm in the upper stratosphere. However, the H₂O change near the tropical tropopause is nearly zero. It is for this reason that the climate forcing due to CH₄-derived H₂O is small. We would not expect higher resolution near the tropopause to change this result. The stratospheric water vapor feedback due to changing tropospheric climate change may be sensitive to modeling of the cold-trap at the tropopause, but the climate forcing due to CH₄-derived stratospheric H₂O should be less sensitive to resolution of the cold-trap.

[130] The 1880–2000 O₃ change causes cooling of a few tenths of a degree in the stratosphere and warming in the troposphere. The 1880–2000 solar irradiance change, multiplied by four to yield a forcing ~1 W/m², causes substantial stratospheric warming and H₂O increase due to increased absorption of ultraviolet radiation, suggesting that solar variability could be a contributing factor in observed stratospheric water changes. The Pinatubo aerosols, divided by three to make the forcing ~1 W/m², cause warming in the tropical lower stratosphere but cooling at the poles.

Table 3. Climate Forcings, Responses, and Efficacies for Miscellaneous Forcings Tested in GISS Model III

Forcing	Run Name	Fi	Fa	Fa ^a	Fs	Fs ^{*a}	δT_o	ΔT_s	Ei	Ea	Es	Es [*]	Fe ^a
10 × Contrail	E3ACT×10	–	–	–	0.029	0.033 ± 0.05	–0.003	0.031 ± 0.028	–	–	2.34 ± 2.05	2.26	0.068
Solar Irradiance													
–20% S ₀	E2S2	–45.28	–45.87	–	–45.91	–43.20	–1.43	–26.85	1.28	1.26	1.26	1.34	–57.98
–10% S ₀	E2S1	–22.64	–22.94	–	–22.69	–22.24	–0.69	–9.51	0.91	0.90	0.91	0.92	–20.54
–5% S ₀	E2S5	–11.32	–11.47	–	–11.30	–10.85	–0.35	–4.53	0.86	0.85	0.87	0.90	–9.78
–2% S ₀	E2S0	–4.53	–4.59	–4.61	–4.51	–4.29 ± 0.18	–0.13	–1.93 ± 0.05	0.92	0.91	0.93 ± 0.02	0.97	–4.18
+2% S ₀	E2s0	4.53	4.59	4.61	4.52	4.23 ± 0.20	0.14	2.07 ± 0.02	0.99	0.97	0.99 ± 0.01	1.06	4.47
+5% S ₀	E2s5	11.32	11.47	11.51	11.11	10.45	0.33	5.31	1.01	1.00	1.03	1.10	11.47
Lean’s Change	E2SO	0.288	0.299	0.30	–	0.319	–	0.11	0.86	0.83	–	0.77	0.247
4 × Lean’s Change	E2So×4	1.15	1.19	1.20	1.16	1.10	0.04	0.51	0.95	0.92	0.95	1.00	1.10

^aFor Fa[′], Fs^{*}, and Fe definitions, see footnotes a, b, and c of Table 1.

[131] Black carbon aerosols cause warming at low levels that extends across the region of the cold-trap. As a result, BC aerosols cause a significant increase of stratospheric H₂O. Thus BC aerosols could contribute to observed increases of stratospheric H₂O, which are too large to be explained by CH₄ alone [Rosenlof *et al.*, 2001]. We note that Koch [2001] has found that the GISS tracer transport model may move an unrealistic amount of BC to high levels in the troposphere. On the other hand, recent observations of Baumgardener *et al.* [2004] find high concentrations of BC reaching into the lower stratosphere, though the measurements are at high latitudes.

[132] The response to all forcings has a cooling of more than 1°C in much of the stratosphere and ~5°C at the stratopause. Nevertheless, water vapor increases throughout the atmosphere, with the minimum increase about 0.2 ppm near the cold-trap.

[133] The warming maximum in the upper tropical troposphere is a common feature among global climate models. However, two of our forcings that contribute significantly to that warming peak are uncertain. As discussed in section 3.1.4, our ozone change specification has large ozone increase in the upper troposphere and does not account for the possibility that stratospheric O₃ depletion (albeit small at low latitudes) might somewhat mitigate the magnitude of O₃ increase near the tropical tropopause. BC aerosols also contribute to the upper tropospheric warming

in our model, but we are uncertain whether the large amount of upper tropospheric BC in our model is realistic.

4.4. Stream Function

[134] The Brewer-Dobson circulation in the stratosphere is an extension of the seasonally dominant branch of the tropospheric Hadley circulation, as shown by the stream function in the control run (Figure 17). Figure 21 shows that increased CO₂ and the 1880–2000 increase of all well-mixed GHGs cause an intensification of the mean meridional circulation in both the troposphere and stratosphere. This holds in the troposphere for both branches of Hadley cells, the indirect Ferrell cells, and the polar cells.

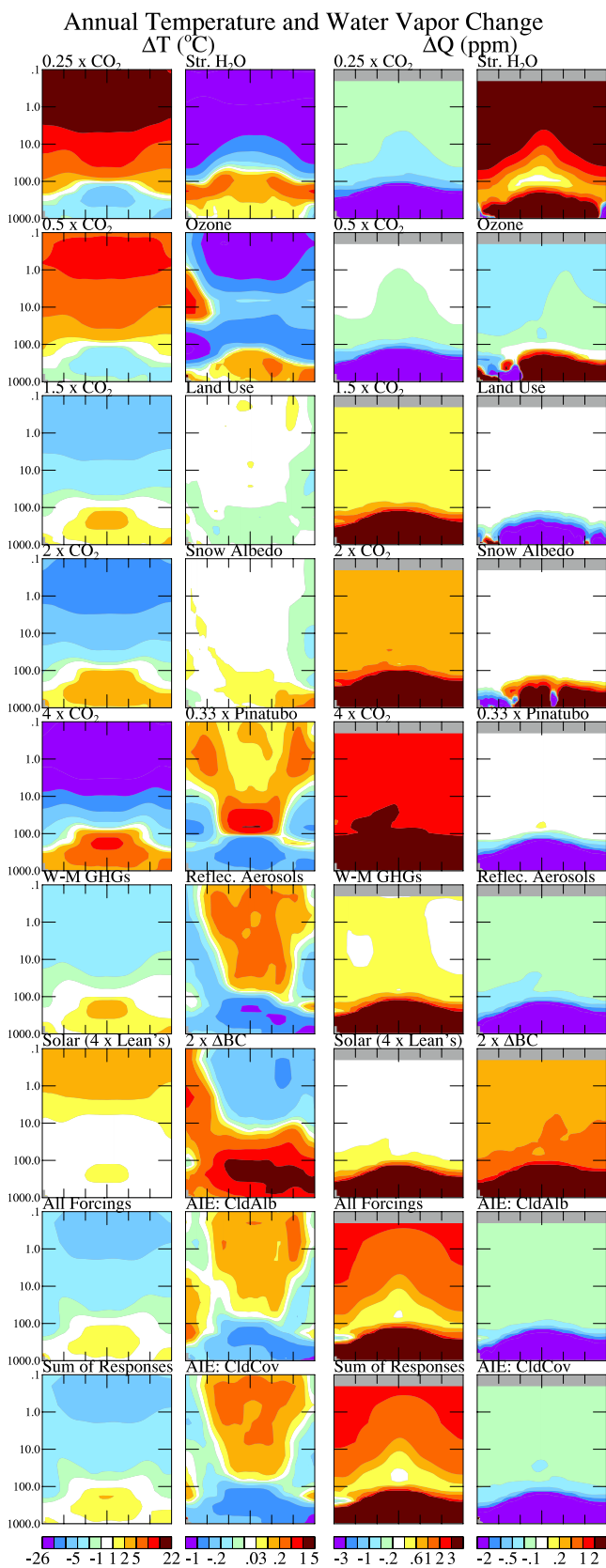
[135] The changes of the mean circulation caused by the GHGs dominate over the effects of other forcings, i.e., the stream function changes due to the GHGs determine the character of the changes when “all forcings” are incorporated. These changes are consistent with the simulated changes in precipitation discussed above, including heavier rainfall in the ITCZ and increased drying in subtropical regions.

[136] The aerosol direct and indirect effects weaken the dominant Hadley cell and the Brewer-Dobson circulation. Industrial BC, by itself, strengthens the Brewer-Dobson circulation in JJA, but weakens it in DJF, a plausible consequence of the Northern Hemisphere location of this forcing. However, these aerosol effects on the mean circulation are subjugated by the larger GHG effects when all

Table 4. Climate Forcings, Responses, and Efficacies for 1880–2000 Changes of Climate Forcing Agents Employed in Transient Simulations With GISS Model III

Forcing	Run Name	Fi	Fa	Fa ^a	Fs	Fs ^{*a}	δT_o	ΔT_s	Ei	Ea	Es	Es [*]	Fe ^a
(a) W-M GHGs	E2GHG	2.52	2.40	2.31	2.55	2.54 ± 0.10	0.14	1.21 ± 0.02	1.04	1.09	1.02 ± 0.02	1.03	2.61
(b) H ₂ O	E2ch4	—	—	—	0.061	0.036 ± 0.01	0.000	0.027 ± 0.01	—	—	0.96 ± 0.31	1.62	0.05
(c) Ozone	E2oz	0.438	0.281	—	0.256	0.203 ± 0.12	0.019	0.107 ± 0.02	0.53	0.82	0.90 ± 0.13	1.14	0.23
(d) Land Use	E2CRP	—	—	—	–0.088	–0.08 ± 0.03	–0.015	–0.042 ± 0.02	—	—	1.02 ± 0.60	1.13	–0.09
(e) Snow Albedo (BC)	E2SNA	0.083	0.082	0.082	0.136	0.14 ± 0.08	0.026	0.065 ± 0.01	1.69	1.71	1.03 ± 0.16	0.95	0.14
(f) Solar (4 × Lean)	E2SOx4	1.15	1.19	1.20	1.16	1.10	0.04	0.51	0.95	0.92	0.95	1.00	1.10
0.33 × Pinatubo	E2PIN	–1.09	–1.01	–0.98	–1.04	–0.94 ± 0.23	–0.02	–0.43	0.84	0.91	0.88	1.00	–0.92
(g) All Trop. Aerosols	E2TRA	–0.41	–0.38	–	–0.52	–1.14	–0.04	–0.28	1.48	1.60	1.14	0.53	–0.60
(g) + (h) Direct + AIE _{CldCov}	E3IE2	—	—	—	–1.39	–1.15	–0.08	–0.64 ± 0.03	—	—	0.99 ± 0.05	1.20	–1.37
“All Forcings” (a + b + c + d + e + 0.25f + g + h)													
All Forcings at Once	E3A18	—	—	—	1.71	1.52	0.09	0.782 ± 0.02	—	—	0.99 ± 0.02	1.11	1.69
Sum of All Responses	—	—	—	—	1.81	—	—	0.856	—	—	1.02	—	1.85

^aFor Fa[′], Fs^{*}, and Fe definitions, see footnotes a, b, and c of Table 1.



forcings are combined. An increase in the strength of the stream function argues against the possibility that long-term stratospheric water vapor increase is due to a slowing of the mean circulation, although it would not rule out such an effect on shorter timescales [Zhou *et al.*, 2001]. The stratospheric O₃ depletion of 1979–1997 works the opposite of increasing CO₂, i.e., the O₃ depletion slows the Brewer-Dobson circulation.

4.5. Zonal Wind and Sea Level Pressure

[137] Figure 22 shows the change in DJF and JJA zonal winds due to the same set of 18 forcings as in the previous figures. Figure 23 shows the change in DJF sea level pressure for these forcings.

[138] Increasing CO₂ speeds up the zonal mean jet stream winds in both DJF and JJA in both hemispheres. These accelerations extend all the way to the surface at latitudes about 50–60 degrees, and they are accompanied by decreasing polar sea level pressure. At 1.5 × CO₂ the effect is still weak in the Northern Hemisphere and the sea level pressure change is small compared to interannual variability (Figure 17). However, because we have ensembles of long runs, the effect on the zonal wind is significant.

[139] Formal significance is somewhat arbitrary, as the number of independent realizations in a single 100 or 120-year run is not well defined. For many of the individual forcings (those with indicated uncertainty ranges in Tables 1–4), as well as the control runs, the indicated responses are results from an ensemble of five runs. A practical measure of significance can be obtained by examining the sequence of CO₂ changes to see if the feature strengthens as the magnitude of the forcing increases.

[140] The effect on zonal winds is at least as strong for the well-mixed GHGs as it is for 1.5 × CO₂, which has about the same forcing. Ozone change contributes in the same sense to this phenomenon. Indeed, anything that warms the troposphere seems to contribute. This is not surprising as a warming troposphere (and a cooling stratosphere) imply that the equator to pole temperature gradient increases at the jet stream level, because the height of the tropopause decreases from equator to pole. Thus those phenomena that cool the troposphere have an effect in the opposite sense to the effect with warming troposphere.

[141] The fact that the increase in zonal winds extends to the surface at 60S is consistent with the strong warming of the Antarctic Peninsula in recent decades [Turner *et al.*, 2005]. O₃ depletion contributes the most to increased zonal wind and decreased polar sea level pressure in the austral summer (Figures 22 and 23), which is the important season for ice melt. Thus there may tend to be some reduction in the warming effects on the Antarctic Peninsula as O₃ recovers in coming decades. However, the well-mixed GHGs contribute substantially to these effects (Figures 22 and 23), so O₃ recovery may not reverse the temperature trend on the Antarctic Peninsula if well-mixed GHGs

Figure 20. Zonal mean temperature and water vapor changes in years 81–120 of coupled model simulations driven by the forcings of Figure 7. The dividing points for the color bars are symmetric about zero with values, from left to right, (1, 2, 5, 10, 15, max), (0.03, 0.1, 0.2, 0.5, 1, max), (0.3, 0.6, 1, 2, 3, max), (0.1, 0.2, 0.5, 1, 2, max).

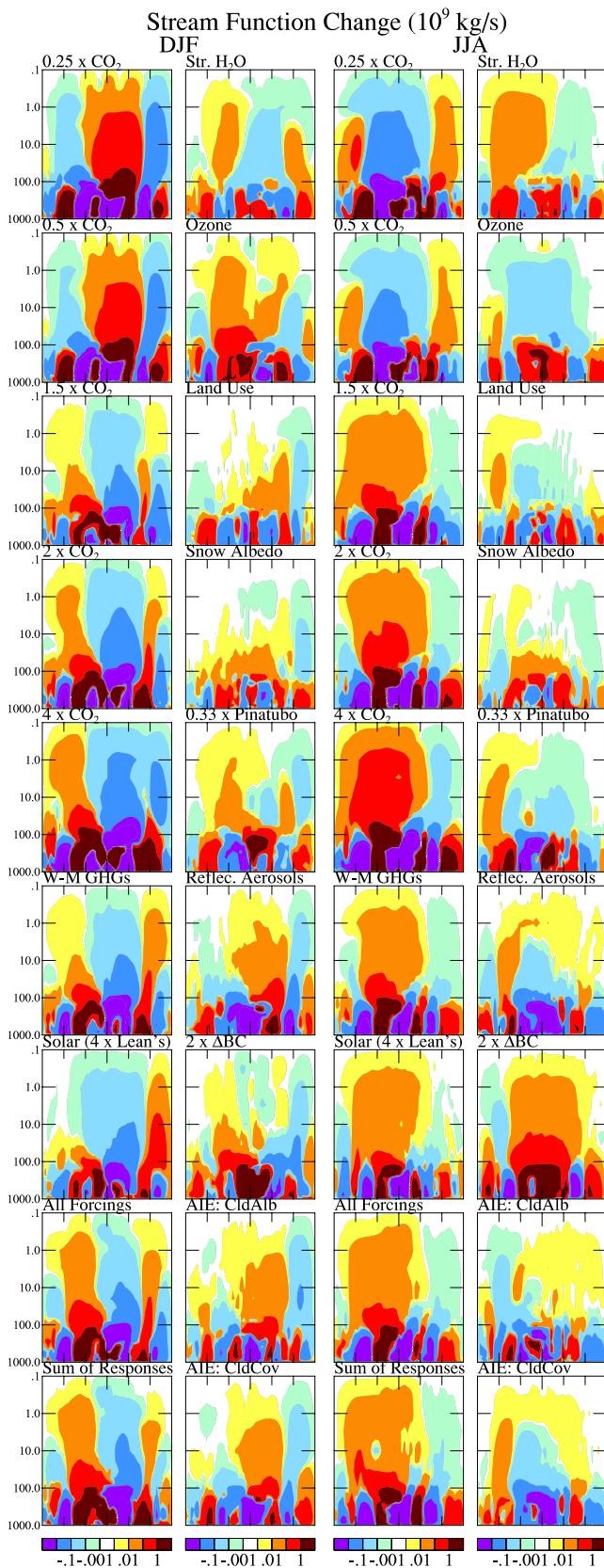


Figure 21. Zonal mean stream function changes in years 81–120 of coupled model simulations driven by the forcings of Figure 7. The dividing points for the color bars are symmetric about zero with values, from left to right, (0.001, 0.01, 0.1, 1, max).

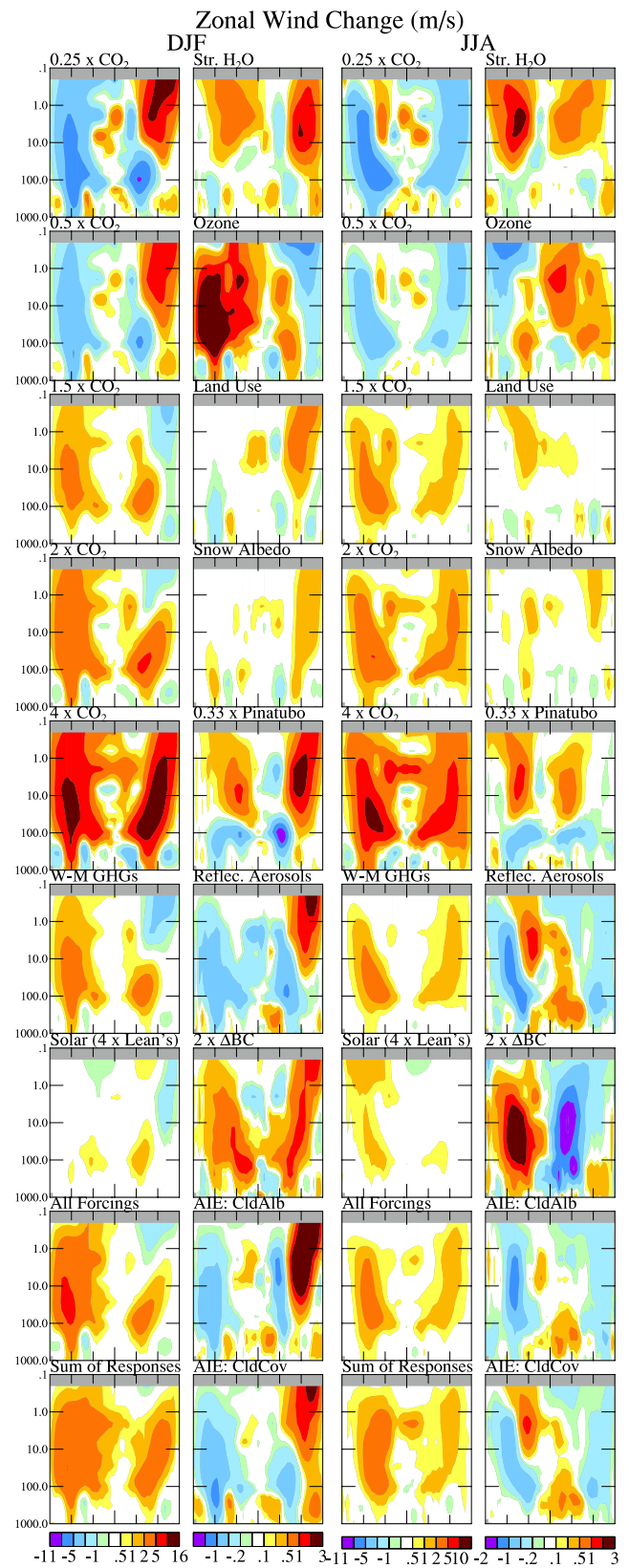


Figure 22. Zonal mean zonal wind changes in years 81–120 of coupled model simulations driven by the forcings of Figure 7. The dividing points for the color bars are symmetric about zero with values, from left to right, (0.5, 1, 2, 5, 10, 16), (0.1, 0.2, 0.5, 1, 1.5, 3), (0.5, 1, 2, 5, 10, 11), (0.1, 0.2, 0.5, 1, 1.5, 3).

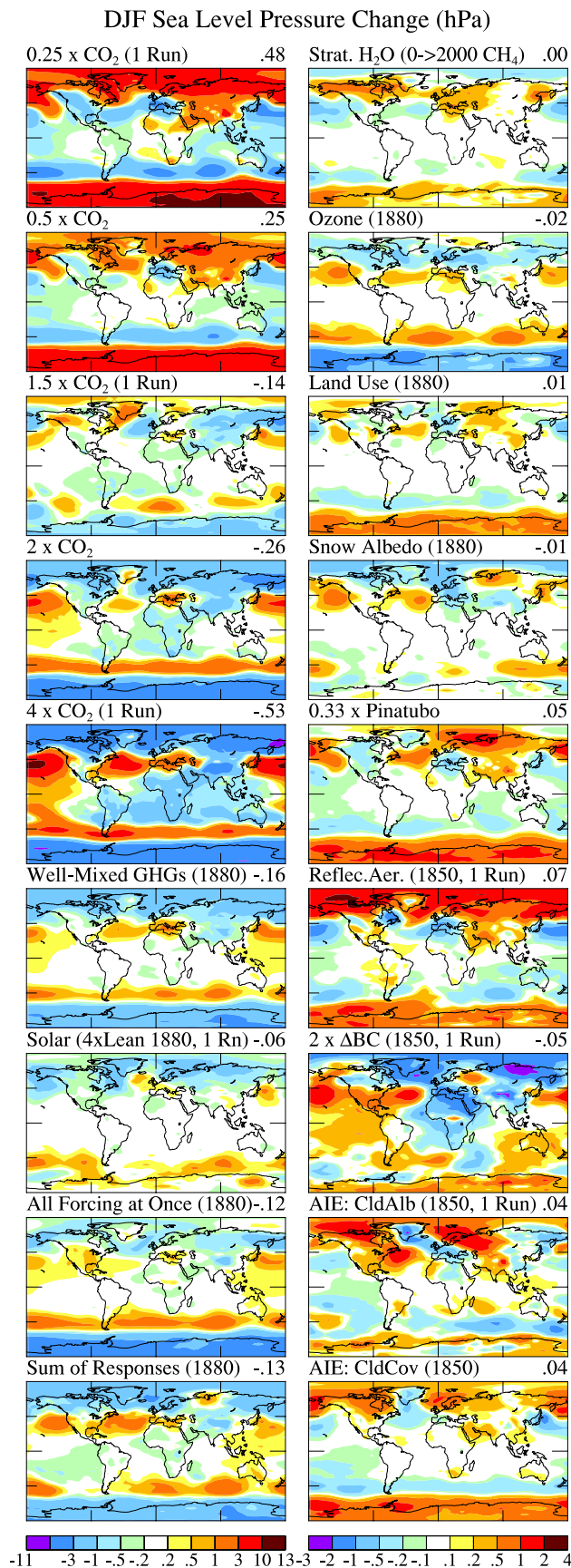


Figure 23. Sea level pressure changes in years 81–120 of coupled model simulations driven by the forcings of Figure 7.

continue to increase rapidly. *Shindell and Schmidt* [2004] discuss this topic further.

[142] The Pinatubo aerosols cause the Northern Hemisphere winter jet stream to accelerate, as expected and as is consistent with the winter warming that generally follows large tropical volcanic eruptions. However, it should be noted that the changes illustrated are the 81–120 year response to a constant forcing, after a large cooling has developed, unlike the situation for a single volcanic eruption. Thus the illustrated sea level pressure change may not be relevant to an actual volcano.

[143] The modeled changes in sea level pressure and zonal winds that occur as the greenhouse gas forcing increases are consistent with an increasingly positive phase of the Arctic Oscillation [*Thompson and Wallace*, 1998]. Such a trend was observed in the last few decades of the 20th century, and a strong tendency for such a trend has been reported in some climate models [*Shindell et al.*, 1999b]. On the other hand, when observations are updated to 2004 there remains little evidence for any trend of the Arctic Oscillation [*Manney et al.*, 2005; *Overland and Wang*, 2005; *Cohen and Barlow*, 2005]. Examination of the large number of long runs summarized in our present figures leaves no doubt that increasing greenhouse gases tend to decrease the modeled winter sea level pressure over the Arctic Ocean, increase the surface pressure in a subpolar-midlatitude band, and increase the zonal wind in the lower stratosphere and troposphere at latitudes 45–55°N. However, this tendency is weak at 1.5 × CO₂ or current levels of well-mixed greenhouse gases. This suggests that we should expect to see a trend toward the positive phase of the Arctic Oscillation, but natural variability could keep this trend from being very obvious for decades.

4.6. Normalized Response

[144] It is natural, in a paper on the efficacy of forcings, to ask whether the spatial patterns of the climate response to different forcing mechanisms become similar if the climate responses are normalized to have the same global mean climate forcing. An indication of this is already provided in Figure 8 for greenhouse gases and in Figure 12 for aerosols, where global maps of ΔTs/Fs are shown.

[145] Figure 24 shows the normalized surface air temperature response, ΔTs/Fs, for all the different forcing mechanisms that we have examined, as well as for the combination of all the forcings. Those forcings that are globally distributed, i.e., the well-mixed GHGs, Pinatubo aerosols, and solar irradiance changes evoke nearly identical normalized responses. Even the aerosol indirect forcings, which are more concentrated in the Northern Hemisphere but include substantial Southern Hemisphere forcing, yield a similar response pattern.

[146] The response to reflective aerosol forcing is larger in the Northern Hemisphere, where most of the aerosols are located, but again the response pattern is quite similar. The response at high latitudes in the Southern Hemisphere, including the sea ice region, is small, but this region is relatively stable to forcings in the current GISS coupled model, perhaps because of excessively deep ocean overturning there, as mentioned in section 2.3 and discussed by *Liu et al.* [2003].

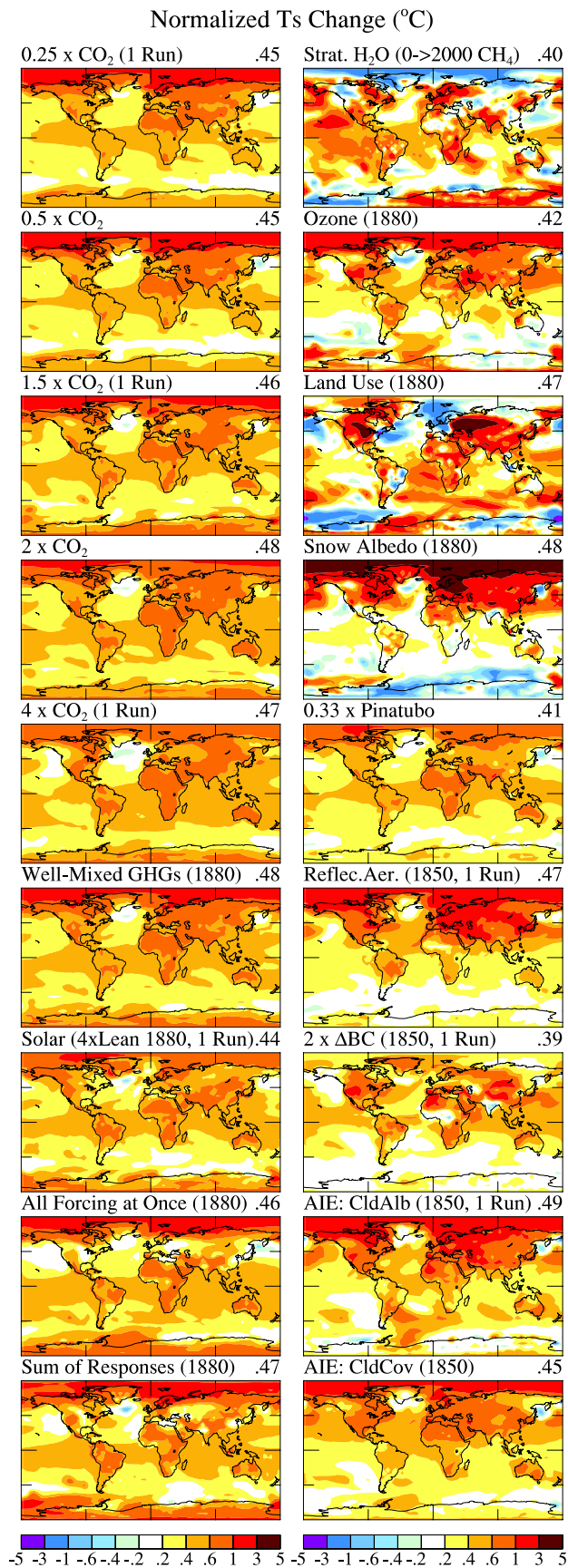


Figure 24. Surface air temperature changes, normalized via division by global mean F_s , in years 81–120 of coupled model simulations driven by the indicated forcings.

[147] Absorbing BC aerosols cause a local cooling in their region of heaviest concentration, the region of biomass burning in Africa. Otherwise BC also evokes a global response having much in common with other forcings, albeit with a moderately smaller global efficacy. The efficacy here refers to the fixed SST forcing, F_s . The efficacy relative to the standard adjusted forcing, F_a , differs even more from unity.

[148] The response to CH_4 -derived stratospheric H_2O is spatially noisy, as expected for such a small forcing, although the ensemble mean has reduced the variability. The snow albedo and land use changes, as surface forcing mechanisms, have increased localized responses in the regions where they occur.

[149] The response pattern to “all forcings at once” is similar to that for the well-mixed greenhouse gases. One implication of this is that, as far as surface air temperature is concerned, it is a fairly good approximation to calculate the net effective climate forcing and simply use an appropriate amount of greenhouse gases to yield that net forcing. Another implication is that it will be difficult to use the spatial pattern of observed temperature change to “fingerprint” responsible forcing mechanisms. Of course other characteristics of the climate response, such as the temperature change versus height, are much more indicative of specific forcings.

5. Efficacies of Climate Forcings

[150] We showed in section 4 that there is considerable coherence in the global response to forcings of the same magnitude, so the use of global forcings as a metric to compare and combine climate forcing agents has more relevance than might have been supposed. F_a is the standard definition for forcing in the past two IPCC reports, and it seems likely to remain so for some time. However, it is useful to consider other forcing definitions and to multiply the forcings by a factor that “corrects” for the fact that some forcing agents are more effective than others. That factor is E , the efficacy of the climate forcing.

[151] Figure 25a shows the global efficacies, E_a , of various climate forcing agents based on the adjusted forcing, F_a . E_a is the global temperature response per unit forcing for a given forcing agent relative to the response per unit forcing for a standard CO_2 forcing from the same initial climate state:

$$E_a = \frac{\Delta T_s / F_a}{\Delta T_s(CO_2) / F_a(CO_2)} \sim \frac{\Delta T_s / F_a}{0.463^\circ C / (W/m^2)}, \quad (5)$$

ΔT_s is obtained from the computed global temperature change in years 81–120 of the GISS coupled climate model. The denominator in (5), and thus the $E_a = 1$ level, is defined from the $1.5 \times CO_2$ experiment. This range of CO_2 normalizing the efficacy, from $1 \times CO_2$ to $1.5 \times CO_2$, is appropriate for analysis of climate change in the past and current centuries, as the CO_2 level in 2000 is ~ 1.27 times the 1880 amount. Although the $1.5 \times CO_2$ experiment is a single run it falls along the line defined by ensembles of runs for lesser and greater CO_2 (Figure 6). The $1.5 \times CO_2$ forcing yields a 100-year response $\Delta T_s = 1.103^\circ C$. F_a for $1.5 \times CO_2$ is $2.39 W/m^2$ for the WMO tropopause

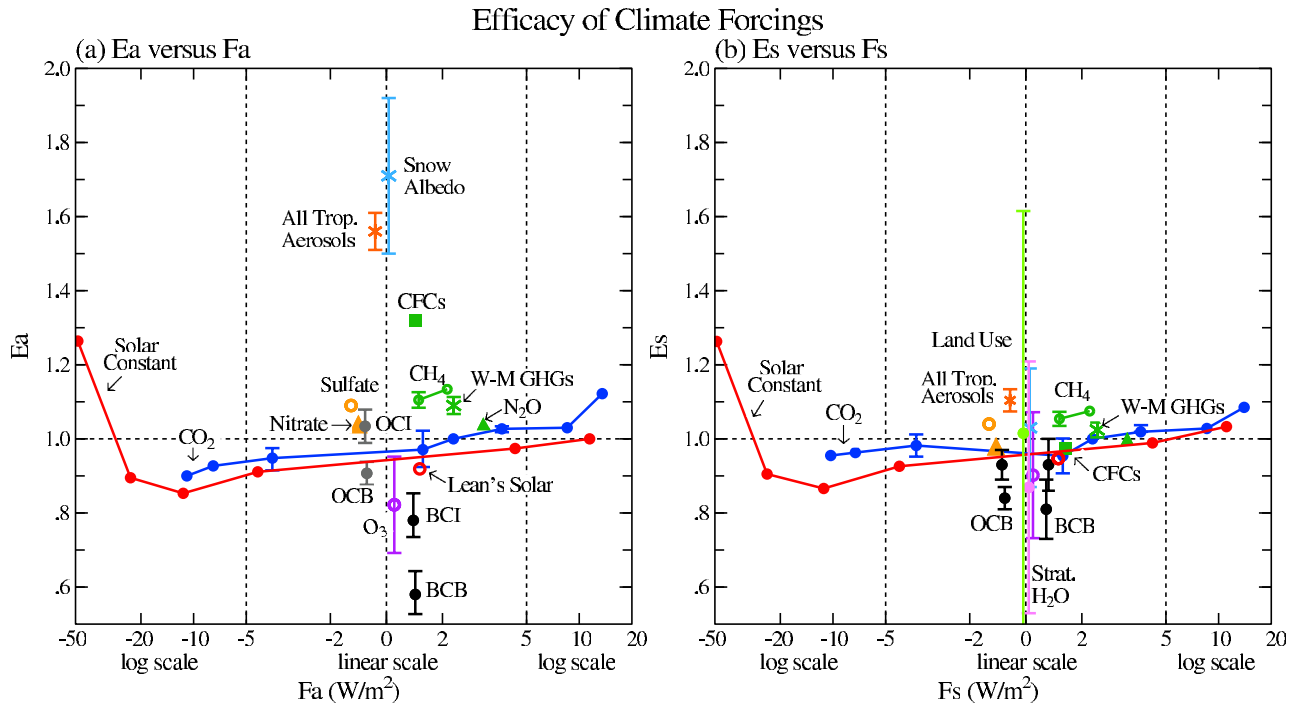


Figure 25. Efficacy of various climate forcing agents for producing global temperature change relative to the global temperature change produced by an equal CO_2 forcing at today's CO_2 amount (mean for $1 \times \text{CO}_2$ to $1.5 \times \text{CO}_2$). The effective forcing is the product of the efficacy and the forcing. (a) Uses the standard definition of climate forcing, F_a , the adjusted forcing; (b) uses the fixed SST forcing, F_s . The fact that the different forcing agents cluster closer to the $E = 1$ line for fixed SST definition of forcing indicates that F_s provides a better measure of expected climate response than does F_a . The positive slope of efficacy curves for changes of solar irradiance or CO_2 amount indicates that (in our climate model, with fixed ice sheet area and fixed vegetation distribution) the 100-year climate response becomes more sensitive as the planet becomes warmer. Upturns in the efficacy at very small and very large solar irradiances or CO_2 amounts correspond to the snowball Earth and runaway greenhouse effects.

definition (Table 1) and 2.37 W/m^2 for the tropopause used by Hansen *et al.* [2002]. Thus $\Delta T_s/F_a \sim 0.463^\circ\text{C/W/m}^2$ for $1.5 \times \text{CO}_2$, with this specific numerical relation being valid for the model III version of GISS modelE.

[152] The principal uncertainty in E_a is in the calculated ΔT_s for the given forcing agent, which depends upon the number of simulations carried out as well as upon the realism of the representation of the forcing agent and the climate model. The standard deviation in the E_s column of Tables 1–4, obtained from the variability of ΔT_s in 5-member ensembles of experiments, applies also to the E_a and E_i columns, after scaling in proportion to the efficacy value.

[153] We use the same normalization, i.e., $\Delta T_s(\text{CO}_2)/F_a(\text{CO}_2) \sim 0.463^\circ\text{C}/(\text{W/m}^2)$, for E_s and E_i as for E_a . Thus although $F_s(1.5 \times \text{CO}_2) \sim F_a(1.5 \times \text{CO}_2)$ so that $E_s(1.5 \times \text{CO}_2) \sim 1.00$, $F_i(1.5 \times \text{CO}_2)$ is $\sim 10\%$ larger than $F_a(1.5 \times \text{CO}_2)$, and as a result $E_i(1.5 \times \text{CO}_2) \sim 0.90$ (Table 1).

[154] Figure 25b shows the efficacies, E_s , based on the fixed SST forcings, F_s :

$$E_s = \frac{\Delta T_s/F_s}{\Delta T_s(\text{CO}_2)/F_a(\text{CO}_2)} \sim \frac{\Delta T_s/F_s}{0.463^\circ\text{C/W/m}^2}. \quad (6)$$

The uncertainty in E_s depends mainly on the uncertainty in the calculated ΔT_s for the given forcing agent, as the

unforced variability in the calculation of F_s in a 100-year run with fixed SST is smaller than the variability in the calculation of ΔT_s with the coupled atmosphere-ocean model.

[155] In this section we discuss three implications of Figure 25. First, there is the positive slope with increasing forcing, for either increasing CO_2 or increasing solar irradiance. This positive slope implies that climate, or at least 100-year climate response as simulated by the GISS climate model, is more sensitive to a positive forcing than to a negative forcing. Second, non- CO_2 gases are more effective at producing global warming than is CO_2 for an equal forcing, with the standard (F_a) definition of forcing. Third, absorbing aerosols (black carbon) are less effective than CO_2 at producing global warming.

5.1. Climate Sensitivity Versus Magnitude of Forcing

[156] Efficacy increases as the forcing increases, albeit only slightly, for forcings that do not take the climate too far away from the current climate, as shown in Figure 25 for a variety of CO_2 and solar irradiance changes. Efficacy is expected to vary as the climate state varies, because the strength of climate feedbacks changes with the climate state. For example, the positive sea ice feedback eventually disappears as sea ice area disappears. Thus, by itself, the sea ice feedback probably would cause the efficacy to slope

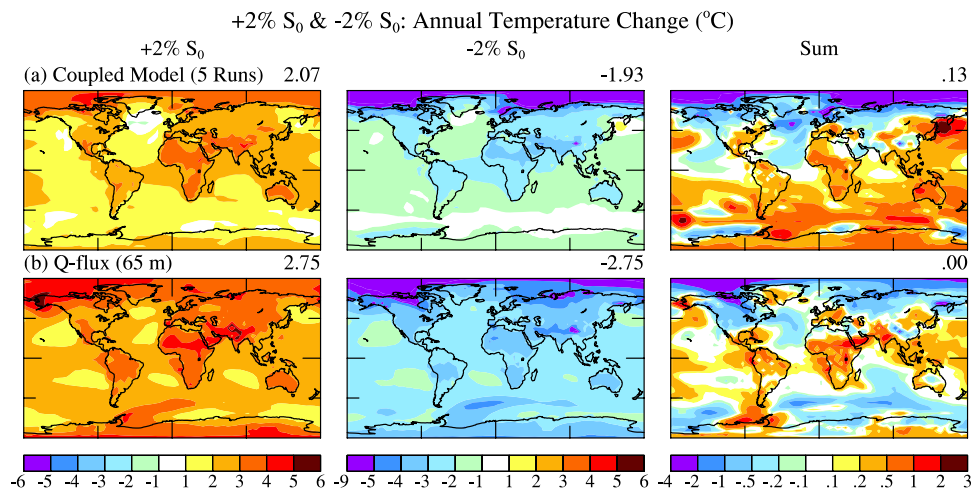


Figure 26. (a) Temperature changes in years 81–120 of coupled model simulations with +2% and –2% solar irradiance changes, and the sum of these responses. (b) Same as Figure 26a, but with the 65-m Q-flux ocean replacing the dynamical ocean C.

upward toward negative forcings. Indeed, if the forcing decreases enough to approach the snowball planet instability [Budyko, 1969], the efficacy should increase rapidly with decreasing forcing, an effect that is apparent for the largest decrease of solar irradiance in Figure 25. Evidently for today’s atmospheric composition other feedbacks, which include water vapor and clouds, cause the efficacy to increase as the forcing increases. Indeed, a large enough CO_2 increase should cause the efficacy to increase rapidly, as the water vapor feedback eventually causes a run-away greenhouse effect [Ingersoll, 1969].

[157] Efficacy also depends on the timescale over which the forcing is allowed to operate. Some feedbacks have a larger impact as the timescale increases, so the relative importance of different feedbacks changes as the timescale increases. Our emphasis is on the 100-year response with a dynamical ocean, because of its practical application to the issue of human impact on climate as outlined by IPCC [2001]. However, it would be informative to investigate the sea ice, water vapor, cloud, and other feedbacks individually over longer timescales (and over a greater range of forcings), which could be done either via a more efficient version of the present climate model, analogous to the “Wonderland” version used in RFCR, or via use of emerging computer capabilities.

[158] We suggest that a useful characterization of climate models can be obtained from a simple pair of model runs in which the solar irradiance is changed by +2% and –2%. Figure 26a shows the sum of the 100-year responses to +2% and –2% changes of the solar irradiance, which yields a net global warming but cooling at middle and high latitudes in the Northern Hemisphere. Obviously the response to the sum of these forcings applied together is identically zero everywhere. The sum of the responses to $2 \times \text{CO}_2$ and $1/2 \text{CO}_2$ (not illustrated here), which are nearly opposite forcings, has cooling in the Northern Hemisphere with a pattern the same as that for the sum of +2% S_0 and –2% S_0 .

[159] But what causes the asymmetric response to positive and negative forcings? One candidate is the timescale of the forcing. The asymmetry of the global mean response is a

reflection of the positive slope of the efficacy versus forcing plot, Figure 25. A positive slope, we have noted, could occur if an increasing strength of the water vapor and cloud feedbacks more than offsets the expected decrease of the sea ice feedback as the planet moves to a warmer state. However, a negative forcing, which cools the ocean surface, may cause deeper ocean mixing and a longer climate response time. The coupled model run of Figure 26a should be extended longer to check this effect better, but an indication is provided by the equilibrium response with the Q-flux ocean, Figure 26b. Indeed, the similar magnitude of the global mean responses for positive and negative forcings suggests that the increasing (global mean) efficacy with increasing forcing may be mainly a timescale effect. The spatial pattern of the temperature change for the sum of the two forcings suggests that the water vapor feedback is increasing and the sea ice feedback is decreasing as the climate passes through the mean (control run) climate.

[160] We infer that the present state of the climate system, at least as represented by our climate model, is in a rather flat region of the efficacy diagram. In that case, and assuming that this flat region of the efficacy diagram represents a minimum between the snowball Earth and runaway greenhouse effect, it is likely that the sensitivity will increase if global temperature increases substantially. We note, however, that prior GISS climate models between model II [Hansen et al., 1983] and SI2000 [Hansen et al., 2002] were more sensitive to a negative forcing than to a positive forcing, as the sea ice feedback was stronger in those models. It is desirable to have a thorough investigation of the factors that determine the present model’s sensitivity and to compare these with other models and relevant data.

[161] The dependence of efficacy on the magnitude of forcing indicated by Figure 25 is derived from a model in which sea ice, water vapor and cloud feedbacks are allowed to operate, but ice sheet and vegetation distributions are constant. The fixed ice sheet area is not a serious limitation for the 100-year (or shorter) timescales. However, the equilibrium (or long-term) efficacy must depend strongly

on the ice sheets, which provide the strongest feedback on 10,000–100,000 year timescales [Hansen *et al.*, 1983]. The vegetation distribution, which can be a feedback on a broad range of timescales, is also fixed in our present model. Vegetation can respond quickly to climate change and have a large effect on regional climate, but it is unlikely that dynamic vegetation would alter qualitatively the intercomparison below of the relative efficacies of different forcing mechanisms. Finally, the carbon cycle provides important feedbacks on a broad range of timescales, especially via atmospheric composition, but this is not relevant to our graphs of efficacy, as we use atmospheric composition as the independent variable.

[162] The efficacy diagram extended over a large range of forcings should have vertical upturns at both the small forcing and large forcing ends, corresponding to the snowball planet and runaway greenhouse instabilities. Indeed, the snowball earth instability is evident for -20% So and there is a hint of the runaway greenhouse at $8 \times \text{CO}_2$. The upturns are expected to be sharper and to occur at smaller forcings for longer timescales. Numerical problems in model parameterizations have hindered more complete exploration of the extremes of the efficacy diagram.

[163] Pleistocene climate variations may create an impression that the Earth's climate is more stable as it heads toward warmer conditions. However, Figure 25 suggests that, on the contrary, the Earth is now in a region of the efficacy diagram in which the climate sensitivity is rather flat with increasing global temperature. Moreover, the sensitivity is likely to increase if the planet becomes significantly warmer.

[164] We note one further implication of Figure 25. When the effectiveness of other forcing mechanisms is compared with that of a CO_2 change, the comparison should be made not only for the same magnitude and sign of the climate forcing, but also from the same base climate state. These conditions are easiest to meet if the same control run is used for all forcings.

5.2. Efficacy of Non- CO_2 Greenhouse Gases

[165] Our calculations indicate that CH_4 , N_2O , and CFCs are more effective at producing climate change than is CO_2 for the same magnitude of climate forcing. The uncertainty in the efficacy is less than the uncertainty in the absolute values of the CH_4 and CO_2 forcings, as their different efficacies are a result of the spatial distribution of the constituents and the spectral distribution of their absorptions.

[166] One source of uncertainty in the efficacies is the noise (unforced variability) in the coupled climate model response to the forcings. We quantify this uncertainty via multiple model runs from different ocean initial conditions. Another factor influencing the calculated efficacies is the definition of tropopause height. We employ the *WMO* [1957] definition of tropopause discussed in section 3, which in our model goes from ~ 100 hPa in the tropics to ~ 200 hPa from middle to high latitudes. If we instead choose a lower tropopause (larger pressure), the forcing (F_a') is less than F_a , but the decrease is smaller for CO_2 than for the other greenhouse gases. For example, with the tropopause employed by Hansen *et al.* [2002], which goes to 300 hPa at the poles, the forcing by CO_2 decreases by

$\sim 1\%$, while the forcings by CH_4 , N_2O and the CFCs decrease by $\sim 9\%$, 6% and 3% , respectively. Thus use of F_a' would make the efficacies of the non- CO_2 gases even larger relative to CO_2 .

[167] One reason that CH_4 , N_2O , and CFCs are more effective than CO_2 at producing climate change is that a greater percentage of the CO_2 forcing comes from high altitudes, where forcings are known to have much smaller efficacies (RFCR). Our present 20-layer model does a good job of simulating the temperature structure throughout the troposphere and stratosphere (Figure 17) from first principles, so we expect it to represent this effect well. CO_2 is well-mixed in our model throughout the stratosphere while CH_4 decreases with height in the stratosphere and changes with latitude based on observations of Minschwaner *et al.* [1998]. The portion of the CO_2 forcing located in the stratosphere is less effective than an equal forcing in the troposphere (RFCR). This vertical distribution effect can account for several percent change of efficacy (RFCR).

[168] Another difference among the forcings is the spectral location of their absorption. Gases whose absorption overlaps strongly with H_2O , as is the case for CO_2 , become relatively less effective as the temperature and absolute humidity increase. The detailed spectral integrations in the radiation treatment of model III should provide a good representation of differences in forcing effectiveness due to spectral location for the primary greenhouse gases. However, CFCs are assumed to be narrow-band absorptions without significant overlap with the primary GHGs. This must partially account for the greater efficacy of the CFC forcing. (This absence of overlap may also cause some overestimate of the CFC forcing in our model.) Still another difference among these forcings is that CO_2 more strongly cools the stratosphere, thus providing a small negative feedback by reducing stratospheric water vapor, or at least reducing the H_2O increase that would otherwise occur because of tropospheric warming.

[169] We are unaware of other factors that would have a significant effect on the relative efficacies of these gases. Thus we believe that the efficacies of non- CO_2 gases in Figure 25 are reasonable. However, it is important to have independent evaluations based on other climate models that realistically simulate stratospheric climate and accurately treat overlapping gaseous absorption.

[170] We anticipate that variations in efficacy should diminish if we employ F_s or F_g , rather than F_a , because F_s and F_g allows some feedbacks, such as semi-direct cloud changes (RFCR), to operate before the flux change is computed. Table 1 and Figure 25 confirm that the efficacy is closer to unity when the forcing is defined by F_s rather than F_a .

[171] Note that F_s “works better” than F_a especially for realistic moderate changes of the forcings, but it has little effect on the efficacy for 10 or 20% solar constant changes. This is as expected. The improvements that occur for BC, CFC or O_3 are a result of the tropospheric temperature profile being allowed to adjust and thus to yield a more realistic flux perturbation for the given forcing. However, the changes in efficacy as solar perturbations become large are primarily a consequence of non-linear responses of climate feedbacks, such as sea ice cover or atmospheric water vapor. These non-linear response are an inherent part

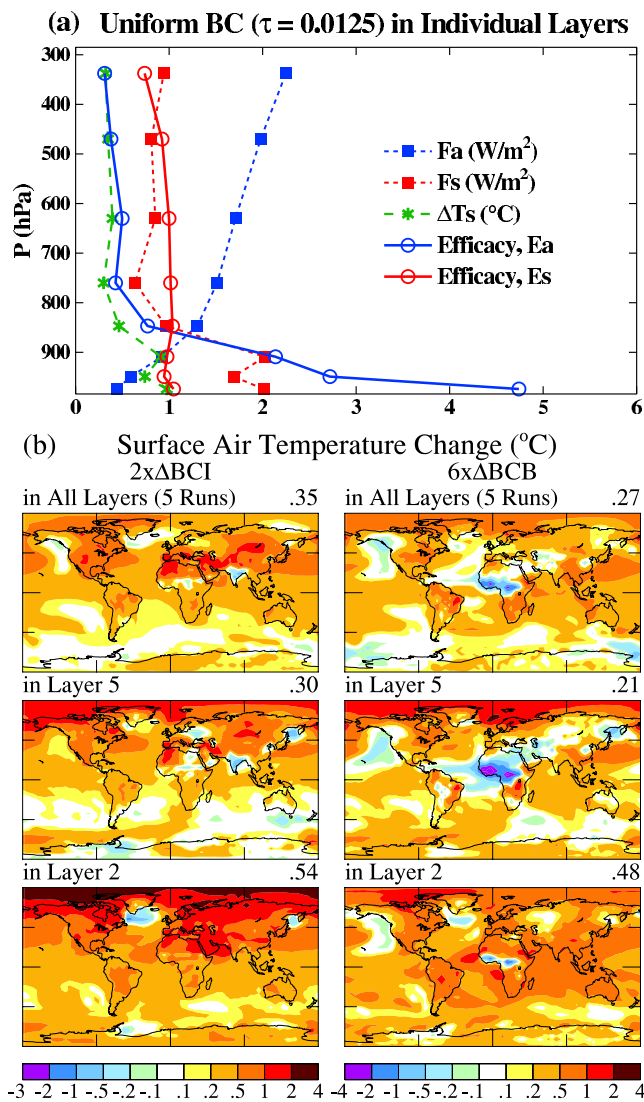


Figure 27. (a) Forcing, 81–120 year surface air temperature response, and efficacy for a globally uniform layer of BC aerosols in each of the eight lowest layers of the GISS model III. (b) Surface air temperature changes in years 81–120 of GISS model III for the same amount and global distribution of BC, but distributed vertically in all layers according to the aerosol transport model of Koch [2001] and in only model layer 5 or layer 2.

of the climate model, and presumably of the real world. It would be possible to “divide out” much of this non-linearity, if we were to normalize the efficacy by dividing by the variable CO_2 forcing rather than the $1 \times CO_2$ to $1.5 \times CO_2$ forcing, but that would introduce another source of noise and make results less transparent.

5.3. Efficacy of Black Carbon

[172] Absorbing aerosols are one of the climate forcing mechanisms for which the radiative forcing is not always indicative of the climate response (RFCR). In other words the efficacy can be much different than unity for absorbing aerosols. For example, we find $E_a = 0.58$ and 0.78 (Table 2) for biomass burning and industrial (fossil fuel) BC aerosols,

respectively, using the spatial distributions of these aerosols produced by the aerosol transport modeling of Koch [2001]. The actual vertical and horizontal distributions of BC aerosols are poorly known. Therefore a more general understanding of the efficacy of the climate forcing by BC aerosols would be useful.

[173] Figure 27a and Table 2 show the results of eight 120-year climate simulations in which BC aerosols were placed in each of the lowest eight layers of the GISS model, one layer at a time. In each case BC was distributed uniformly over the globe with optical depth 0.0125 at visible wavelengths. The instantaneous and adjusted forcings, F_i and F_a , are practically equal, both increasing from about $0.4 W/m^2$ when the BC is in the lowest layer to more than $2 W/m^2$ when BC is in the upper troposphere.

[174] The global warming in response to the uniform BC distribution is close to $1^{\circ}C$ when BC is in the planetary boundary layer (PBL), i.e., in one of the lowest three model layers, and it is about $0.3^{\circ}C$ when BC is in the free troposphere. As a result, the efficacy, E_a , decreases drastically as the BC is moved higher into the atmosphere. In the lowest model layer $E_a \sim 5$, and in all three of the layers beneath the 900 hPa level $E_a > 2$. In the free troposphere $E_a \sim 0.5$, and E_a is even less in the upper troposphere. F_a is entirely misleading as a predictor of climate response, as has been noted previously [RFCR; Cook and Highwood, 2004].

[175] The large change of E_a with height for BC aerosols is due in part to the “semi-direct” effect of absorbing aerosols on cloud cover (RFCR). Heating of the layer containing the aerosols reduces the cloud cover within that layer, but, because the heating inhibits convection from the layer below, it increases cloud cover in the lower layer. The reality of a semi-direct effect on cloud cover has been verified by observations [Ackerman *et al.*, 2000] and large-eddy simulations of marine stratocumulus clouds [Johnson *et al.*, 2004]. Johnson [2005], using a single column model, finds that the cloud schemes in some GCMs substantially underestimate the semi-direct effect. The realism of the simulated semi-direct effect depends on the realism of the simulated profile of low clouds, including their dependence on atmospheric stability, and on the realism of the simulated profile of BC. The GISS model includes a prognostic cloud water scheme based on cloud thickness [Del Genio *et al.*, 2005; Schmidt *et al.*, 2005]. Model III parameterizes boundary layer turbulence and uses an improved second order closure model to represent turbulence throughout the troposphere [Cheng *et al.*, 2002], achieving a more realistic profile of low clouds than previous GISS models. We believe that the present model provides a meaningful estimate of BC climate effects, but comparisons with more detailed models and observations are needed.

[176] Figure 27a also includes results of 100-year F_s runs for BC aerosols placed individually in each of the lowest eight model layers. F_s differs greatly from F_a . Unlike F_a , F_s provides a good prediction of the global temperature change, i.e., the efficacy E_s is near unity.

[177] Figure 27b and Table 2 show the 81–120 year climate response when BC industrial and BC biomass aerosols are placed entirely in level 2 or in level 5, in both cases using the geographical distribution of aerosols from

the transport model of Koch [2001]. In other words, these simulations allow us to test the sensitivity of the results to the height of the aerosols with a fixed realistic geographic distribution of aerosols.

[178] We conclude that, if the BC aerosols are entirely above the PBL (in the 700–800 hPa) region, the global warming is not much (about 20%) less than it is with the BC vertical distribution from Koch’s modeling. On the other hand, if the BC aerosols are in the PBL, the global warming is 50–100% larger than with Koch’s vertical distribution. Koch [2001] notes that her aerosols are distributed rather high in the atmosphere relative to meager available observations. If the actual BC vertical distribution has a greater proportion of aerosols in the PBL than in Koch’s model, then we have probably underestimated the climate effect of the BC aerosols and their efficacy. It is safe to say that the Koch vertical distribution does not over-estimate the BC forcing and efficacy, because the result is close to what it would be with all of the BC in the middle to upper troposphere, where it is least effective as a forcing.

[179] Roberts and Jones [2004] recently reported results of calculations using the Hadley Centre climate model for climate sensitivity to fossil fuel black carbon. They obtained a climate sensitivity of 0.56°C per W/m² for BC versus 0.91°C per W/m² for CO₂. Thus their fossil fuel BC efficacy, ~62%, is less than the efficacy of 79% that we find for fossil fuel BC. Roberts and Jones [2004] note that the vertical distribution of BC in their model may be weighted too much toward higher altitudes, which would reduce their net efficacy. However, a qualitatively similar statement may apply to the vertical distribution of BC in our model. Cook and Highwood [2004], using a simplified general circulation model in idealized situations, obtain an efficacy versus aerosol height comparable to that in our model. As discussed by Johnson [2005], it will be necessary to evaluate the ability of each GCM to simulate low level clouds and the sensitivity of cloud cover to aerosol heating in order to determine the realism of the model estimates of the aerosol forcing efficacy.

[180] BC aerosols reduce the flux of solar radiation reaching the surface and can cause regional cooling, as seen in regions of biomass burning in Africa and industrial BC in India (Figure 27b). However, on global average BC causes substantial warming of surface air. Biomass BC is less effective at causing warming than fossil fuel BC, because the biomass BC is more heavily weighted toward low latitudes where the efficacy is less (RFCR) and because biomass BC on the average is at greater altitudes where its efficacy is less (Figure 27a).

6. Effective Climate Forcings

[181] The product of a forcing and its efficacy is the effective forcing,

$$F_e = E_a F_a = \sim \frac{\Delta T_s}{0.463^\circ\text{C}/(\text{W}/\text{m}^2)}, \quad (7)$$

where the indicated specific numerical relation is valid for the model III version of GISS modelE. The efficacy, defined as the ability (relative to CO₂) of a given forcing (per unit

forcing) to produce global temperature change (equation (5)), is defined for other forcing definitions via

$$F_e = E_a F_a = E_s F_s = E_i F_i. \quad (8)$$

Use of the effective forcing has the merit of allowing use of a mixture of different forcing definitions, when that is necessary. Of course the primary burden in obtaining the efficacy is the need to compute ΔT_s via 120-year climate simulations. However, once the efficacy of a given forcing agent is known, it does not need to be recomputed for alternative values of the forcing far from the extremes of snowball Earth or runaway greenhouse effect.

[182] Consideration of the efficacy of climate forcings and indirect climate forcings can alter the relative importance of different climate forcing agents. In section 8.1 we show alternative presentations of climate forcings in the industrial era to illustrate the impact of efficacy and indirect effects. We also discuss the question of which forcing definition is most appropriate for use in policy considerations about long-term climate change. First, however, we must clarify our use of the terms forcings, indirect forcings, and climate feedbacks.

[183] Distinctions among forcings, indirect forcings, and climate feedbacks need not be rigid. Flexibility can help improve and quantify understanding of climate change mechanisms. It places a burden on the practitioner to make the usage clear, but that is not difficult. We illustrate with a few examples.

6.1. Alternative Forcing Definitions

[184] It is useful to consider alternative definitions of climate forcings, such as F_i , F_a , F_g and F_s , each of which has merits and disadvantages. F_i is a true forcing, because climate is fixed while F_i is calculated. However, in some cases it is unrepresentative of the climate response, i.e., E_i is far from unity, perhaps even negative. Besides, if one is interested in the response to climate forcings that remain present for years, the instantaneous energy flux is less relevant than the flux perturbation that quickly comes into being as a result of fast adjustment processes. It is for this reason that F_a “works better,” in the sense of providing a better indication of the expected climate response, and therefore it has become the standard forcing definition [IPCC, 2001]. F_i and F_a depend upon how the tropopause is defined. F_s , and presumably F_g , usually “work better” than F_i or F_a and they are independent of the tropopause, but F_g requires programming effort and F_s and F_g require more computing time than F_i and F_a . For the sake of interpreting climate responses to forcings, and for comparing results among different investigators, it would be valuable for researchers to report the values of as many of these forcings as practical.

[185] We suggest that multiple forcing definitions have merit, and there is no need to be apologetic about any of the definitions. However it is important to make clear which forcing definition is being used, and to recognize the implications about which feedback mechanisms are included. For example, because the tropospheric temperature and cloud cover adjust to the presence of the forcing agent in the cases of F_s and F_g , these forcing definitions include the “semi-direct” effect of absorbing aerosols on clouds

[RFRCR; *Johnson et al.*, 2004] as part of the forcing, while F_i and F_a do not include the semi-direct effect. F_s and F_g may show greater “model-dependence” than F_i and F_a , because they involve much more “physics” than radiation. Thus, if different models calculate and report several of the forcings, it will be easier to analyze reasons for differences among climate responses.

6.2. Climate Feedbacks

[186] Climate mechanisms can be feedbacks on some timescales while being forcings on other timescales. The area of ice sheets is a climate feedback on millennial timescales, while it is a fixed boundary condition on short timescales. If we compare eras with different ice sheet areas, e.g., glacial and interglacial times, the change in ice sheet area is a forcing. The concept of ice sheets as a forcing has proved useful for empirically inferring the climate sensitivity relevant to century and shorter timescales [*Hansen et al.*, 1984, 1993; *Hoffert and Covey*, 1992]. The empirical climate sensitivity inferred in this way is a function of all fast feedbacks in the climate system, such as changes of sea ice, clouds and water vapor. Recently a number of models seem to have converged on a sensitivity [*Kerr*, 2004] comparable to that inferred from paleoclimate data ($\sim 3^\circ\text{C}$ for doubled CO_2). By itself this result might indicate only that the models are using similar methods, as the feedback processes are highly parameterized and remain difficult to simulate with accuracy and confidence. However, the paleoclimate data naturally incorporate all relevant processes, so it is reassuring that the theoretical and empirical approaches yield similar results.

[187] *Lea* [2004] infers an empirical tropical climate sensitivity of $4.4\text{--}5.6^\circ\text{C}$ for doubled CO_2 from paleoclimate data. This result is consistent with our inference of a global sensitivity of $\sim 3^\circ\text{C}$, because *Lea* includes the effect of ice sheet changes as a feedback. As shown by climate simulations with ice sheets removed [*Hansen et al.*, 1984], as well as by our simulations in this paper for regional forcings such as tropospheric aerosols, non-tropical forcings yield a substantial tropical response (more than half as large as the tropical response to a globally uniform forcing of the same global mean value). The $\sim 3^\circ\text{C}$ sensitivity that we derive includes only the fast feedback processes (water vapor, clouds, sea ice) that are allowed to operate in our model, consistent with the common definition of climate sensitivity relevant to anthropogenic climate effects [*Charney*, 1979; *IPCC*, 2001].

6.3. Indirect Climate Forcings

[188] There is flexibility in the degree to which indirect forcings are associated with primary climate forcing mechanisms, and there is merit in alternative choices. The climate forcing associated with each of the measured or estimated changes of atmospheric composition or boundary conditions over a given period, say the industrial era, provides basic data. However, it is useful to also associate indirect effects with primary forcing mechanisms. For example, the increase of stratospheric H_2O that accompanies increased CH_4 was examined above. This effect is well understood, confirmed by observations, and thus it is appropriately included as part of the total (direct plus indirect) CH_4 climate forcing. The total

forcing is a relevant metric for evaluating strategies aimed at reducing human-made climate effects.

[189] How far should we go in assigning indirect effects? Results of *Stuber et al.* [2005] imply that it makes sense to include even some second generation indirect effect in a total forcing, an example being the change of stratospheric O_3 and, subsequently, stratospheric H_2O as a net effect of solar irradiance variations. A practical answer is to include only those indirect effects that are large enough to be significant (relative to the primary forcings, e.g., they should show up in a bar graph of all the forcings) and that can be calculated with a reasonable degree of confidence.

7. Applications

[190] We estimate the efficacy of two non- CO_2 forcings: methane and soot. Besides CO_2 , methane and soot are potentially the largest global anthropogenic forcings, although estimates of the soot forcing have varied widely [*Ramaswamy et al.*, 2001; *Hansen et al.*, 2000; *Jacobson*, 2001; *Penner*, 2001; *Penner et al.*, 2003]. We define soot as the carbonaceous aerosol product of fossil fuel and biomass burning, including BC and OC, with the distinction between BC and OC made on the basis of optical properties [*Chylek et al.*, 2003; *Hansen et al.*, 2004].

7.1. Methane

7.1.1. Direct CH_4 Forcing

[191] The direct CH_4 forcing based on the analytic relationship of *Hansen et al.* [2000] is $F_a = 0.59 \text{ W/m}^2$ for the change from pre-anthropogenic amount (650 ppb [*Petit et al.*, 1999]) to 2000 (1752 ppb), $F_a = 0.55 \text{ W/m}^2$ for the change from 1750 (700 ppb) to 2000, and $F_a = 0.46 \text{ W/m}^2$ for the change from 1880 (837 ppb) to 2000. Our calculated F_a for 1750–2000 is about 15% larger than the IPCC estimate [*Ramaswamy et al.*, 2001] of $F_a = 0.48 \text{ W/m}^2$ for the period 1750–1998, but it is smaller than the CH_4 forcing obtained by *Jain et al.* [2000] from narrow-band radiation calculations using the CH_4 global distribution measured by satellite. *Jain et al.* [2000] obtained $F_a = 0.601 \text{ W/m}^2$ for the period 1750–1992, which increases to 0.62 W/m^2 for the 1750–2000 period. However, they suggest that their narrow-band calculations could be an over-estimate by 11%, which would reduce their 1750–2000 forcing to $F_a = 0.55 \text{ W/m}^2$. Thus their reduced forcing is in close agreement with our estimate.

[192] The variation in estimated forcings among different models arises not only from imprecision in the radiation schemes. The results also depend on the manner in which a global mean is calculated and how the tropopause is defined. We use the clouds, water vapor and other climate variables saved from a control run of model III, allow one year for the stratospheric temperature to adjust to the presence of the forcing agent, and then integrate another year to obtain the annual global flux change at the top of the atmosphere (F_a). As mentioned in section 3, we use the WMO tropopause definition, as available at the web site given in section 3. If, instead, we use the fixed tropopause level specified by *Hansen et al.* [2002], which declines from 100 hPa at low latitudes to 300 hPa at the pole, F_a decreases by about 9%. Thus with this prior definition of the tropo-

pause, the efficacy of CH₄ as a forcing would have been even higher, of the order of $\sim 120\%$.

[193] The absorption coefficients determining the CH₄ climate forcing in the present GISS GCM, the model III version of modelE [Schmidt *et al.*, 2005], were chosen to match the forcing specified by the relationships in Table 1 of Hansen *et al.* [2000], which has been employed for the past several years in GISS models. However, these forcings do not necessarily achieve the potential accuracy of the current GISS radiation scheme in model III [Lacis and Oinas, 1991; Schmidt *et al.*, 2005], which utilizes 15 non-contiguous spectral intervals to model overlapping cloud, aerosol and gaseous absorption of solar radiation and 33 correlated k-intervals from non-contiguous spectral regions for long-wave radiation. The coefficients in this current radiation scheme need to be “tuned” to fit the best possible line-by-line calculations, a procedure that will be carried out over the next year or two. For our present discussion, i.e., section 7.1, except where specified otherwise, we employ the Fa relationship of Hansen *et al.* [2000]. We estimate, partly subjectively, the 1σ uncertainty in Fa (CH₄) as being of the order of 10%.

[194] We conclude from our present study that the efficacy of the direct CH₄ forcing is $E_a \sim 110 \pm 2\%$, where the indicated uncertainty is the 1σ variation in our ensemble of climate model runs (Table 1). Thus the effective CH₄ forcing for the period 1750–2000 is $\sim 0.6 \text{ W/m}^2$ for the CH₄ direct effect alone. This direct CH₄ forcing is $\sim 40\%$ of the CO₂ forcing for the same period.

7.1.2. Indirect CH₄ Effect via Stratospheric H₂O

[195] Figure 9 indicates that the 20-layer model with model top above the stratosphere (Figure 1) does a reasonable job of simulating the H₂O produced by oxidation of CH₄. The model’s vertical resolution is sufficient to do a good job of simulating the thermal structure of the stratosphere (Figure 17), and thus the model should be able to calculate accurately the radiative impact of the added H₂O.

[196] We found (Figure 9) that CH₄ oxidation causes little water vapor increase near the tropopause, where an added greenhouse gas would be effective at influencing surface temperature (RFCR). As a result, the forcing Fs due to CH₄-derived H₂O is only 0.11 W/m^2 for the CH₄ increase from no CH₄ to year 2000 CH₄, 0.07 W/m^2 for 1750–2000, and 0.06 W/m^2 for 1880–2000. These Fs values are also the effective forcings, as five 120-year model runs yielded $E_s = 0.96 \pm 0.31$, not significantly different than unity (Table 1). Thus the CH₄-derived H₂O forcing is small, increasing the direct CH₄ forcing by $\sim 10\%$.

7.1.3. Indirect CH₄ Effect via Tropospheric O₃

[197] A larger indirect effect of increasing CH₄ occurs via tropospheric O₃. Prather and Ehhalt [2001] in IPCC [2001] credit $\sim 45\%$ of the anthropogenic tropospheric O₃ forcing to CH₄. Given the tropospheric O₃ forcing $F_a \sim 0.34 \text{ W/m}^2$ (section 3.1.4) [IPCC, 2001], we estimate the CH₄ indirect effect via O₃ as $\sim 0.15 \text{ W/m}^2$.

[198] We found a tropospheric O₃ efficacy of 82% (Table 1). Thus the effective forcing due to the indirect effect of CH₄ on tropospheric O₃ is $\sim 0.13 \text{ W/m}^2$.

7.1.4. Direct Plus Indirect CH₄ Effective Forcing

[199] Our estimate for the 1750–2000 direct effective forcing by CH₄ is $\sim 0.60 \text{ W/m}^2$. The effective indirect forcings via stratospheric H₂O and tropospheric O₃ are

$\sim 0.07 \text{ W/m}^2$ and $\sim 0.13 \text{ W/m}^2$, respectively. Thus the total effective CH₄ forcing is $\sim 0.80 \text{ W/m}^2$. Given that the direct forcing (Fa) of CH₄ is 0.55 W/m^2 , this implies an overall, direct plus indirect, efficacy of $\sim 145\%$. The direct plus indirect CH₄ effective forcing for 1750–2000 is thus $\sim 50\%$ of the CO₂ forcing.

7.2. Soot

[200] We define soot as the carbonaceous aerosol product of incomplete combustion, including both BC and OC components. Soot climate forcing is very uncertain, because it comprises four terms, two being positive and two being negative. The positive terms are the direct forcing by BC aerosols and the snow albedo effect of soot. The negative terms are the direct effect of OC aerosols and the indirect effect on clouds of both BC and OC. Each term is uncertain by a factor of two or more. Measurements are inadequate in all cases, but the snow albedo and indirect aerosol effects are particularly poorly constrained. Nevertheless, we hazard a strawman estimate.

[201] We calculate a fossil fuel BC (BCI) forcing $F_a = +0.49 \text{ W/m}^2$ and an efficacy $E_a = 78\%$. Efficacies, of course, include the semi-direct effect and all climate feedbacks, as they are inferred from 120-year climate simulations. The effective forcing for BCI is thus $+0.38 \text{ W/m}^2$ for the change of BCI between 1850 and 2000. Our climate model simulations for OCI yield $F_a = -0.13 \text{ W/m}^2$, $E_a \sim 100\%$, but the division of OC between OCI and OCB in our model is from aerosol transport model results [Koch, 2001] that assumed emission OC/BC ratios of 4 for fossil fuel (industrial) emissions and 7.9 for biomass burning emissions. In part because this assumed OC/BC ratio is intended to account for secondary OC formation (which is primarily of natural origin), it assigns a higher proportion of the OC to fossil fuels than estimated by most researchers. Thus as our partly subjective estimate for the effective forcing by fossil fuel OCI we take -0.10 W/m^2 .

[202] Any estimate of uncertainties is necessarily partly subjective. A formal error analysis including emissions uncertainties and the multiple steps in forcing computations would yield a large uncertainty. However, there are empirical constraints such as the AERONET observations analyzed by Sato *et al.* [2003]. Contrary to the claim of Reddy *et al.* [2005], Sato *et al.* [2003] did not filter the AERONET data with single scatter albedo retrievals. The Sato *et al.* [2003] analysis was performed on $\tau_{\text{absorption}}$ specifically to avoid such problems and it incorporated all values of $\tau_{\text{absorption}}$. Our partly subjective 1σ error estimate for BCI is $\pm 33\%$ for BCI and $\pm 50\%$ for OCI direct forcings.

[203] The soot effect on snow albedo is poorly constrained. HN cite various observations in support of their estimate of 0.17 W/m^2 . We take 0.15 W/m^2 as our central estimate and divide this 0.10 W/m^2 for fossil fuel soot and 0.05 W/m^2 for biomass burning. This subdivision is based in part on tracer transport calculations [Koch and Hansen, 2005] in which the sources of soot deposited in the Arctic and other regions were tracked. We take the efficacy of this forcing as 170%, although, as discussed above, it could be higher if the BC effect on sea ice albedo is closer to that assumed by Hansen and Nazarenko [2004]. Our subjective 1σ error estimate is $\pm 65\%$.

Table 5. Climate Forcing Estimates for Fossil Fuel and Biomass Burning Soot^a

Forcing, W/m ²	Efficacy	Effective Forcing, W/m ²
<i>Fossil Fuel Soot</i>		
BCI = +0.48	78%	+0.38 ± 0.12
OCI = -0.10	100%	-0.10 ± 0.05
BCsnow = +0.1	170%	+0.17 ± 0.10
AIEsoot		-0.20 ± 0.10
		sum +0.25 ± 0.20
<i>Biomass Burning Soot</i>		
BCB = +0.17	58%	+0.10 ± 0.05
OCB = -0.12	91%	-0.11 ± 0.05
BCsnow = +0.05	170%	+0.08 ± 0.05
AIEsoot		-0.30 ± 0.15
		sum -0.23 ± 0.17

^aBCI, black carbon industrial; OCI, organic carbon industrial; AIE, aerosol indirect effect.

[204] We have argued on several grounds that the total aerosol indirect effect is of the order of -1 W/m^2 and that most of this is via $\text{AIE}_{\text{CldCvT}}$, i.e., cloud cover change. We show elsewhere [Hansen *et al.*, 2005] that an aerosol indirect forcing of this amount yields reasonable agreement with observed climate change. The question is: how much of this indirect forcing should be “credited” to soot? On the one hand, fresh soot is not very hydrophilic and thus not a prime condensation nuclei for cloud drops. On the other hand, after hours or days, soot tends to become coated with acids and thus to become more hydrophilic. Clarke *et al.* [1997] has found cases in which most aerosols include a soot core.

[205] Lohmann *et al.* [2000] suggest that the sulfate indirect effect could be small compared with the soot indirect effect, especially when they assume external mixing. This is at least in part a result of the assumed particles sizes, $0.01 \mu\text{m}$ for BC, $0.02 \mu\text{m}$ for OC, and $0.07 \mu\text{m}$ for sulfate, which results in relatively few sulfate particles. Also, the contribution of soot to the net indirect effect may be reduced via the suggested soot particles glaciation indirect effect that reduces mid-level clouds [Lohmann, 2002].

[206] Our forcing estimate assigns 50% of the aerosol indirect effect to soot, with 20% being fossil fuel soot and 30% biomass burning soot. The larger portion for biomass is because most emission estimates have larger amounts for biomass than for industrial sources, and, unlike the case for snow albedo, the predominance of biomass aerosols in tropical regions is not a reason to downgrade their contribution. It can be argued that the proportion of the indirect aerosol effect we have assigned to soot is too large, as we have neglected the contribution of anthropogenic soil dust. Our neglect of anthropogenic soil dust is another reason to think that we have not underestimated the soot indirect effect. However, recent estimates [Tegen *et al.*, 2004; Miller *et al.*, 2004] suggest that the anthropogenic portion of soil dust is moderate, perhaps less than 10%. Our subjective 1σ error estimate for the soot indirect effect is $\pm 50\%$ of the estimated values.

[207] Table 5 summarizes our forcing estimates. The central estimate for the fossil fuel soot effective forcing is $+0.25 \text{ W/m}^2$, which is 17% of the CO_2 forcing for the same 1850–2000 period. The estimated 1σ uncertainty,

$\pm 0.20 \text{ W/m}^2$, indicates that the fossil fuel soot forcing is probably in the range between 0.05 and 0.45 W/m^2 , corresponding to 3–30% of the CO_2 forcing. The same uncertainty estimate implies that it is highly likely, but not certain, that the net fossil fuel soot forcing is positive, i.e., that it contributes to global warming. Biomass burning soot, on the other hand, almost certainly yields a negative forcing, i.e., it has a net cooling effect, as concluded by others [Penner *et al.*, 1992; Jacobson, 2004]. We refer here only to the aerosol products of biomass burning. Gaseous products of biomass burning probably cause a positive forcing [Jacobson, 2004], but steady state biomass burning should not have much effect on atmospheric gaseous composition.

[208] The calculations in Table 5 refer to an estimated average OC/BC ratio. Some fossil fuel sources of soot have a much lower OC/BC ratio [Bond *et al.*, 2004; Novakov *et al.*, 2005]. Sources with low OC/BC offer a greater potential to reduce global warming than suggested by Table 5.

8. Discussion

[209] We summarize here several inferences from the climate simulations. We encourage other uses of these systematic simulations, which are available at <http://www.giss.nasa.gov/data/efficacy>.

8.1. Climate Forcings and Effective Climate Forcings

[210] Inevitably a variety of definitions of climate forcing will be employed. That is not a problem, provided the definition is stated clearly. Interpretation of climate change studies and intercomparisons will be aided if forcings are calculated and reported for more than one forcing definition.

[211] Several forcing definitions have merit. F_a , the standard definition, is close to being a pure forcing and requires little computational effort. F_s and F_g are independent of tropopause definition and provide better indications of the climate response, although we have not been able to verify F_g results with the GISS climate model. The disadvantage of F_s and F_g is that they require climate model runs of at least several years. F_s can be readily computed for all forcing mechanisms, and it is easy to assure that the same prescription is used in different climate models. F_s^* is usually a good approximation of F_s , as shown by Tables 1–4, where F_s^* uses 10-year coupled model simulations with fixed forcing for regression of the top-of-atmosphere flux to $\Delta T_S = 0$.

[212] Table 4 shows that for practical purposes, at least for climate forcings agents of the past century, the a priori fixed SST forcing, F_s , which we defined via equation (1), serves to quantify the forcing agents of interest almost as well as the a posteriori effective climate forcing F_e . Because F_s is straightforward to compute, it is easy to assure consistency if it is applied among different climate models. Thus we suggest that F_s may provide a useful tool for comparing results of different models, as well as for analysis of climate change simulations of a given model. If F_s were computed, preferably for individual forcings as well as all forcings operating together, and made available along with results of climate simulations, it would be much more feasible to analyze and compare results from different climate models.

[213] The effective climate forcing, F_e , the product of a forcing and its efficacy, can be used for more refined

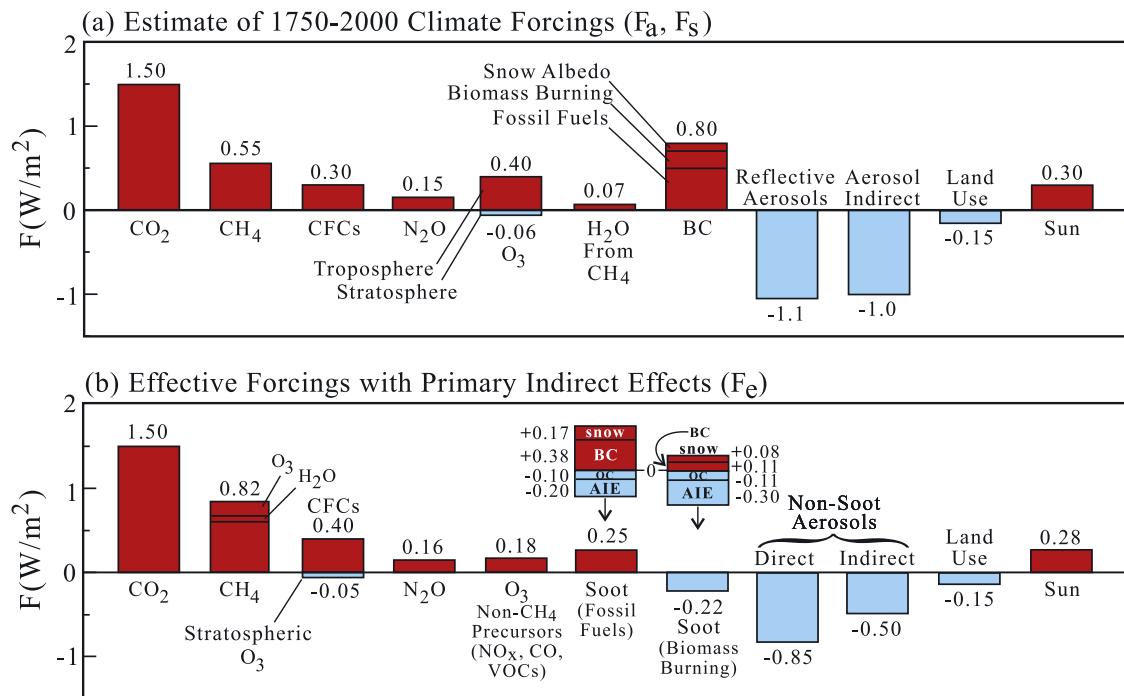


Figure 28. (a) A specific estimate of climate forcings for 1750–2000. (b) Same as Figure 28a, but with the effective forcing partially sorted by sources.

assessment of climate change mechanisms. There is merit in displaying alternative organizations of the effective forcings. At the most basic level the forcings are based on the measured or inferred changes of atmospheric composition, surface properties, and solar irradiance. At a second level some forcings are rearranged to associate indirect effects with a root cause. For example, that portion of the O₃ increase due to increased CH₄ should be associated with CH₄, and aerosol indirect effects might be apportioned among the different aerosols. A third breakdown would be in terms of emission sources, with the multiple emissions from a given source grouped together. Such successive levels of forcing assignment are necessarily approximate because of nonlinearities in combining different sources, but such estimates are needed for policy considerations.

[214] Figure 28 provides an example of the influence of “efficacies” on estimated climate forcings and the effect of grouping of forcings with major indirect effects. Figure 28a is a “plausible estimate” of forcings for the period 1750–2000 based as much as possible on measured composition changes. The reflective aerosol forcing is less than that in Table 2, in accord with recent simulations with the GISS aerosol transport model that yield smaller sulfate negative forcings (D. Koch, private communication, 2004). The 0.8 W/m^2 for BC, the same as in Hansen et al. [2002], is assumed to be 0.5 W/m^2 from fossil fuels, 0.2 W/m^2 from biomass burning, and 0.1 W/m^2 from snow albedo change. The land-use forcing is larger for 1750–2000 than that for 1880–2000 (Table 3). The net climate forcing in Figure 28a is 1.76 W/m^2 .

[215] Figure 28b shows the effective forcings, i.e., after multiplication by efficacies. The total effective forcing, 1.82 W/m^2 , is practically unchanged by the efficacies as some forcings increased and others decreased. Figure 28b

also groups some indirect effects. Figure 28b does a better job than Figure 28a of making clear the practical significance of different forcing mechanisms. CH₄ is shown to be a major positive (warming) forcing, while the net forcing by soot is much smaller than the positive component from the direct BC effect. Figure 28b makes clear that CH₄, not soot, is the second largest contributor to global warming. However, in interpreting the importance of soot as a climate forcing, bear in mind that one source of soot can provide a very different net forcing than another source, as discussed below.

[216] Which climate forcing definition is most appropriate for use in policy discussions about long-term climate change? As we move along the chain from Fi to Fe, we expect the forcing to provide a better and better indication of the climate impact of the forcing. However, the further we go along that chain the more feedbacks and thus the more model dependence we have introduced; also the computational burden increases. A practical criterion might be when we have reached a point such that the forcing is not qualitatively misleading about the climate impact and the quantitative result is within the range of other uncertainties, for example, uncertainties due to model dependence. Fa apparently fails this criterion for BC aerosols and O₃. We suggest that Fs is probably sufficient, although a case could also be made for Fe, and in either case we suggest that straightforward indirect effects, such as O₃ and stratospheric H₂O produced by CH₄, should be added to the direct forcing.

8.2. Climate Sensitivity Versus Forcing

[217] The greater variability of climate in colder periods during the Pleistocene [Alley et al., 1995; Petit et al., 1999] might encourage the notion that climate sensitivity decreases as the Earth becomes warmer. Although formation of

continental ice sheets on long timescales can produce a dominant climate feedback, our climate model suggests that climate sensitivity associated with the combination of all fast feedback processes (water vapor, clouds, sea ice) may actually increase as global warming increases. This matter is relevant to anthropogenic global warming as well as interpretation of warm climates in the Earth's past, such as the Pliocene.

[218] The efficacy curve for the Earth must have an overall U-shape, with sharp upturns to snowball Earth on the left side and runaway greenhouse on the right. Our calculations for a range of CO₂ forcings (Figure 25) suggest that the present climate of the Earth is near the minimum that must exist between the two instabilities (though it is conceivable that there are multiple relative minima between the extremes). There is evidence in geologic data that the Earth was far to the left of the minimum about 500–700 million years ago, and indeed the Earth plunged into the snowball Earth state (*Chandler and Sohl* [2000] have argued that “slushball” would be a more accurate description) but managed to escape, probably with the help of continued volcanic emissions of greenhouse gases during the snowball state [*Hoffman et al.*, 1998; *Hoffman and Schrag*, 2002]. The luminosity of the sun has subsequently increased ~6%, so it is unlikely that the Earth could return to the snowball state. However, the luminosity of the sun, a main sequence star, will continue to increase as it ages toward the red giant state [*Jastrow*, 1967]. Thus it would be interesting to fill out the efficacy diagram (Figure 25) to its full range, allowing prediction of the date of the Earth's runaway greenhouse demise, a state from which there is no escape.

[219] Although Figure 25 suggests that the Earth is on a flat portion of the efficacy diagram, GISS model II [*Hansen et al.*, 1983] had climate sensitivity increasing toward negative forcings (RFCR). In our transient simulations for 1880–2003 submitted to IPCC, sea ice change is smaller than suggested by limited observations. Thus it is uncertain whether the positive slope of efficacy versus forcing in Figure 25 is representative of the present state of the real world. It would be informative to see results from other GCMs analogous to our Figure 25, and to analyze the contributions of the primary feedbacks. However, regardless of the precise value of the sea ice feedback, Figure 25 does not support the notion that the Earth, being in a warm interglacial period, is therefore in a relatively stable climate state. Indeed, it seems likely that, as global warming continues, the Earth will move toward a steeper positive gradient of the efficacy curve.

[220] This discussion refers to the usual definition of climate sensitivity [*Charney*, 1979], which includes only fast feedback processes. As noted in section 6.2, ice sheets are treated as a feedback in some discussions about climate change on long timescales. In that case the inferred climate sensitivity is larger [*Lea*, 2004] and the shape of the efficacy curve versus forcing would also change.

8.3. Methane

[221] The importance of CH₄ as a forcing of global warming is enhanced by its efficacy, $E_a \sim 110\%$, as well as by its indirect effects via stratospheric H₂O and tropo-

spheric O₃. These indirect effects increase the practical efficacy of CH₄ to ~145%. The CH₄ forcing between 1750 and 2000 is thus ~0.8 W/m², about 50% of the CO₂ forcing.

[222] *Hansen and Sato* [2004] point out that a decrease of non-CO₂ forcings by 0.5 W/m², as opposed to the typical projection of an increase by ~0.5 W/m² [*IPCC*, 2001], makes a huge difference in the plausibility of avoiding dangerous anthropogenic global warming. We suggest that the potential effectiveness of CH₄ in alleviating global warming is not always fully appreciated and that CH₄ should receive greater weight in strategies for slowing global warming.

8.4. Soot

[223] Evaluation of soot climate forcing is difficult because the amount and spatial distribution of soot is not well measured, the forcing depends strongly on aerosol location, especially its altitude, internal mixing of aerosols alters the forcing, and there are large poorly known indirect effects of soot on snow albedo and cloud properties.

[224] Despite these complications, we conclude that, on average, fossil fuel soot provides a positive forcing, while biomass burning soot produces a negative forcing. Thus reduction of fossil fuel soot, in and of itself, could help slow global warming. Actions to reduce soot that also reduce sulfate aerosols require further assessment to determine the net climate effect. However, if sulfate reductions are being pursued in any case, reduction of soot can ameliorate the warming effect from reduced sulfates.

[225] Furthermore, our estimate of effective forcing is calculated for a mean OM/BC ratio ~3.4 (OC/BC ~ 2.6) for fossil fuels. This ratio may exaggerate the OC contribution [*Novakov et al.*, 2005], and in any case certain sources of soot have much smaller OC/BC, e.g., emissions from diesel fuels have OC/BC as small as 1 or less [*Bond et al.*, 2004]. Reduction of such soot sources has the potential to reduce global warming. The effect for a specific source can be quantified by adjusting the OC contribution in Table 5 appropriately. The resulting soot forcing must be multiplied by the fraction of global BC emissions represented by that source.

8.5. Regional Climate Change

[226] Many climate forcings produce unique regional responses that must be investigated on a case-by-case basis. Land use changes [*Myhre and Myhre*, 2003; *Matthews et al.*, 2003] and heavy regional aerosol pollution [*Ramanathan et al.*, 2001; *Menon et al.*, 2002b] are two examples. Nevertheless, we find that most forcings tend to evoke a response of global climate characteristics, such as the mean meridional circulation, in proportion to the effective forcing. We suggest that the net effective climate forcing, and thus global temperature change, have merit as simple metrics of global climate change with relevance even to some aspects of regional climate change.

[227] We note that global warming is attended by increased intensity of the Hadley circulation, with greater rainfall in the ITCZ and more intense drying in the subtropics. These effects of increasing greenhouse gases survive the addition of other known climate forcings in our climate simulations.

[228] A practical implication is that global warming is likely to cause increased drought in the Southwest United States, the Mediterranean region, the Middle East, and an expanding Sahelian region in Africa, and increased rainfall in the Eastern United States. This model result is consistent with empirical evidence of strong droughts in the Southwest United States during past warm climates [Cook *et al.*, 2004]. As the importance of greenhouse gases relative to aerosols increases, we expect that these climate tendencies may become more apparent.

[229] One region that we find to be particularly susceptible to regional forcings is the Arctic (section 4.2). Climate response to anthropogenic ozone change and snow albedo change is concentrated in the Arctic and may be responsible for a substantial fraction of observed warming and sea ice loss. This suggests that reductions of these air pollutants, and their precursors, especially methane, may be an essential component of an effective strategy to slow anthropogenic climate change in the Arctic.

[230] **Acknowledgments.** We thank Andy Ackerman, Matt Barlow, David Fahey, Mark Jacobson, Ben Johnson, David Lea, Ulrike Lohmann, Phil Mote, Joyce Penner, Bill Randel, Alan Robock, Glenn Shaw, Keith Shine, and Nicola Stuber for data and comments on a draft manuscript, Darnell Cain and Lilly DelValle for technical assistance, and NASA Earth Science Research Division managers Jack Kaye, Don Anderson, Phil DeCola, Tsengdar Lee, and Eric Lindstrom, and Hal Harvey of the Hewlett Foundation for research support.

References

- Ackerman, A. S., O. B. Toon, D. E. Stevens, A. J. Heymsfield, V. Ramanathan, and E. J. Welton (2000), Reduction of tropical cloud cover by soot, *Science*, **288**, 1042–1047.
- Ackerman, A. S., M. P. Kirkpatrick, D. E. Stevens, and O. B. Toon (2004), The impact of humidity above stratiform clouds on indirect aerosol climate forcing, *Nature*, **432**, 1014–1017.
- Albrecht, B. A. (1989), Aerosols, cloud microphysics, and fractional cloudiness, *Science*, **245**, 1227–1230.
- Alley, R. B., A. J. Gow, S. J. Johnson, J. Kipfstuhl, D. A. Meese, and T. Thorsteinsson (1995), Comparison of deep ice cores, *Nature*, **373**, 393–394.
- Andronova, N. G., E. V. Rozanov, F. Yang, M. E. Schlesinger, and G. L. Stenchikov (1999), Radiative forcing by volcanic aerosols from 1850 to 1994, *J. Geophys. Res.*, **104**, 16,807–16,826.
- Baumgardner, D., G. Kok, and G. Raga (2004), Warming of the Arctic lower stratosphere by light absorbing particles, *Geophys. Res. Lett.*, **31**, L06117, doi:10.1029/2003GL018883.
- Betts, R. A. (2001), Biogeophysical impacts of land use on present-day climate: Near-surface temperature and radiative forcing, *Atmos. Sci. Lett.*, **2**, 39–51.
- Bleck, R. (2002), An oceanic general circulation model framed in hybrid isopycnic-Cartesian coordinates, *Ocean Modell.*, **4**, 55–88.
- Bohren, C. F. (1986), Applicability of effective-medium theories to problems of scattering and absorption by nonhomogeneous atmospheric particles, *J. Atmos. Sci.*, **43**, 468–475.
- Bond, T. C., D. G. Streets, K. F. Yarber, S. M. Nelson, J. H. Woo, and Z. Klimot (2004), A technology-based global inventory of black and organic carbon emissions from combustion, *J. Geophys. Res.*, **109**, D14203, doi:10.1029/2003JD003697.
- Boucher, O., and M. Pham (2002), History of sulfate aerosol radiative forcings, *Geophys. Res. Lett.*, **29**(9), 1308, doi:10.1029/2001GL014048.
- Brovkin, V., S. Sitch, W. Von Bloh, M. Claussen, E. Bauer, and W. Cramer (2004), Role of land cover changes for atmospheric CO₂ increase and climate change during the last 150 years, *Global Change Biol.*, **10**, 1253–1266, doi:10.1111/j.1365-2486.2004.00812.x.
- Budyko, M. I. (1969), The effect of solar radiation variations on the climate of the earth, *Tellus*, **21**, 611–619.
- Chandler, M. A., and L. E. Sohl (2000), Climate forcings and the initiation of low-latitude ice sheets during the Neoproterozoic Varanger glacial interval, *J. Geophys. Res.*, **105**, 20,737–20,756.
- Charney, J. (1979), *Carbon Dioxide and Climate: A Scientific Assessment*, 33 pp., Natl. Acad. Sci. Press, Washington, D. C.
- Cheng, Y., V. M. Canuto, and A. M. Howard (2002), An improved model for the turbulent PBL, *J. Atmos. Sci.*, **59**, 1550–1565.
- Christiansen, B. (1999), Radiative forcing and climate sensitivity: The ozone experience, *Q. J. R. Meteorol. Soc.*, **125**, 3011–3035.
- Chylek, P., G. Videen, D. Ngo, R. G. Pinnick, and J. D. Klett (1995), Effect of black carbon on the optical properties and climate forcing of sulfate aerosols, *J. Geophys. Res.*, **100**, 16,325–16,332.
- Chylek, P., S. G. Jennings, and R. Pinnick (2003), Soot, in *Encyclopedia of Atmospheric Sciences*, edited by J. R. Holton, Elsevier, New York.
- Clarke, A. D., and K. J. Noone (1985), Soot in the Arctic snowpack: A cause for perturbations in radiative transfer, *Atmos. Environ.*, **19**, 2045–2053.
- Clarke, A. D., T. Uehara, and J. N. Porter (1997), Atmospheric nuclei and related aerosol fields over the Atlantic: Clean subsiding air and continental pollution during ASTEX, *J. Geophys. Res.*, **102**, 25,281–25,292.
- Cohen, J., and M. Barlow (2005), The NAO, the AO, and global warming: How closely related?, *J. Clim.*, in press.
- Cook, E. R., C. Woodhouse, C. M. Eakin, D. M. Meko, and D. W. Stahle (2004), Long-term aridity changes in the western United States, *Science*, **306**, 1015–1018.
- Cook, J., and E. J. Highwood (2004), Climate response to absorbing aerosols in an Intermediate General Circulation Model, *Q. J. R. Meteorol. Soc.*, **130**, 175–191.
- Del Genio, A. D., W. Kovari, M. S. Yao, and J. Jonas (2005), Cumulus microphysics and climate sensitivity, *J. Clim.*, in press.
- Dickinson, R. E. (1975), Solar variability and the lower atmosphere, *Bull. Am. Meteorol. Soc.*, **36**, 1240–1248.
- Feichter, J., E. Roeckner, U. Lohmann, and B. Liepert (2004), Nonlinear aspects of the climate response to greenhouse gas and aerosol forcing, *J. Clim.*, **17**, 2384–2398.
- Fleming, E. L., C. H. Jackman, R. S. Stolarski, and D. B. Considine (1999), Simulation of stratospheric tracers using an improved empirically based two-dimensional model transport formulation, *J. Geophys. Res.*, **104**, 23,911–23,934.
- Forster, P. M. F. (1999), Radiative forcing due to stratospheric ozone changes 1979–1997, using updated trend estimates, *J. Geophys. Res.*, **104**, 24,395–24,399.
- Forster, P. M. F., and K. P. Shine (1997), Radiative forcing and temperature trends from stratospheric ozone changes, *J. Geophys. Res.*, **102**, 10,841–10,855.
- Forster, P. M. F., and K. P. Shine (1999), Stratospheric water vapor changes as a possible contributor to observed stratospheric cooling, *Geophys. Res. Lett.*, **26**, 3309–3312.
- Forster, P. M. F., and K. P. Shine (2002), Assessing the climate impact of trends in stratospheric water vapor, *Geophys. Res. Lett.*, **29**(6), 1086, doi:10.1029/2001GL013909.
- Forster, P. M. F., R. S. Freckleton, and K. P. Shine (1997), On aspects of the concept of radiative forcing, *Clim. Dyn.*, **13**, 547–560.
- Forster, P. M. F., M. Blackburn, R. Glover, and K. P. Shine (2000), An examination of climate sensitivity for idealized climate change experiments in an intermediate general circulation model, *Clim. Dyn.*, **16**, 833–849.
- Gent, P. R., J. Willebrand, T. J. McDougall, and J. C. McWilliams (1995), Parameterizing eddy-induced tracer transports in ocean circulation models, *J. Phys. Oceanogr.*, **25**, 463–474.
- Gillett, N. P., M. F. Wehner, S. F. B. Tett, and A. J. Weaver (2004), Testing the linearity of the response to combined greenhouse gas and sulfate aerosol forcing, *Geophys. Res. Lett.*, **31**, L14201, doi:10.1029/2004GL020111.
- Gregory, J. M., W. J. Ingram, M. A. Palmer, G. S. Jones, P. A. Stott, R. B. Thorpe, J. A. Lowe, T. C. Johns, and K. D. Williams (2004), A new method for diagnosing radiative forcing and climate sensitivity, *Geophys. Res. Lett.*, **31**, L03205, doi:10.1029/2003GL018747.
- Grenfell, T. C., B. Light, and B. Sturm (2002), Spatial distribution and radiative effects of soot in the snow and sea ice during the SHEBA experiment, *J. Geophys. Res.*, **107**(C10), 8032, doi:10.1029/2000JC000414.
- Griffies, S. M. (1998), The Gent-McWilliams skew flux, *J. Phys. Oceanogr.*, **28**, 831–841.
- Gultepe, I., and G. A. Isaac (1999), Scale effects on averaging cloud droplet and aerosol number concentrations: observations and models, *J. Clim.*, **12**, 1268–1279.
- Haigh, J. D. (1994), The role of stratospheric ozone in modulating the solar radiative forcing of climate, *Nature*, **370**, 544–546.
- Haigh, J. D. (1999), Modelling the impact of solar variability on climate, *J. Atmos. Sol. Terr. Phys.*, **61**, 63–72.
- Hansen, J. (2002), Air pollution as a climate forcing, 169 pp., NASA Goddard Inst. for Space Stud., New York.
- Hansen, J. (2004), Defusing the global warming time bomb, *Sci. Am.*, **290**, 68–77.
- Hansen, J., and L. Nazarenko (2004), Soot climate forcing via snow and ice albedos, *Proc. Natl. Acad. Sci.*, **101**, 423–428.

- Hansen, J., and M. Sato (2004), Greenhouse gas growth rates, *Proc. Natl. Acad. Sci.*, *101*, 16,109–16,114.
- Hansen, J., W. C. Wang, and A. A. Lacis (1978), Mount Agung eruption provides test of a global climate perturbation, *Science*, *199*, 1065–1068.
- Hansen, J., D. Johnson, A. Lacis, S. Lebedeff, P. Lee, D. Rind, and G. Russell (1981), Climate impact of increasing atmospheric carbon dioxide, *Science*, *213*, 957–966.
- Hansen, J., G. Russell, D. Rind, P. Stone, A. Lacis, S. Lebedeff, R. Ruedy, and L. Travis (1983), Efficient three-dimensional global models for climate studies: Models I and II, *Mon. Weather Rev.*, *111*, 609–662.
- Hansen, J., A. Lacis, D. Rind, G. Russell, P. Stone, I. Fung, R. Ruedy, and J. Lerner (1984), Climate sensitivity: Analysis of feedback mechanisms, in *Climate Processes and Climate Sensitivity*, *Geophys. Monogr. Ser.*, vol. 29, edited by J. E. Hansen and T. Takahashi, pp. 130–163, AGU, Washington, D. C.
- Hansen, J., A. Lacis, R. Ruedy, M. Sato, and H. Wilson (1993), How sensitive is the world's climate?, *Natl. Geogr. Res. Explor.*, *9*, 142–158.
- Hansen, J., M. Sato, and R. Ruedy (1995), Long-term changes of the diurnal temperature cycle: Implications about mechanisms of global climate change, *Atmos. Res.*, *37*, 175–209.
- Hansen, J., et al. (1996), A Pinatubo climate modeling investigation, in *Global Environment Change*, edited by G. Fiocco, D. Fua, and G. Visconti, *NATO ASI Ser., Ser. 1*, *42*, 233–272.
- Hansen, J., M. Sato, and R. Ruedy (1997a), Radiative forcing and climate response, *J. Geophys. Res.*, *102*, 6831–6864.
- Hansen, J., et al. (1997b), Forcings and chaos in interannual to decadal climate change, *J. Geophys. Res.*, *102*, 25,679–25,720.
- Hansen, J., M. Sato, A. Lacis, and R. Ruedy (1997c), The missing climate forcing, *Philos. Trans. R. Soc. London B*, *352*, 231–240.
- Hansen, J., M. Sato, A. Lacis, R. Ruedy, I. Tegen, and E. Matthews (1998), Climate forcings in the Industrial Era, *Proc. Natl. Acad. Sci. U. S. A.*, *95*, 12,753–12,758.
- Hansen, J., M. Sato, R. Ruedy, A. Lacis, and V. Oinas (2000), Global warming in the twenty-first century: An alternative scenario, *Proc. Natl. Acad. Sci. U. S. A.*, *97*, 9875–9880.
- Hansen, J., et al. (2002), Climate forcings in Goddard Institute for Space Studies SI2000 simulations, *J. Geophys. Res.*, *107*(D18), 4347, doi:10.1029/2001JD001143.
- Hansen, J., T. Bond, B. Cairns, H. Gaeggler, B. Liepert, T. Novakov, and B. Schichtel (2004), Carbonaceous aerosols in the Industrial Era, *Eos Trans. AGU*, *85*, 241, 244.
- Hansen, J., et al. (2005), Earth's energy imbalance: Confirmation and implications, *Science*, *308*, 1431–1435, doi:10.1126/science.1110252.
- Henderson-Sellers, A., and V. Gornitz (1984), Possible climatic impacts of land cover transformations with particular emphasis on tropical deforestation, *Clim. Change*, *6*, 231–257.
- Hoffert, M. I., and C. Covey (1992), Deriving global climate sensitivity from paleoclimate reconstructions, *Nature*, *360*, 573–576.
- Hoffman, P. F., and D. P. Schrag (2002), The snowball Earth hypothesis: Testing the limits of global change, *Terra Nova*, *14*, 129–155.
- Hoffman, P. F., A. J. Kaufman, G. P. Halverson, and D. P. Schrag (1998), A neoproterozoic snowball Earth, *Science*, *281*, 1342–1346.
- Ingersoll, A. P. (1969), The runaway greenhouse: A history of water on Venus, *J. Atmos. Sci.*, *26*, 1191–1198.
- Intergovernmental Panel on Climate Change (IPCC) (2001), *Climate Change 2001: The Scientific Basis*, edited by J. T. Houghton et al., Cambridge Univ. Press, New York.
- Jacobson, M. Z. (2001), Strong radiative heating due to the mixing state of black carbon in atmospheric aerosols, *Nature*, *409*, 695–697.
- Jacobson, M. Z. (2004), The short-term cooling but long-term warming due to biomass burning, *J. Clim.*, *17*, 2909–2926.
- Jain, A. K., B. P. Briegleb, K. Minschwaner, and D. J. Wuebbles (2000), Radiative forcings and global warming potentials of 39 greenhouse gases, *J. Geophys. Res.*, *105*, 20,773–20,790.
- Jastrow, R. (1967), *Red Giants and White Dwarfs*, 176 pp., HarperCollins, New York.
- Jensen, E., and O. Toon (1994), Ice nucleation in upper troposphere: Sensitivity to aerosol number density, temperature, and cooling rate, *Geophys. Res. Lett.*, *21*, 2019–2022.
- Johnson, B. T. (2005), The semi-direct aerosol effect: Comparison of a single column model with large-eddy simulation for marine stratocumulus, *J. Clim.*, *18*, 119–130.
- Johnson, B. T., K. P. Shine, and P. M. Forster (2004), The semi-direct aerosol effect: Impact of absorbing aerosols on marine stratocumulus, *Q. J. R. Meteorol. Soc.*, *130*, 1407–1422.
- Joshi, M., K. Shine, M. Ponater, N. Stuber, R. Sausen, and L. Li (2003), A comparison of climate response to different radiative forcings in three general circulation models: Towards an improved metric of climate change, *Clim. Dyn.*, *20*, 843–854.
- Kaufman, Y. J., I. Koren, L. A. Remer, D. Rosenfeld, and Y. Rudich (2005), The effect of smoke, dust, and pollution aerosol on shallow cloud development over the Atlantic Ocean, *Proc. Natl. Acad. Sci.*, *102*, 11,207–11,212.
- Kerr, R. (2004), Three degrees of consensus, *Science*, *305*, 932–933.
- Klein Goldewijk, K. (2001), Estimating global land use change over the past 300 years: The HYDE database, *Global Biogeochem. Cycles*, *15*, 417–433.
- Koch, D. (2001), Transport and direct radiative forcing of carbonaceous and sulfate aerosols in the GISS GCM, *J. Geophys. Res.*, *106*, 20,311–20,332.
- Koch, D., and J. Hansen (2005), Distant origins of Arctic black carbon: A Goddard Institute for Space Studies ModelE experiment, *J. Geophys. Res.*, *110*, D04204, doi:10.1029/2004JD005296.
- Koch, D., D. Jacob, I. Tegen, D. Rind, and M. Chin (1999), Tropospheric sulfur simulation and sulfate direct radiative forcing in the Goddard Institute for Space Studies general circulation model, *J. Geophys. Res.*, *104*, 23,799–23,822.
- Lacis, A. A., and V. Oinas (1991), A description of the correlated k-distribution method for modeling nongrey gaseous absorption, thermal emission, and multiple scattering in vertically inhomogeneous atmospheres, *J. Geophys. Res.*, *96*, 9027–9063.
- Lacis, A. A., D. J. Wuebbles, and J. A. Logan (1990), Radiative forcing of climate by changes of the vertical distribution of ozone, *J. Geophys. Res.*, *95*, 9971–9981.
- Lacis, A. A., J. Hansen, and M. Sato (1992), Climate forcing by stratospheric aerosols, *Geophys. Res. Lett.*, *19*, 1607–1610.
- Lacis, A. A., B. E. Carlson, and J. E. Hansen (2000), Retrieval of atmospheric N₂O, O₃, aerosol optical depth, effective radius and variance information from SAGE II multispectral extinction measurements, *Appl. Math. Comput.*, *116*, 133–151.
- Large, W. G., J. C. McWilliams, and S. C. Doney (1994), Oceanic vertical mixing: a review and a model with a nonlocal boundary layer parameterization, *Rev. Geophys.*, *32*, 363–403.
- Lea, D. W. (2004), The 100 000-yr cycle in tropical SST, greenhouse forcing, and climate sensitivity, *J. Clim.*, *17*, 2170–2179.
- Lean, J. (2000), Evolution of the sun's spectral irradiance since the Maunder Minimum, *Geophys. Res. Lett.*, *27*, 2425–2428.
- Liao, H., J. H. Seinfeld, P. J. Adams, and L. J. Mickley (2004), Global radiative forcing of coupled tropospheric ozone and aerosols in a unified general circulation model, *J. Geophys. Res.*, *109*, D16207, doi:10.1029/2003JD004456.
- Liu, J., G. A. Schmidt, D. G. Martinson, D. Rind, G. L. Russell, and X. Yuan (2003), Sensitivity of sea ice to physical parameterizations in the GISS global climate model, *J. Geophys. Res.*, *108*(C2), 3053, doi:10.1029/2001JC001167.
- Lohmann, U. (2002), A glaciation indirect aerosol effect caused by soot aerosols, *Geophys. Res. Lett.*, *29*(4), 1052, doi:10.1029/2001GL014357.
- Lohmann, U., and J. Feichter (2005), Global indirect aerosol effects: A review, *Atmos. Chem. Phys.*, *5*, 715–737.
- Lohmann, U., and G. Lesins (2002), Stronger constraints on the anthropogenic indirect aerosol effect, *Science*, *299*, 1012–1015.
- Lohmann, U., J. Feichter, J. E. Penner, and R. Leaitch (2000), Indirect effect of sulfate and carbonaceous aerosols: A mechanistic treatment, *J. Geophys. Res.*, *105*, 12,193–12,206.
- Lovelock, J. E., R. J. Maggs, and R. A. Rasmussen (1972), Atmospheric dimethyl sulphide and the natural sulphur cycle, *Nature*, *237*, 452–453.
- Manabe, S., and R. T. Wetherald (1975), The effects of doubling the CO₂ concentration on the climate of a general circulation model, *J. Atmos. Sci.*, *32*, 3–15.
- Mann, M. E., M. A. Cane, S. E. Zebiak, and A. Clement (2005), Volcanic and solar forcing of the tropical Pacific over the past 1000 years, *J. Clim.*, *18*, 447–456.
- Manney, G. L., K. Kruger, J. L. Sabutis, S. A. Sena, and S. Pawson (2005), The remarkable 2003–2004 winter and other recent warm winters in the Arctic stratosphere since the late 1990s, *J. Geophys. Res.*, *110*, D04107, doi:10.1029/2004JD005367.
- Matthews, H. D., A. J. Weaver, M. Eby, and K. J. Meissner (2003), Radiative forcing of climate by historical land cover change, *Geophys. Res. Lett.*, *30*(2), 1055, doi:10.1029/2002GL016098.
- Matthews, H. D., A. J. Weaver, K. J. Meissner, N. P. Gillett, and M. Eby (2004), Natural and anthropogenic climate change: Incorporating historical land cover change, vegetation dynamics and the global carbon cycle, *Clim. Dyn.*, *22*, 461–479.
- McCormick, M. P., L. W. Thomason, and C. R. Trepte (1995), Atmospheric effects of Mt. Pinatubo eruption, *Nature*, *373*, 399–404.
- Menon, S., and A. Del Genio (2005), Evaluating the impacts of carbonaceous aerosols on clouds and climate, in *Human-Induced Climate Change: An Interdisciplinary Assessment*, edited by M. E. Schlesinger et al., Cambridge Univ. Press, New York, in press.

- Menon, S., A. D. Del Genio, D. Koch, and G. Tselioudis (2002a), GCM simulations of the aerosol indirect effect: Sensitivity to cloud parameterization and aerosol burden, *J. Atmos. Sci.*, *59*, 692–713.
- Menon, S., J. Hansen, L. Nazarenko, and Y. Luo (2002b), Climate effects of black carbon aerosols in China and India, *Science*, *297*, 2250–2253.
- Mickley, L. J., D. J. Jacob, and D. Rind (2001), Uncertainty in preindustrial abundance of tropospheric ozone: Implications for radiative forcing calculations, *J. Geophys. Res.*, *106*, 3389–3399.
- Mickley, L. J., D. J. Jacob, B. D. Field, and D. Rind (2004), Climate response to the increase in tropospheric ozone since preindustrial times: A comparison between ozone and equivalent CO₂ forcings, *J. Geophys. Res.*, *109*, D05106, doi:10.1029/2003JD003653.
- Miller, R. L., I. Tegen, and J. Perlwitz (2004), Surface radiative forcing by soil dust aerosols and the hydrologic cycle, *J. Geophys. Res.*, *109*, D04203, doi:10.1029/2003JD004085.
- Minnis, P., J. K. Ayers, R. Palikonda, and D. Phan (2004), Contrails, cirrus trends, and climate, *J. Clim.*, *17*, 1671–1685.
- Minschwaner, K., R. W. Carver, B. P. Briegleb, and A. E. Roche (1998), Infrared radiative forcing and atmospheric lifetimes of trace species based on observations from UARS, *J. Geophys. Res.*, *103*, 23,243–23,253.
- Mishchenko, M. I., B. Cairns, J. E. Hansen, L. D. Travis, R. Burg, Y. J. Kaufman, J. V. Martins, and E. P. Shettle (2004), Monitoring of aerosol forcing of climate from space: Analysis of measurement requirements, *J. Quant. Spectrosc. Radiat. Transfer*, *88*, 149–161.
- Mitchell, T. D., T. R. Carter, P. D. Jones, M. Hulme, and M. New (2004), A comprehensive set of high-resolution grids of monthly climate for Europe and the globe: The observed record (1901–2000) and 16 scenarios (2001–2100), *Tyndall Working Pap.*, *55*, 30 pp. (Available at <http://www.tyndall.ac.uk>)
- Myhre, G., and A. Myhre (2003), Uncertainties in radiative forcing due to surface albedo changes caused by land use changes, *J. Clim.*, *16*, 1511–1524.
- Novakov, T., S. Menon, T. Kirchstetter, D. Koch, and J. Hansen (2005), Aerosol organic carbon to black carbon ratios: Analysis of published data and implications for climate forcing, *J. Geophys. Res.*, doi:10.1029/2005JD005977, in press.
- Oinas, V., A. A. Lacis, D. Rind, D. Shindell, and J. E. Hansen (2001), Radiative cooling by stratospheric water vapor: Big differences in GCM results, *Geophys. Res. Lett.*, *28*, 2791–2794.
- Overland, J. E., and M. Wang (2005), The Arctic climate paradox: The recent decrease of the Arctic Oscillation, *Geophys. Res. Lett.*, *32*, L06701, doi:10.1029/2004GL021752.
- Penner, J. E. (2001), Aerosols, their direct and indirect effects, chap. 5, pp. 289–348, in *Climate Change 2001: The Scientific Basis*, edited by J. T. Houghton et al., Cambridge Univ. Press, New York.
- Penner, J. E., R. E. Dickinson, and C. A. O'Neill (1992), Effects of aerosol from biomass burning on the global radiation budget, *Science*, *256*, 1432–1434.
- Penner, J. E., D. H. Lister, D. J. Griggs, D. J. Dokken, and M. McFarland (Eds.) (1999), *Aviation and the Global Atmosphere*, 373 pp., Cambridge Univ. Press, New York.
- Penner, J. E., S. Y. Zhang, and C. C. Chuang (2003), Soot and smoke may not warm climate, *J. Geophys. Res.*, *108*(D21), 4657, doi:10.1029/2003JD003409.
- Petit, J. R., et al. (1999), 420,000 years of climate and atmospheric history revealed by the Vostok deep Antarctic ice core, *Nature*, *399*, 429–436.
- Ponater, M., S. Marquart, R. Sausen, and U. Schumann (2005), On contrail climate sensitivity, *Geophys. Res. Lett.*, *32*, L10706, doi:10.1029/2005GL022580.
- Prather, M., and D. Ehhalt (2001), Atmospheric chemistry and greenhouse gases, chap. 4, pp. 239–287, in *Climate Change 2001: The Scientific Basis*, edited by J. T. Houghton et al., Cambridge Univ. Press, New York.
- Quass, J., O. Boucher, and F. M. Breon (2004), Aerosol indirect effects in POLDER satellite data and the Laboratoire de Meteorologie Dynamique-Zoom (LMDZ) general circulation model, *J. Geophys. Res.*, *109*, D08205, doi:10.1029/2003JD004317.
- Ramanathan, V., P. J. Crutzen, J. T. Kiehl, and D. Rosenfeld (2001), Aerosols, climate, and the hydrological cycle, *Science*, *294*, 2119–2124.
- Ramankutty, N., and J. A. Foley (1999), Estimating historical changes in global land cover: Croplands from 1700 to 1992, *Global Biogeochem. Cycles*, *13*, 997–1027.
- Ramaswamy, V., et al. (2001), Radiative forcing of climate change, chap. 6, pp. 349–416, in *Climate Change 2001: The Scientific Basis*, edited by J. T. Houghton et al., Cambridge Univ. Press, New York.
- Randel, W. J., and F. Wu (1999), A stratospheric ozone trends data set for global modeling studies, *Geophys. Res. Lett.*, *26*, 3089–3092.
- Randel, W. J., F. Wu, A. Gettelman, J. M. Russell, J. M. Zawodny, and S. J. Oltmans (2001), *J. Geophys. Res.*, *106*, 14,313–14,325.
- Reddy, M. S., O. Boucher, N. Bellouin, M. Schulz, Y. Balkanski, J. L. Dufresne, and M. Phan (2005), Estimates of global multicomponent aerosol optical depth and direct radiative perturbation in the Laboratoire de Meteorologie Dynamique general circulation model, *J. Geophys. Res.*, *110*, D10S16, doi:10.1029/2004JD004757.
- Reichler, T., M. Dameris, R. Sausen, and D. Nodorp (1996), A global climatology of the tropopause height based on ECMWF analyses, *Inst. Phys. Atmos. Rep.* *57*, 23 pp., Dtsch. Forsch. fur Luft und Raumfahrt, Wessling, Germany.
- Rind, D., P. Lonergan, and K. Shah (2000), Modeled impact of cirrus cloud increases along aircraft flight paths, *J. Geophys. Res.*, *105*, 19,927–19,940.
- Roberts, D. L., and A. Jones (2004), Climate sensitivity to black carbon aerosol from fossil fuel combustion, *J. Geophys. Res.*, *109*, D16202, doi:10.1029/2004JD004676.
- Robock, A. (2000), Volcanic eruptions and climate, *Rev. Geophys.*, *38*, 191–219.
- Rosenlof, K. H., et al. (2001), Stratospheric water vapor increases over the past half-century, *Geophys. Res. Lett.*, *28*, 1195–1198.
- Rothrock, D. A., Y. Yu, and G. A. Maykut (1999), Thinning of the arctic sea ice cover, *Geophys. Res. Lett.*, *26*, 3469–3472.
- Rotstajn, L. D., and J. E. Penner (2001), Indirect aerosol forcing, quasi forcing and climate response, *J. Clim.*, *20*, 2960–2975.
- Russell, G. L., J. R. Miller, and D. H. Rind (1995), A coupled atmosphere-ocean model for transient climate change, *Atmos. Ocean*, *33*, 683–730.
- Russell, P. B., et al. (1996), Global to microscale evolution of the Pinatubo volcanic aerosol derived from diverse measurements and analyses, *J. Geophys. Res.*, *101*, 18,745–18,763.
- Sagan, C., O. B. Toon, and J. Pollack (1979), Anthropogenic albedo changes and Earth's climate, *Science*, *206*, 1363–1368.
- Sato, M., J. Hansen, M. P. McCormick, and J. P. Pollack (1993), Stratospheric aerosol optical depths, 1850–1990, *J. Geophys. Res.*, *98*, 22,987–22,994.
- Sato, M., J. Hansen, D. Koch, A. Lacis, R. Ruedy, O. Dubovik, B. Holben, M. Chin, and T. Novakov (2003), Global atmospheric black carbon inferred from AERONET, *Proc. Natl. Acad. Sci.*, *100*, 6319–6324.
- Schmidt, G. A., et al. (2005), Present day atmospheric simulations using GISS ModelE: Comparison to in-situ, satellite and reanalysis data, *J. Clim.*, in press.
- Schnaiter, M., C. Linke, O. Mohler, K. H. Naumann, H. Saathoff, R. Wagner, and U. Schurath (2005), Absorption amplification of black carbon internally mixed with secondary organic aerosol, *J. Geophys. Res.*, doi:10.1029/2005JD006046, in press.
- Sharma, S., D. Lavoue, H. Cachier, L. A. Barrie, and S. L. Gong (2004), Long-term trends of the black carbon concentrations in the Canadian Arctic, *J. Geophys. Res.*, *109*, D15203, doi:10.1029/2003JD004331.
- Shaw, G. E. (1983), Bio-controlled thermostat involving the sulfur cycle, *Clim. Change*, *5*, 297–303.
- Shaw, G. E. (1987), Aerosols as climate regulators: A climate biosphere linkage?, *Atmos. Environ.*, *21*, 985–986.
- Shindell, D., and G. Fulavegi (2002), An exploration of ozone changes and their radiative forcing prior to the chlorofluorocarbon era, *Atmos. Chem. Phys.*, *2*, 363–374.
- Shindell, D., and G. A. Schmidt (2004), Southern Hemisphere climate response to ozone changes and greenhouse gas increases, *Geophys. Res. Lett.*, *31*, L18209, doi:10.1029/2004GL020724.
- Shindell, D., D. Rind, N. Balachandran, J. Lean, and P. Lonergan (1999a), Solar cycle variability, ozone, and climate, *Science*, *284*, 305–308.
- Shindell, D., R. L. Miller, G. A. Schmidt, and L. Pandolfo (1999b), Simulation of recent northern winter climate trends by greenhouse-gas forcing, *Nature*, *399*, 452–455.
- Shindell, D., G. A. Schmidt, R. L. Miller, and D. Rind (2001), Northern Hemisphere winter climate response to greenhouse gas, volcanic, ozone, and solar forcing, *J. Geophys. Res.*, *106*, 7193–7210.
- Shindell, D., G. Fulavegi, and N. Bell (2003a), Preindustrial-to-present-day radiative forcing by tropospheric ozone from improved simulations with the GISS chemistry-climate GCM, *Atmos. Chem. Phys.*, *3*, 1675–1702.
- Shindell, D., G. A. Schmidt, R. L. Miller, and M. E. Mann (2003b), Volcanic and solar forcing of climate change during the preindustrial era, *J. Clim.*, *16*, 4094–4106.
- Shindell, D., G. A. Schmidt, M. E. Mann, and G. Fulavegi (2004), Dynamic winter climate response to large tropical volcanic eruptions since 1600, *J. Geophys. Res.*, *109*, D05104, doi:10.1029/2003JD004151.
- Shine, K. P. (2005), Comment on “Contrails, cirrus trends and climate,” *J. Clim.*, in press.
- Shine, K. P., and P. M. Forster (1999), The effect of human activity on the radiative forcing of climate change: A review, *Global Planet. Change*, *20*, 205–225.
- Shine, K. P., J. Cook, E. J. Highwood, and M. M. Joshi (2003), An alternative to radiative forcing for estimating the relative importance of climate change mechanisms, *Geophys. Res. Lett.*, *30*(20), 2047, doi:10.1029/2003GL018141.

- Smith, C. A., J. D. Haigh, and R. Tuomi (2001), Radiative forcing due to trends in stratospheric water vapor, *Geophys. Res. Lett.*, *28*, 179–182.
- Soden, B. I., R. T. Wetherald, G. L. Stenchikov, and A. Robock (2002), Global cooling after the eruption of Mount Pinatubo: A test of climate feedback by water vapor, *Science*, *296*, 727–730.
- Sokolik, I. N., and O. Toon (1996), Direct radiative forcing by anthropogenic airborne mineral aerosols, *Nature*, *381*, 681–683.
- Stenchikov, G., K. Hamilton, A. Robock, V. Ramaswamy, and M. D. Schwarzkopf (2004), Arctic oscillation response to the 1991 Pinatubo eruption in the SKIHI general circulation model with a realistic quasi-biennial oscillation, *J. Geophys. Res.*, *109*, D03112, doi:10.1029/2003JD003699.
- Stuber, N., M. Ponater, and R. Sausen (2005), Why radiative forcing might fail as a predictor of climate change, *Clim. Dyn.*, *24*, 497–510.
- Tegen, I., and I. Fung (1995), Contribution to the mineral aerosol load from land surface modification, *J. Geophys. Res.*, *100*, 18,707–18,726.
- Tegen, I., M. Werner, S. P. Harrison, and K. E. Kohfeld (2004), Relative importance of climate and land-use in determining present and future global soil dust emissions, *Geophys. Res. Lett.*, *31*, L05105, doi:10.1029/2003GL019216.
- Thompson, D. W. J., and J. M. Wallace (1998), The Arctic Oscillation signature in the wintertime geopotential height and temperature fields, *Geophys. Res. Lett.*, *25*, 1297–1300.
- Turner, J., S. R. Colwell, G. J. Marshall, T. A. Lachlan-Cope, A. M. Carleton, P. D. Jones, V. Lagun, P. A. Reid, and S. Iagovkina (2005), Antarctic climate change during the last 50 years, *Int. J. Climatol.*, *25*, 279–294.
- Twomey, S. (1977), The influence of pollution on the shortwave albedo of clouds, *J. Atmos. Sci.*, *34*, 1149–1152.
- Warren, S. G., and W. J. Wiscombe (1985), Dirty snow after nuclear war, *Nature*, *313*, 467–470.
- Wetherald, R. T., and S. Manabe (1975), The effects of changing the solar constant on the climate of a general circulation model, *J. Atmos. Sci.*, *32*, 2044–2059.
- Wong, S., W. C. Wang, I. S. A. Isaksen, T. K. Berntsen, and J. K. Sundet (2004), A global climate-chemistry model study of present-day tropospheric chemistry and radiative forcing from changes in tropospheric O₃ since the preindustrial period, *J. Geophys. Res.*, *109*, D11309, doi:10.1029/2003JD003998.
- Wong, T., B. A. Wielicki, and R. B. Lee (2004), Decadal variability of Earth radiation budget deduced from satellite altitude corrected ERBE/ERBS nonscanner data, paper presented at 13th Conference on Satellite Meteorology and Oceanography, Am. Meteorol. Soc., Norfolk, Va., 20–24 Sept. (Available at <http://asd-www.larc.nasa.gov/~tak/wong/r47.pdf>)
- World Meteorological Organization (WMO) (1957), Meteorology: A three-dimensional science, Second session of the commission for aerology, *WMO Bull.*, *6*(4), 134–138.
- Zhou, X. L., M. A. Geller, and M. Zhang (2001), The cooling trend of the tropical cold point tropopause temperatures and its implications, *J. Geophys. Res.*, *106*, 1511–1522.
-
- I. Aleinov, M. Bauer, S. Bauer, N. Bell, M. Chandler, G. Faluvegi, D. Koch, J. Lerner, L. Nazarenko, Ju. Perlwitz, M. Sato, and S. Zhang, Columbia University Earth Institute, New York, NY 10025, USA.
- B. Cairns and Ja. Perlwitz, Department of Applied Physics and Applied Mathematics, Columbia University, New York, NY 10025, USA.
- V. Canuto, A. Del Genio, T. Hall, J. Hansen, N. Kiang, A. Lacis, R. Miller, D. Rind, A. Romanou, G. Russell, G. A. Schmidt, D. Shindell, and S. Sun, NASA Goddard Institute for Space Studies, New York, NY 10025, USA. (jhansen@giss.nasa.gov)
- Y. Cheng, K. Lo, V. Oinas, R. Ruedy, N. Tausnev, and M. Yao, SGT Incorporated, New York, NY 10025, USA.
- E. Fleming and C. Jackman, NASA Goddard Space Flight Center, Greenbelt, MD 20771, USA.
- A. Friend and M. Kelley, Laboratoire des Sciences du Climat et de l'Environnement, Orme des Merisiers, F-91198 Gif-sur-Yvette Cedex, France.
- J. Lean, Naval Research Laboratory, Washington, DC 20375, USA.
- S. Menon and T. Novakov, Lawrence Berkeley National Laboratory, Berkeley, CA 94720, USA.
- P. Minnis, B. Wielicki, and T. Wong, NASA Langley Research Center, Hampton, VA 23681, USA.
- P. Stone, Center for Meteorology, Massachusetts Institute of Technology, Cambridge, MA 02139, USA.
- D. Thresher, Department of Earth and Environmental Sciences, Columbia University, New York, NY 10025, USA.